Mariana Antas Rebocho da Costa
Licenciatura em Biologia Celular e Molecular

Uncovering the role of blood vessels during spinal cord regeneration in zebrafish

Dissertação para obtenção do Grau de Mestre em
Genética Molecular e Biomedicina

Orientador: Doutora Ana Ribeiro, Instituto de Medicina Molecular – João Lobo Antunes

Co-orientador: Professora Doutora Leonor Saúde, Instituto de Medicina Molecular – João Lobo Antunes

Presidente: Professora Doutora Alexandra Fernandes

Arguente: Professor Doutor Sérgio Dias

FACULDADE DE CIÊNCIAS E TECNOLOGIA
UNIVERSIDADE NOVA DE LISBOA

Setembro 2018

2018

Uncovering the role of blood vessels during spinal cord regeneration in zebrafish

Mariana Antas Rebocho da Costa
Licenciatura em Biologia Celular e Molecular

Uncovering the role of blood vessels during spinal cord regeneration in zebrafish

Dissertação para obtenção do Grau de Mestre em Genética Molecular e Biomedicina, Faculdade de Ciências e Tecnologia, Universidade Nova de Lisboa

Orientadores: Ana Ribeiro e Leonor Saúde

Setembro 2018

Uncovering the role of blood vessels during spinal cord regeneration in zebrafish

Acknowledgments

Bem, por onde começar?

Acaba um assim o ano da tese de Mestrado. Aquele que todos os alunos de mestrado temem mas no qual, no fundo, têm uma expectativa e entusiasmo imensos, já que para muitos de nós é a primeira longa experiência de trabalho num grupo de investigação no qual temos de desenvolver um projecto que vai ser o nosso "bebé". E tal como um bebé, este projecto precisou de muito carinho, paciência, dedicação e tempo (muitooo tempo). Mas tudo acaba, e com a escrita desta dissertação, está (quase) finalizado este capítulo na vida desta estudante de Mestrado e é hora de agradecer a todas as pessoas que fizeram com que esta experiência pudesse acontecer ou que apenas deram o seu tempo e apoio total ao longo deste ano.

Antes de tudo, queria agradecer à Professora Leonor Saúde, a melhor chefe que alguém pode ter. Desde ter aceite no seu grupo está miúda que não sabia muito bem se queria ou iria gostar de fazer investigação, às reuniões semanais para discutir os resultados que podiam não ser fantásticos, mas que com uma pitada de otimismo eram novas possibilidades e incentivavam a manter a cabeça erguida e não desmotivar. Um grande obrigada por tudo!

Quero também agradecer imenso à minha orientadora, Ana Ribeiro, por me ter ensinado todas as técnicas essenciais para este projecto. Foste uma professora fantástica (e a Alice também, que tecnicamente estava presente nesta altura)! Obrigada por me teres apoiado ao longo deste ano, de me teres ajudado e dado uns empurrõezinhos quando precisei (principalmente em partes durante a escrita desta dissertação, quando eu não sabia muito bem por onde pegar). Obrigada por nestas últimas semanas teres sido um apoio constante e uma guia e teres tornado possível a entrega desta tese a tempo (não sei o que faria sem os teus feedbacks tão rápidos)! OBRIGADA!

Ao melhor grupo de investigação, obrigado por me terem acolhido tão bem. Guida, obrigada por toda a ajuda no lab (embora tu digas que eu não dou trabalho nenhum) e por teres iniciado o contrabando de suculentas lindas que se estão a dar maravilhosamente na minha varanda; Isaura, obrigada pelo apoio e pelos concelhos nos protocolos que correram menos bem (#rnaemspinalcordémentira); e Diogo, obrigada pelas tuas sugestões e ajuda e pelas gargalhadas nas horas de almoço do grupo, não sei como é no CEDOC, mas aqui foi louvável 😂! A todos um enorme obrigada!! Às meninas da Fish Facility, que no fundo são como uma extensão do laboratório, obrigada! Lara, obrigado por me teres recebido, por me teres introduzido no mundo do peixe-zebra, por me teres acompanhado nas minhas primeiras semanas no iMM e por me ensinado as técnicas básicas que todos os utilizadores deste modelo deveriam saber e de o teres feito com tanto entusiamos, boa vontade e com essa tua atitude relaxada e animada. Obrigada por tudo! Aida, minha companheira de trocas de vídeos de gatos e de fails e de gosto musical impecável, quero agradecer todo o teu apoio, toda a tua ajuda durante este ano, principalmente a tratar

das minhas linhas e a fazer os screens quando eu já não sabia se os peixes eram verdes ou azuis ou quando tinha tanta coisa para fazer que o que me apetecia mesmo encostar a um cantinho e não me mexer. Obrigada por seguires as minhas maluquices e implementares comigo o dia mensal da batata frita, porque na verdade toda a gente precisa de um diazinho (ou mais) de comida de conforto. Obrigada principalmente por nestas duas semanas de stress intensivo teres tentado quebrar os momentos de tensão de escrita a desoras, és fantástica (but u know that 😉). Quero agradecer ainda à Filipa por todo o apoio, sugestões e dicas como "veterena" de MGMB e por a certa altura ter sido ao mesmo tempo minha professora em algumas técnicas e minha aluna em SCI, foi engraçado, és uma boa professora e espero ter sido uma boa professora para ti (pelo menos lesionas que é uma maravilha! Eheheh). Obrigada ainda à Carolina. Desejo-te imensa sorte no teu mestrado! (para o ano és tu assim)

Agradeço também à equipa de Bioimaging do IMM por todo o apoio e ajuda que me deram ao longo de todo este ano, principalmente ao António Temudo que me deu a minha primeira (e única, até agora) aula de bioimaging e me incentivou a utilizar o equipamento maravilhoso (~~quando lhe apetece~~) que é o Lighsheet. Agradeço ainda à Anna Pezzarossa pela ajuda e contributo que deu para este trabalho.

Quero agradecer à Mariana (ainda não oficialmente bioimaging, but one day!) por ser aquela amiga que eu não estava à espera de encontrar, por ser a minha companheira durante todo este ano no iMM e a pessoa com quem eu posso contar e falar sem me importar de dizer as maiores baboseiras à face da terra. U DA GURL! Quero também agradecer à Dalila que, desde o início, me deu dicas sobre o que esperar deste ano e para escrever esta dissertação, que me ajudou e apoio ao longo de todo este processo e que foi outra amizade com a qual eu não contava. Obrigada meninas! No fundo, somos a #iMMMScrew!

Quero agradecer aos meus amigos e família que, embora não tenham estado envolvidos directamente no projecto em termos laboratoriais, foram o meu apoio exterior. Às minhas meninas, Ana, Catarinas e Joana, obrigada por todo o apoio, por terem ouvido os desabafos, por serem a melhor distração com os nossos lanches e as nossas sessões de filmes de terror. Desculpem não ter estado tão presente nos últimos tempos, mas a "época final" de uma tese faz destas coisas. De qualquer das formas um enorme obrigada! (e viva o abalam ou o flower power, não sei bem, são coisas um bocado contraditórias, não?).

Obrigada aos amigos do mesmo percurso académico, à Laura, por estar presente desde o primeiro dia de faculdade, literalmente desde que nos conhecemos somos amigas. És a melhor sabes? Obrigada ao Magalhães pelas parvoíces e pelas discussões de arte. A estas duas pérolas de LBCM, obrigada por estarem sempre a uma mensagem de distância se for necessário. À Rita e ao Martins, colegas de licenciatura e de mestrado, obrigada por estes últimos dois anos de companheirismo, de parvoíces e, agora, de stress conjunto por termos de estar a escrever esta dissertação. Está quase a acabar!

Por último, e provavelmente mais importante, quero agradecer à minha família pelo apoio que me deram nesta aventura. Quero agradecer principalmente à minha mãe e ao Santana por terem sido o meu apoio

não só nestes anos de mestrado mas desde sempre! Nada disto era possível sem o vosso apoio incondicional, incentivo e, sim, não era possível sem a vossa preocupação (embora muitas seja vezes excessiva, convenhamos). Um Obrigado Gigante!

E agora sim, o último obrigado vai mesmo para o meu gato que é um fofo e eu não o ia deixar fora disto, obviamente!

Até à próxima aventura!

Abstract

The spinal cord is the region of the central nervous system responsible for the bidirectional relay of information between the brain and the rest of the body. For this reason, damages to the spinal cord can result in devastating consequences. Spinal cord injury (SCI) occurs due to a physical trauma and causes loss of motor and sensitive function. Additionally, the initial trauma provokes the disruption of the blood-spinal cord barrier (BSCB). This results in the leakage of blood to the tissue, further damaging the spinal cord. In mammals, like humans and mice (*Mus musculus*), endogenous attempts to repair the resulting damage occur, however, these attempts are mostly unsuccessful due to the present of growth-inhibitory molecules and structures. As such, no significant recovery is accomplished. By contrast, zebrafish (*Danio rerio*) are able to regenerate their spinal cord and previous work from our lab showed that, during regeneration, the injured tissue revascularizes and that blood flow is observed in these vessels.

In this work, we followed the recovery of the BSCB during spinal cord regeneration in zebrafish at different timepoints after injury. Our results showed that the reestablishment of the BSCB occurred between 3 dpi and 7 dpi, indicating that the new blood vessels rapidly become functional in zebrafish. In addition, in order to study the importance of revascularization after SCI, we attempted to inhibit the angiogenic process that occurs during spinal cord regeneration. Our preliminary results suggest that the inhibition of angiogenesis results in impaired motor function. However, the cellular and molecular mechanisms involved are not yet understood.

These results allow a better understanding of the regenerative process in zebrafish and may provide clues regarding the fundamental differences that exist between this animal model and mammals.

Keywords: Spinal Cord, Spinal Cord Injury, Blood-Spinal Cord Barrier, Regeneration, Angiogenesis, Zebrafish.

Sumário

A medula espinhal é a região do sistema nervoso central responsável pela troca bidirecional de informação entre o cérebro e o resto do corpo. Desta forma, qualquer dano que afete a medula resulta em consequências devastadoras para o indivíduo. As lesões vertebro-medulares (LVM) são causadas por um trauma físico e têm como consequências a perda da função motora e sensorial. Este trauma pode ainda levar à disrupção da função da barreira hematoencefálica (BHE) da medula, provocando uma hemorragia que promove a deterioração do tecido nervoso. Nos mamíferos, como por exemplo em humanos e em murganho (*Mus musculus*), ocorre uma tentativa endógena de reparação dos danos causados. No entanto, devido à existência de substâncias e estruturas que inibem estas tentativas, nenhuma melhoria significativa ocorre a longo prazo. Por outro lado, o peixe-zebra (*Danio rerio*) é capaz de regenerar a medula espinhal após uma lesão. Estudos feitos pelo nosso laboratório indicam também que, durante o processo regenerativo, ocorre uma revascularização do tecido lesado e, nestes vasos, é ainda possível observar fluxo sanguíneo.

Neste trabalho, estudámos o restabelecimento da BHE em peixe-zebra, utilizando amostras com diferentes dias após a lesão. Os resultados obtidos apontam para a recuperação da BHE entre o terceiro e o sétimo dia após a lesão, indicando que os vasos recentemente formados rapidamente se tornam funcionais. Adicionalmente, tentámos inibir a formação de novos vasos durante o processo regenerativo de modo a estudar a importância da revascularização após uma LVM. Os resultados preliminares indicam que a inibição da revascularização parece resultar numa diminuição da função motora. No entanto, os mecanismos celulares e moleculares envolvidos neste processo não são claros.

Os resultados obtidos neste trabalho contribuem para uma melhor compreensão do processo regenerativo em peixe zebra e poderão fornecer informações e pistas sobre as diferenças existentes entre o peixe-zebra e os mamíferos.

Palavras-chave: Medula Espinhal, Lesões Vertebro-Medulares, Barreira Hematoencefálica, Regeneração, Angiogénese, Peixe-zebra

Table of Contents

Figure index

Abbreviation and Symbols

Abbreviations

Ang - Angiopoetin

BSCB - Blood-Spinal Cord Barrier

CFP - Cerulean fluorescent protein

CNS - Central nervous system

CSF - Cerebrospinal fluid

dpi - Days post injury

ECs - Endothelial cells

EGFP or GFP - (Enhanced) Green fluorescent protein

FGF - Fibroblast growth factor

h - hour

HS - heat-shock

hpf - Hours post fertilization

ISVs - Intersomitic vessels

KDRL – VEGFR-2 like

PDGF-β - Platelet-derived growth factor

PFA - Paraformaldehyde

qPCR – Quantitative polymerase chain reaction

SCI - spinal cord injury

sFLT1 - soluble form of VEGFR-1

TGF - Transforming growth factor

VEGF - Vascular endothelial growth factor

VEGFR-1 (also known as FLT1) - Vascular endothelial growth factor receptor 1

VEGFR-2 (also known as KDR) - Vascular endothelial growth factor receptor 2

Symbols

% - percentage

ºC – degrees Celsius

M – molar concentration

v/v – volume per volume

w/v – weight per volume

µm – micrometer

µL – microliter

± - plus-minus

Chapter 1. Introduction

1.1 Spinal Cord

1.1.1 Function, structure and composition

The spinal cord is a narrow tube composed of nervous tissue and is a major component of the central nervous system (CNS). It contacts with the brain through an orifice in the skull, the foramen magnum, and is protected by the vertebral column (**Figure 1.1**), extending through the spinal canal of each vertebra. Additionally, the spinal cord is also protected by the meninges, three membranes of connective tissue that directly cover the CNS, and by the cerebrospinal fluid (CSF) (Marcus *et al*., 2014; Van de Graaff, 2011). The spinal cord has two main functions: the conduction of impulses, processing sensory information and providing bidirectional relay between the brain and remaining organs and tissues; and the integration of reflexive involuntary movements, with different nerve pathways than those initiated voluntarily by the brain (Marcus *et al*., 2014; Van de Graaff, 2011).

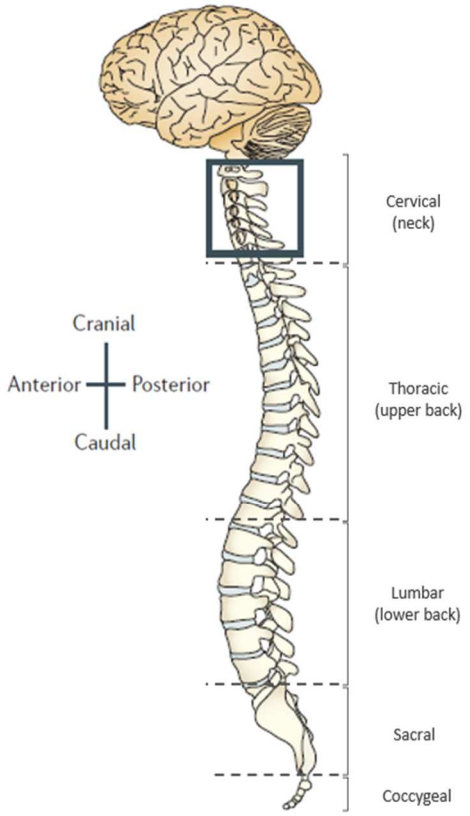

Figure 1.1 – Central nervous system. Representation of the CNS regarding the body axis. The vertebral column surrounds and protects the spinal cord (as seen in **boxed area**) and can be divided 5 different levels: cervical, thoracic, lumbar, sacral and coccygeal (Adapted from Thuret *et al.*, 2006)

Transverse cuts of the spinal cord allow the identification of two distinct areas, the white matter and the grey matter (**Figure 1.2**). The white mater is the outermost part of the spinal cord, consisting of glial cells and bundles of myelinated axons of sensory and motor fibers, running to and from the brain, respectively. The grey matter is the innermost part of the spinal cord and consists of cell bodies and

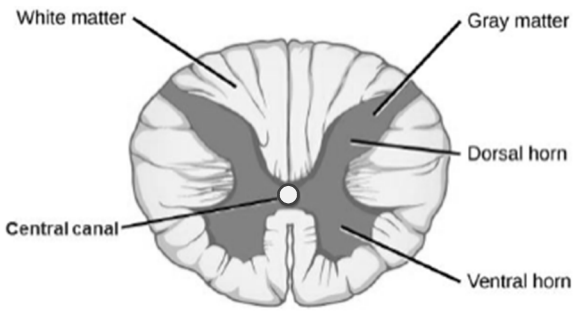

Figure 1.2 – Spinal cord transverse section. Representation of the grey matter and white matter regions of the spinal cord, as well as the dorsal and ventral horns and the central canal (adapted from OpenStax Anatomy & Physiology, Rice University, 2013)

synapses, neuroglia and unmyelinated interneurons. These two regions are organized in a butterfly-like shape, in which the grey matter is surrounded by the white matter, with two dorsal horns and two ventral horns (Marcus *et al*., 2014; Mescher, 2013; Van de Graaff, 2011).

Although it is the least complex of the CNS elements, the spinal cord is still composed of various cell types with specific functions and distinct distribution. One of the main cell types are neurons, which form a complex network that receives information, like sensory intakes, and generates motor responses. As previously mentioned, the cell bodies and the axons of neurons in the spinal cord have distinct locations, the grey matter and the white matter, respectively. Different types of glial cells provide the support and maintenance needed for the nervous tissue survival, such as oligodendrocytes, astrocytes, microglia and ependymal cells. Oligodendrocytes produce myelin sheaths, which wrap around axons and give electrical insulation, allowing the efficient transmission of the electric impulse. Astrocytes, the most numerous type of glial cells, are responsible for not only regulating metabolic exchanges but also directly influencing the metabolism of surrounding cell types. Microglia are motile antigen-presenting cells of the CNS, responsible for the immune surveillance of these tissues. Finally, ependymal cells line the central canal of the spinal cords, are responsible for the circulation of the CSF and are a source of adult neural stem cells. (Marcus *et al*., 2014; Meletis *et al.*, 2008; Mescher, 2013).

1.1.2 Spinal cord vasculature

The spinal cord, as the rest of the CNS, is a highly energy-demanding tissue. It is, therefore, of special importance the existence of an organized and tightly controlled vascular system, in order to provide cells with oxygen and nutrients and remove metabolic waste, maintaining the homeostasis of the tissue (Attwell and Laughlin, 2001; Martirosyan *et al.*, 2011).

1.1.2.1 Vascular structure and blood supply

In general, the blood supply of the spinal cord is achieved by two distinct systems, the central and the peripheral system (**Figure 1.3**). Both are supplied by the radicular artery, that runs along the nerve root, and then splits into anterior and posterior radicular arteries. Both of these arteries then connect to longitudinal vessels along the spinal cord, the anterior radicular artery with the anterior spinal artery and the posterior radicular artery with the left and right posterior spinal arteries. Numerous anastomoses, connecting the spinal arteries, exist around the spinal cord, forming an irregular network of vessels called spinal arterial plexus, or simply vasocorona. The central system is derived from the arterial spinal artery, being supplied by the sulcocommissural artery. It irrigates roughly two-thirds of the spinal cord: the anterior and the anterior portion of the posterior grey matter, and the inner portions of the white matter. The peripheral system is composed by the posterior spinal arteries and the vasocorona, and it supplies the outer portion of the white matter and the posterior portion of the posterior grey matter (**Figure 1.3 A**) (Martirosyan *et al.*, 2011; Mautes *et al.*, 2000; Tventen, 1976).

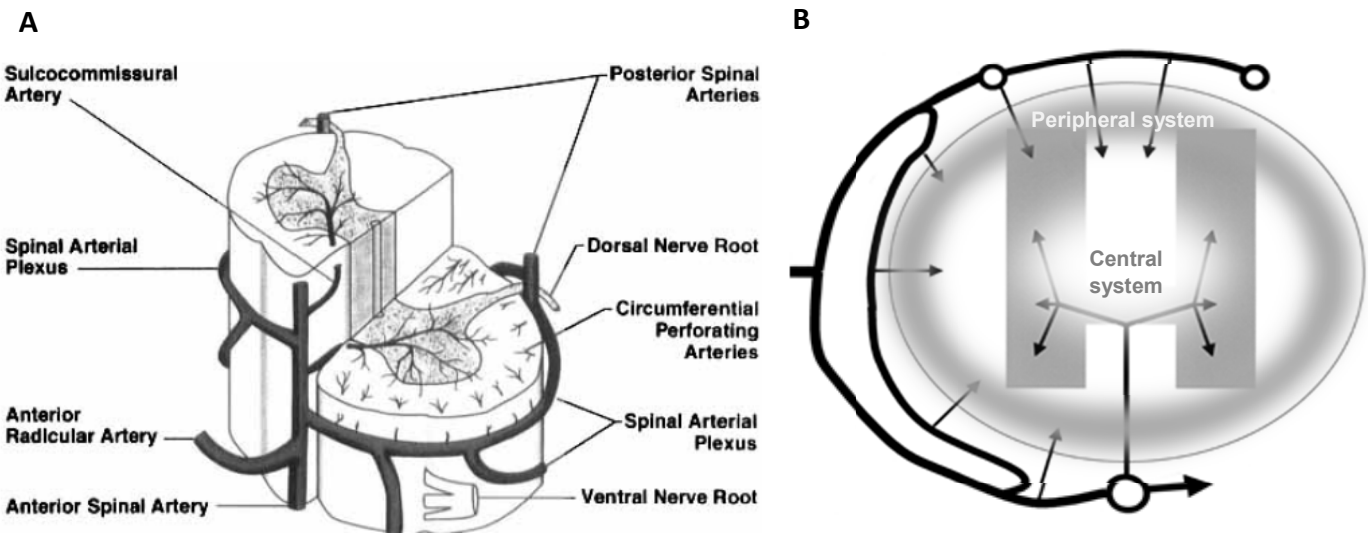

Figure 1.3 – **Spinal cord vasculature and blood supply**. (**A**) General representation of the main arteries irrigating the spinal cord and (**B**) of the blood supply and flow (arrows) to the peripheral and central systems of the spinal cord. (**A** –Cheshire *et al.*, 1996; **B** – Adapted from Mautes *et al*., 2000)

Although there is no connection between the capillary beds of the central and peripheral systems, in an intermediate zone there is an overlap of their terminal branches, being indirectly supplied by one system or the other. As the blood flow in each system is different, with a centrifugal flow in the central system and a centripetal flow in the peripheral system (**Figure 1.3 B**), a watershed zone is established. These zones are characterized by the inexistence of direct blood supply and are, therefore, dependent on the overlapping vasculature. In case of interruption of the blood supply, as occurs in spinal cord injuries (SCI), these zones are particularly vulnerable (Martirosyan *et al.*, 2011; Mautes *et al.*, 2000).

1.1.2.2 Blood - Spinal Cord Barrier

As arteries get thinner and blood vessels reach the intramedullary territory, the blood - spinal cord barrier (BSCB) is established (**Figure 1.4**). This vascular specialization occurs at the capillary level and involves pericytes, basal lamina, and astrocytes. Capillaries are the smallest blood vessels in diameter, with just one endothelial cell (EC) of thickness, and lack smooth muscle, having instead pericytes with stabilizing and contractile functions. Unlike the capillaries that exist in the peripheral circulation, those of the BSCB are characterized by the absence of cell membrane fenestration and the existence of tight junctions between neighbouring ECs. These cells are then surrounded by a continuous basal lamina, where pericytes are attached. Surrounding the outer surface of the capillaries, astrocytic foot processes are essential to the development and maintenance of the barrier mechanism, modulating the properties of the other BSCB components via secretory mechanisms (Bartanusz *et al.*, 2011; Mautes *et al.*, 2000; Van de Graaff, 2011).

The BSCB, through the existence of physical and molecular barriers, regulates the transport of molecules into the nervous tissue and restricts the contact of potentially toxic agents, such as metabolic

waste or pathogens, with the spinal cord. This way, a stable microenvironment, necessary for the normal neuronal function, is established (Bartanusz *et al.*, 2011; Mautes *et al.*, 2000).

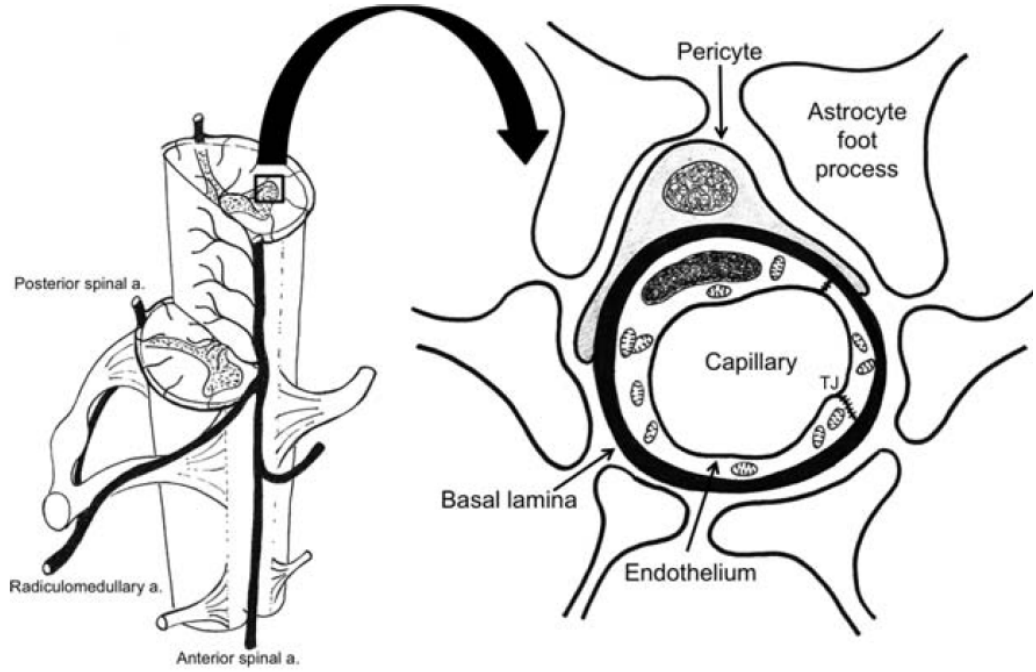

Figure 1.4 – **Representation of the blood - spinal cord barrier**. This specialized vascular structure is composed of epithelial cells, joined by tight junctions (TJ), basal lamina surrounding the capillary, pericytes and astrocyte foot processes, which prevent the direct contact of the vasculature with the surrounding nervous tissue. (Bartanusz et al., 2011)

1.2 Spinal cord injury

Although the spinal cord is protected by the vertebrae and the meninges, it is a relatively soft and fragile tissue, with very little collagen and fibrous components and, as such, is especially susceptible to damage directly inflicted to the vertebral column (Mescher, 2013).

1.2.1 General description and types of spinal cord injury

Spinal cord injury is a highly disabling injury and is defined as a damage to the spinal cord, which can result from a contusion, compression, laceration or maceration, causing a temporary or permanent change in its function, bellow the injury site, like loss of sensation and partial or total paralysis, and it may also affect the performance of multiple organs (Ahuja *et al.*, 2017; Kang *et al.*, 2018, Thuret *et al.*, 2006).

It can be divided in two categories: traumatic SCI, that occurs due to an external physical impact, like falls, motor vehicle accidents, sport-related accidents, violence, *etc.*; or non-traumatic SCI, which can be the result of acute or chronic illnesses, such as vertebral spondylosis, tumorous compression, infections, vascular ischemia and congenital or degenerative diseases (Ahuja *et al.*, 2017; Kang *et al.*, 2018).

1.2.2 Epidemiology

According to data provided by the World Health Organization (WHO) in 2013, between 250 000 and 500 000 people world-wide suffer from SCI each year, with the most common cause being falls, followed by motor vehicle crashes and violence, all of them preventable.

Recent information indicates that, with the rise in human activity, the incidence of traumatic SCI also increased, being estimated that it varies from 13.019 cases per million individuals to 163.420 cases per million individuals. Most SCI patients are male (79,8%) and the age profile of SCI patients has a bimodal distribution, with most cases happening in patients with 15 to 29 years of age and, although with a smaller number of cases but growing, in patients with more than 50 years of age. (Ahuja *et al.*, 2017; Kang *et al.*, 2018).

The mortality of SCI patients, although having improved over time, is still 1,5 times to 5 times higher to that of the general population. The survival, longevity and quality of life of SCI patients are positively correlated with less severe injuries and SCI affecting lower levels of the spinal cord like at the lumbar or sacral level, as opposed to more severe injuries and those affecting higher levels, like lesions in the cervical and high thoracic regions (Chamberlain *et al.*, 2015, Kirshblum et al. 2011).

1.2.3 Physiological events after spinal cord injury

The events that occur after a traumatic spinal cord injury can be temporally divided into acute (< 48 hours), subacute (> 48 hours to 14 days), intermediate (14 days to 6 months) and chronic (> 6 months) phases (**Figure 1.5**), and physiologically divided into primary and secondary injuries (Ahuja *et al.*, 2017).

The primary injury happens immediately after a physical trauma to the vertebral column, leading to the compression or transection of the spinal cord tissue. It instantly causes neural cell death, axon damage and demyelination, which results in an immediate loss of motor and sensory function. The disruption of the BSCB also ensues, causing a severe haemorrhage at the injury site and exposing the spinal cord to immune cells and pro-inflammatory molecules. As a consequence, swelling of the tissues occurs, further compressing the injured spinal cord. These events describe the acute phase of the injury (**Figure 1.5 A**) and, over time, lead to the spread of the damage to adjacent areas, resulting in a secondary injury. The consequent cell death and axonal retraction, the absence of a functional microvasculature, the presence of pro-apoptotic, of pro-inflammatory and of cytotoxic molecules and the resulting activation of immune cells, all aid in the maintenance of an acute inflammatory response that is described as a subacute phase of the injury (**Figure 1.5 B**) (Ahuja *et al.*, 2017; Oudega, 2012; Tewari *et al.*,2010).

The intermediate to chronic phase (**Figure 1.5 C**) is characterized by the decrease of the acute inflammatory response and is marked by the endogenous attempts at remyelination (Wang *et al.*, 2017)

and vascular repair (Oudega, 2012) and by the expression of regeneration associated genes (Tetzlaff et al. 1991) and remodelling of the neural circuitry (Dietz *et al.*, 2009). However, and even if in some cases some functional recovery is observed years after the injury, these self-repair attempts are mostly unsuccessful due to the development of growth-inhibitory structures, like a scar, with reactive astrocytes, that surrounds and isolates fluid filled cystic cavities where cell death occurred. In addition, the presence of growth-inhibitory molecules, like myelin debris and other molecules released by degenerating oligodendrocytes, and lack of functional vasculature further hinder the self-repair process (Ahuja *et al.*, 2017; Oudega, 2012).

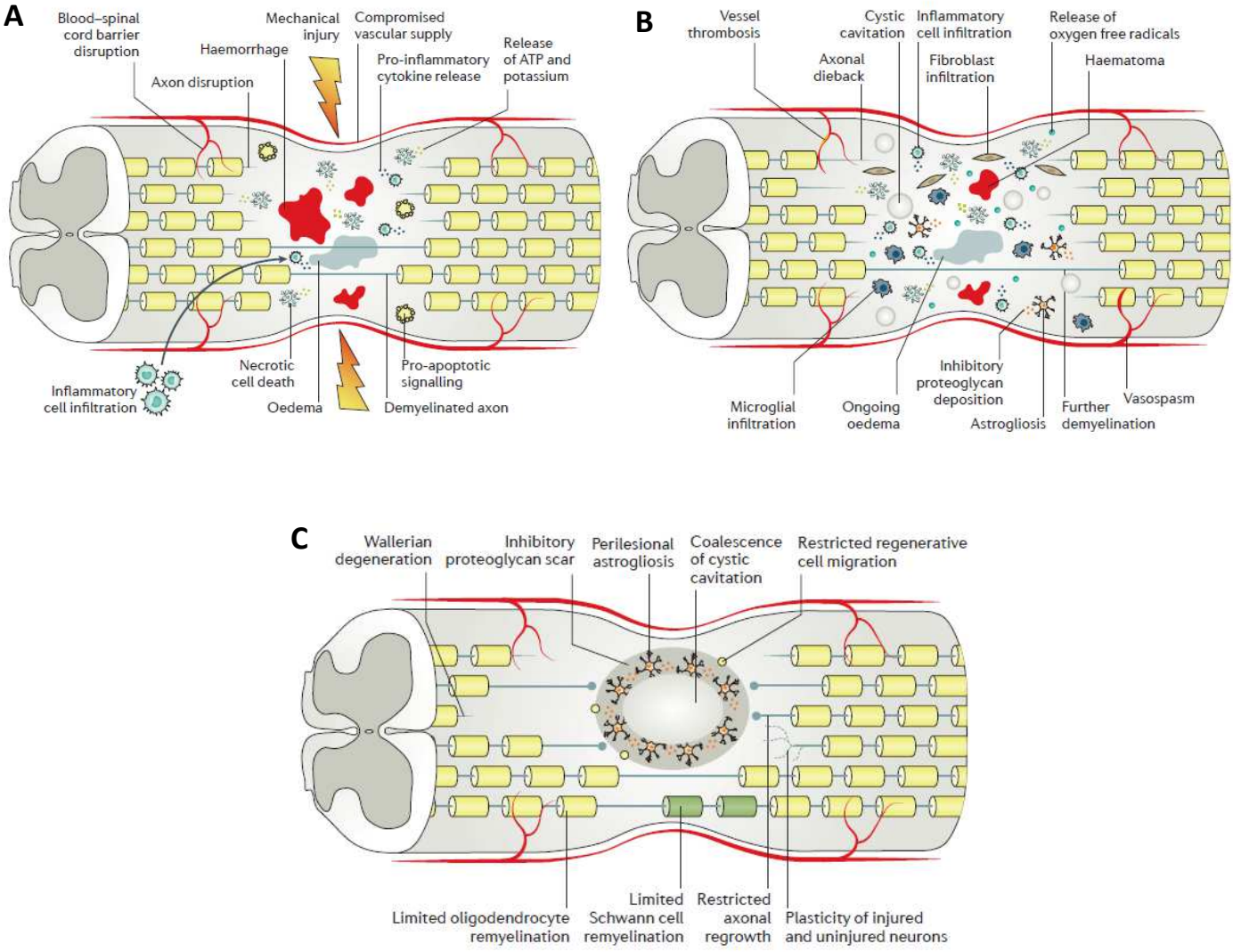

Figure 1.5 – **Events after spinal cord injury**. Main events that occur, after a mechanical injury to the spinal cord. (**A**) In the acute phase, death by necrosis and apoptosis, axonal disruption, swelling of the tissue, BSCB disruption and severe haemorrhage are observed and the beginning of the inflammatory response occurs. (**B**) In the subacute phase, an increased inflammatory response occurs due to the production/release of pro-inflammatory molecules and the invasion of immune cells, further damaging the tissue. (**C**) The intermediate to chronic phase is marked by the presence of a cystic cavity surrounded by a glial scar, composed of reactive astrocytes, that restricts endogenous attempts at a functional recovery. (Ahuja *et al.*, 2017)

1.2.3.1 Blood - Spinal Cord Barrier disruption

The disruption of the BSCB is a major event after SCI (**Figure 1.6**). As previously mentioned, the destruction of blood vessels at the injury site leads to the consequent contact between nervous tissue and toxic blood components, further increasing cell death. Additionally, the shear stress from the initial trauma may damage blood vessels in adjacent areas, leaving them hyperpermeable, allowing the passage

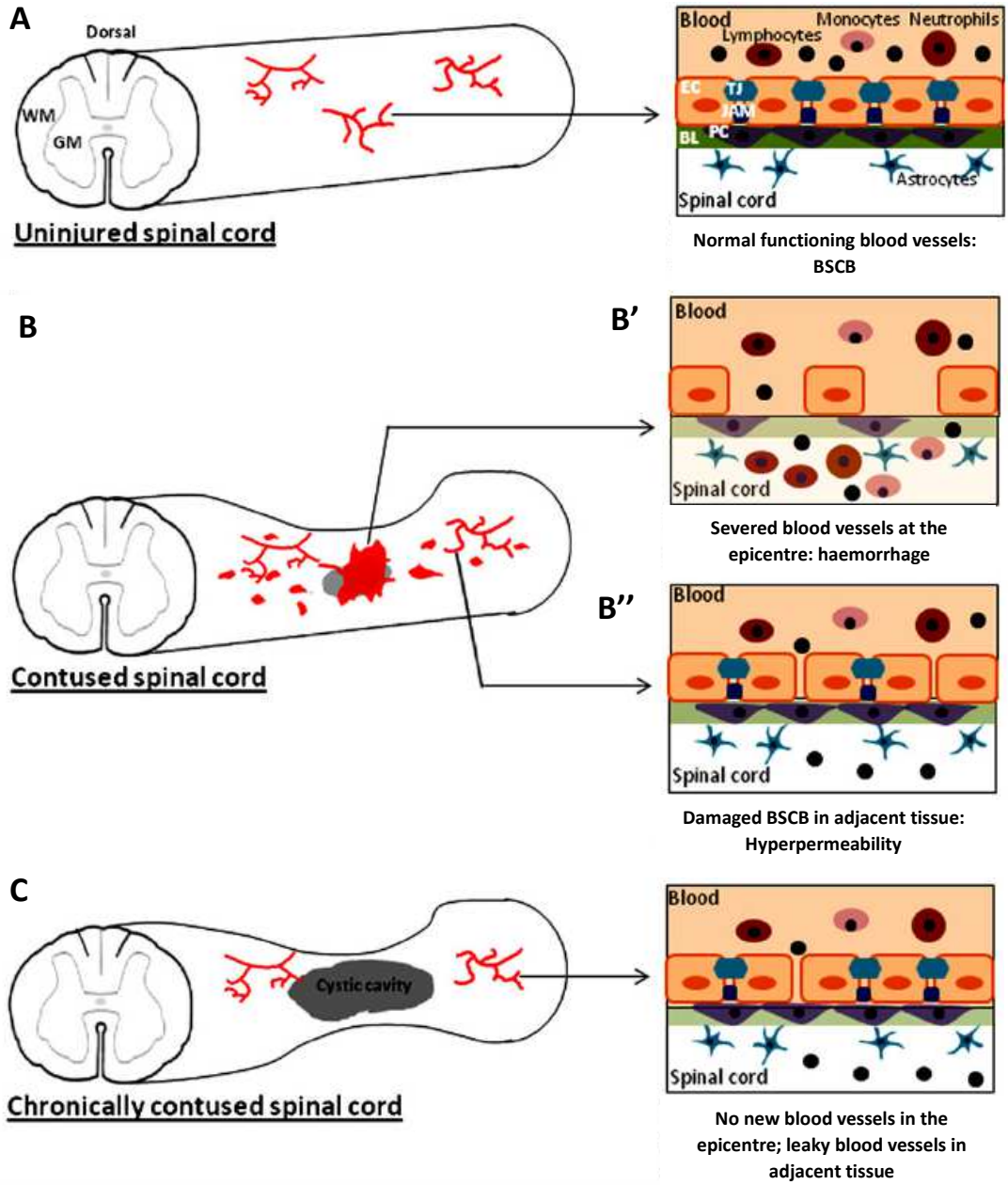

Figure 1.6 – **Blood - Spinal cord barrier disruption after spinal cord injury**. (**A**) BSCB in a healthy spinal cord. Blood and nervous tissue are physically separated by a vascular specialization, maintaining the homeostasis of the spinal cord tissue. (**B**) Disruption of the BSCB after a physical trauma. Blood vessels are severed at the injury site (**B'**), causing haemorrhage and, consequently, loss of homeostasis and cell death. At the periphery of the injury (**B''**), the BSCB is damage and blood components leak to the tissue. (**C**) In a chronically contused spinal cord, no new blood vessels are formed at the injury site and BSCB in peripheral areas continue to be hyperpermeable. **WM** – white matter, **GM** – grey matter, **EC**-endothelial cells, **TJ** – tight junctions, **PC** – pericytes, **BL** – basal lamina, **JAM** - junction adhesion molecules (Oudega, 2012)

of immune cells and toxic molecules, further damaging the spinal cord tissue. Through time, an angiogenic response fails to take place. As a consequence, no new blood vessels are formed in the epicentre of the injury, impairing the normal blood supply to this area. In adjacent regions, new and old blood vessels remain leaky, being a continuous source of damage to the already hurt tissue (**Figure 1.6 C**) (Oudega, 2012). The leakiness of the peripheral vessels may result from the detachment of pericytes from the blood vessels and their migration to the injury site, where they differentiate into fibroblast-like cells and contribute for the formation of the stromal component of the glial scar (Goritz et al., 2011).

1.2.4 Complications and current treatments

Besides the immediate loss of sensation and of motor function, many other complications can arise from a spinal cord injury. In most cases, patients suffer from spasticity (involuntary muscle contractions), pressure ulcers, excessive neuro-inflammation and consequent neuropathic pain. Bladder control is affected and, in many cases, bowel control is also affected. In more severe SCI cases, like in cervical and high thoracic lesions, autonomous nervous function can be affected, resulting in loss of core temperature control, cardiovascular and respiratory complications. Furthermore, SCI patients, due to the seriousness of this type of injury and the future obstacles they face, are especially susceptible to experience anxiety and develop depression (Ahuja *et al.*, 2017; Hagen, 2015).

Although there is no effective treatment for SCI, neuroprotective interventions can be applied to minimize loss of neural tissue and improve quality of life. It is therefore important to provide efficient and effective medical care right after injury. Non-pharmacological treatments involve the surgical decompression of the spinal cord right after injury, rehabilitation to prevent muscle waste and, in cases of subacute phase SCI or chronic motor-incomplete SCI, to recover as much function as possible, functional electrical stimulation. Pharmacological approaches involve the use of medication to reduce the inflammation and swelling of the spinal cord, control pain, manage spasticity and improve bowel and bladder function. (Ahuja *et al.*, 2017; Baptiste and Fehling, 2007; Cristante *et al.*, 2012) Cell transplantation therapies, like of neural stem cells, present a interesting method to improve sensory and motor function in chronic SCI patients, with some studies in phase I human clinical trials (Curtis *et al.*, 2018; Thuret *et al.*, 2006). However, a better understanding regarding the mechanisms involved to promote the potential functional recovery is still needed as well as further investigation about their safety and risks in human applications (Assinck *et al.,* 2017).

1.2.5 Spinal cord injury experimental models

SCI not only has devastating physical, psychological and social consequences for the patients and their families but is also a financial burden due to the continued need for medical care. Due to this, new therapeutic strategies to treat these patients are being pursued with the help of experimental models. (Tewari *et al.*,2010). The use of different injury models and the use of animal models to understand the mechanisms behind the pathophysiological response after SCI has been essential.

Three different models for SCI, that mimic specific clinical features, have been established: the transection model, the contusion model and the compression model (**Figure 1.7**). The transection model (**Figure 1.7 A**) includes all forms of lacerations, from small incisions and dorsal or lateral hemisections to complete cuts of the spinal cord, and has a more contained area of damage. Despite not being a very common type of SCI in humans, this model is used in studies where direct axonal growth, through the glial scar, is of interest. The contusion model (**Figure 1.7 B**) is produced by a focal impact on the spinal cord, most commonly dorsal, giving rise to an anatomically incomplete injury with a rim of spared white matter, the formation of cavities inside the spinal cord and with spread of the damage to areas adjacent to the injury. Contusions are the most common type of SCI in humans and therefore, this model is of particular relevance in terms of human SCI pathology. It is experimentally performed using a weight drop method or an impactor. The compression model (**Figure 1.7 C**) has the same pathophysiological consequences as the contusion model, however, rather than a focal force, a lateral or dorsal force is generally applied with the use of forceps, clips or specialized apparatus. Compression models have a broader dorsal and rostral impact and can have a bigger effect on lateral white matter areas than contusion models. The severity of this type of injury can vary depending on the instrument used and the duration of compression (McDonough, 2012; Oudega, 2012).

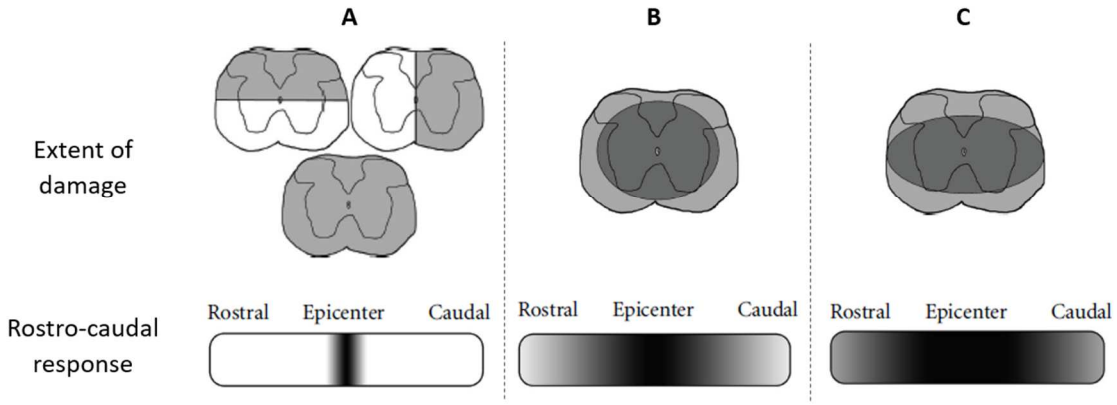

Figure 1.7 –Spinal cord injury models. Main types of experimentally induced spinal cord injuries models, (**A**) transection model, (**B**) contusion model and (**C**) compression model, and the respective extent of damage, seen from a tranverse section, and rostro-caudal response, with darker areas being more affected than lighter areas. (adapted from McDounough, 2012)

Mammal models like rat (*Rattus norvegicus*) or mouse (*Mus musculus*) are valuable SCI models as they emulate the locomotor and sensory deficits that happen in humans after a SCI, not being able to recover to their initial state. Although larger animals and non-human primates have more similarities with humans regarding the physiological response to SCIs, rodent models are better suited for preliminary studies since they are relatively smaller and cheaper to maintain, have better understood anatomy and genome, bigger availability of genetic tools, and less regulatory requirements and ethical restrictions. In contrast with these models, animals that are capable of regeneration during adulthood are used in order to understand and compare the pathophysiological, cellular and molecular differences during SCI and provide hints to improve the repair process in non-regenerating animals. An example of

an animal model with regenerative abilities is the zebrafish (*Danio rerio*) (Sharif-Alhoseini *et al.*, 2017; Steward and Willenberg, 2017).

1.2.5.1 Zebrafish as a spinal cord injury model

Zebrafish, a small teleost fish, is a well known developmental model due to characteristics like having external fertilization and development, being optically transparent until early adulthood and having a rapid development, with the completion of embryogenesis after 5 days post fertilization. Furthermore, only one couple can produce a high number of offsprings (100-300 embryos), providing statistically significant sample size and facilitating the maintenance of zebrafish lines. Since these fish exhibit a high degree of similarities with mammals regarding molecular pathways and mechanisms, and due to the variety of genetic tools and mutant and transgenic lines currently available, zebrafish present an interesting and less expensive model to use in preliminary studies. (Kari *et al.*, 2007)

As previously mentioned, zebrafish has regenerative abilities, being able to regenerate fins, jaw, heart, pancreas, liver, kidney and, of course, CNS structures, like the spinal cord (Gemberling *et al.*, 2013). Although the result after SCI in vastly different to that of mammals, the spinal cord cellular architecture is relatively similar and therefore useful to study the regenerative process (Dias Quiroz and Echeverri, 2013; Hui *et al.*, 2010)

Transection and compression models of spinal cord injury can be performed in zebrafish (Becker and Becker, 2008; Fang *et al.*, 2012). After SCI, loss of swimming behaviour is observed mainly due to the paralysis of the posterior portion of the body, bellow the injury site. In compression models, very little movement is observed 3 days after the injury, when compared to unlesioned fish. Movement progressively increases after 15 days and an almost complete recovery of swimming ability is observed 1 month after injury. In a complete transection of the spinal cord, 42 days after injury, axonal projections of brainstem neurons with spinal projection are seen beyond the injury site and fish show almost complete recovery of their normal swimming behaviour (Becker and Becker, 2008; Hui *et al.*, 2010).

Pathophysiological analysis show that, after a compression injury, adult zebrafish spinal cord experiences cell death of both neurons and glial cells, rupture of blood vessels, with consequent haemorrhage and release of immune cells and pro-inflammatory molecules to the spinal cord. This follows what is observed in mammals. However, and in contrast to the SCI response in mammals, apoptotic cell death and macrophage infiltration reach a peak earlier, at 1 day and 2-3 days after injury, respectively, decreasing afterwards. Furthermore, the formation of a glial scar is not observed in zebrafish (Ghosh and Hui, 2018; Hui *et al.*, 2010).

Much is still unknown regarding zebrafish spinal cord regeneration. However, several studies have demonstrated that recovery of function correlates not only with an efficient axonal regrowth but also with the generation of new motor neurons, originated from ependymo-radial glial cells. This

indicates a permissiveness of the environment of the adult zebrafish spinal cord for axonal regeneration and a plasticity in terms of cell differentiation and network integration (Becker and Becker, 2008; Becker and Becker, 2014; Hui *et al.*, 2010; Reimer *et al.*, 2008).

Despite these findings, not many studies focus on the vascular recovery during spinal cord regeneration in zebrafish, even though vascular integrity is essential in the maintenance of homeostasis and its disruption contributes to the spread of the secondary injury in mammals, as previously mentioned. Information regarding the recovery of the vasculature after SCI could be essential in establishing new players and/or mechanisms that, together with other biological or pharmacological strategies, could be applied to efficiently restore the malfunctioning vasculature in mammal SCIs (Oudega, 2012)

1.3 Blood vessel formation

The two main processes from which new blood vessels arise are called vasculogenesis and angiogenesis (**Figure 1.8**). Vasculogenesis mainly occurs during development and is defined as a process where epithelial precursor cells, also known as angioblasts, differentiate and join to form a primitive vascular network (*de novo* formation). Angiogenesis is the development of new blood vessels from pre-existing ones and can be divided in sprouting angiogenesis with proliferation of ECs, and in intussusceptive angiogenesis, where a split in pre-existing blood vessels occurs (Kolte *et al.*, 2015).

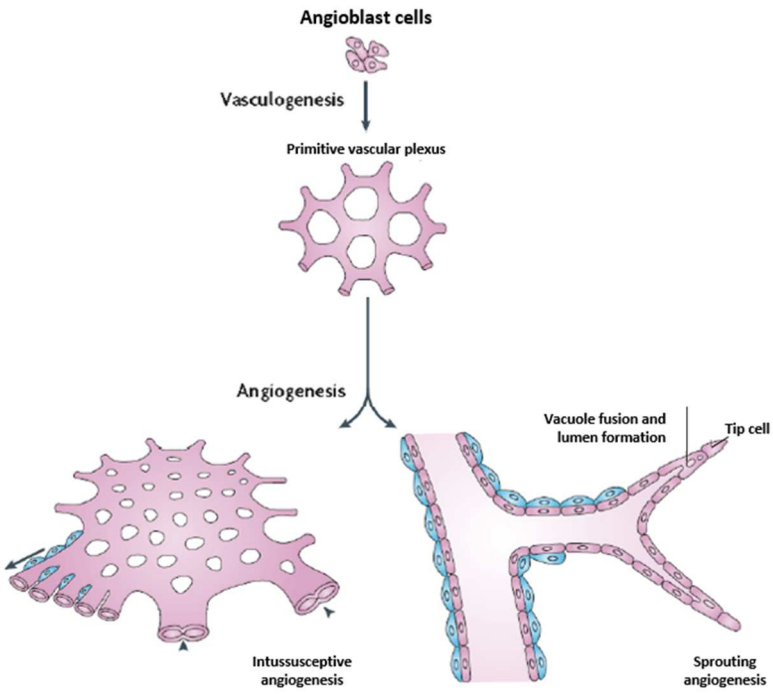

Figure 1.8 – Mechanisms of blood vessel formation. During development, blood vessels are formed by vasculogenesis, through the differentiation of angioblasts. The vascular network is then extended by angiogenesis, which can occur by EC proliferation – sprouting angiogenesis; and by the split of pre-existing vessels – intussusceptive angiogenesis. (Adapted from Ten Dijke and Arthur, 2007)

1.3.1 Sprouting angiogenesis

Sprouting angiogenesis occurs both during development and in adulthood, in normal and pathological conditions. This process was first described in 1977, by Ausprunk and Folkman, during tumour growth. It can be divided in: **(i)** degradation of the basement membrane, mediated by matrix

metalloproteinases; (**ii**) ECs proliferation and migration into the connective tissue, with specialization into tip and stalk cells; (**iii**) contact of ECs and cord formation; (**iv**) lumen formation and (**v**) establishment of anastomosis to establish functional capillary loops, with synthesis of new basement membrane and recruitment of pericytes. (Kolte *et al.*, 2015; Ribatti and Crivellato, 2012).

1.3.1.1 Main cellular and molecular players

The angiogenic process is regulated by pro- and anti-angiogenic factors that exist in a dynamic balance, in physiological conditions. ECs can remain quiescent for years. However, in response to tissue damage or oxygen and nutrient deprivation, the molecular angiogenic balance is disturbed and angiogenic sprouting is initiated. This process requires ECs to take different roles and morphologies, giving rise to tip cells, which primarily migrate, and stalk cells, that mainly proliferate. Tip cells extend numerous filopodia and respond to angiogenic stimuli, guiding the new branch vessel. Stalk cells are responsible for the formation of tubes, branches and of the nascent vascular lumen. After the formation of new blood vessels, tip cells adopt a lumenized, immobile phenotype that promotes vessel integrity and stabilization, not responding to angiogenic clues. (Kolte *et al.*, 2015; Ribatti and Crivellato, 2012)

The main regulator of the angiogenic process is the vascular endothelial growth factor (VEGF) pathway (**Figure 1.9**). Tip cell migration is driven by a gradient of VEGF, drifting away from the parent blood vessel, while stalk cells proliferate and lumenize as a response to VEGF concentration. Tip cells filopodia express VEGF receptor 2 (VEGFR-2, also known as KDR or FLK1), a tyrosine kinase receptor that positively responds to VEFG and activates a angiogenic cascade. VEGFR-1 (also known as FLT1), can have a membranar (mFLT1) or soluble form (sFLT1) and is mainly expressed in stalk cells. It is involved in guidance of tip cells, preventing their outward migration through the reduction of VEGF availability, and limiting tip cell formation, therefore having an anti-angiogenic effect. Interference with these receptors can result in angiogenic defects, such as increase of sprouting and vascularization in case of loss of VEGFR-1 and defects of sprouting in cases of blockade of VEFGR-2. The opposite effects are seen in case of increase of each receptor (Chappel and Bautch, 2010; Chappel *et al.*, 2012; Matsuoka *et al.*, 2016; Ribatti and Crivellato, 2012).

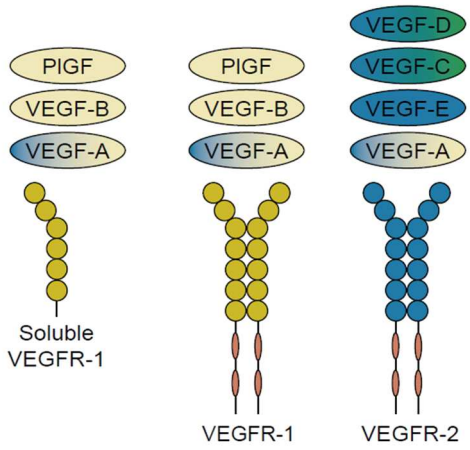

Figure 1.9 – VEGF receptors expressed by endothelial cells and VEGF specificity. Differents types of VEGFs, including placenta growth factor (PIGF) bind in a specific manner to different VEGFR, having distinct downstream effects. (Adapted from Cross *et al*, 2003)

Other pathways also have an important contribute to the angiogenic process, such as the Notch pathway, and other factors, like the fibroblast growth factor (FGF), angiopoetin (Ang), platelet-derived

growth factor (PDGF)-β and transforming growth factor (TGF) work together with VEGFs and regulate vessel proliferation, migration and maturation (Chappel and Bautch, 2010; Chappel *et al.*, 2012; Kolte *et al.*, 2015; Ribatti and Crivellato, 2012; Ten Dijke and Arthur, 2007).

1.3.1.2 Angiogenesis during spinal cord injury

As previously mentioned, after SCI in mammals, an attempt at vascular repair occurs. However, no blood vessels are formed at the injury site and, in areas adjacent to the injury, the newly formed blood vessels are not functional, allowing the leakage of their contents to the spinal cord tissue, further damaging it. The use of different strategies to promote the revascularization of the spinal cord after injury, like the use of biomaterials coupled with pro-angiogenic molecules (Haggerty et al., 2018; Rao et al., 2018), the delivery of pro-angiogenic factors to the injury site (Yu et al., 2016) or use of microRNAs (Hu et al., 2015), have resulted in an improvement of motor function, pointing to the importance of tissue revascularization for spinal cord regeneration.

In zebrafish, the recovery of the vasculature seems to follow the regenerative process of the spinal cord. Previous work done in our lab (**Figure 1.10**), using the zebrafish compression model, showed that, since injury and until 15 days post injury (dpi), there is an increase of blood vessels at the injury site, followed by a decrease in number and a vascular reorganization seen at 30 and 60 dpi. It is worth to note that these images represent just a portion of the spinal cord vasculature (160 μm), due to restraints from the method of image acquisition used. Additionally, blood flow, through cardiac injection of a fluorescence compound at 7 dpi, was observed, indicating that, at this timepoint, the BSCB is reestablished. A functional swimming assay, done 1 day before injury and until 15 dpi, confirms an improvement of swimming ability after injury. These results could potentially indicate a correlation between the repair of the vasculature and the recovery of motor function that occurs during the regenerative process of the spinal cord (Maçarico, 2014).

In summary, while SCI in mammals results in the absence of new blood vessels at the injury site, the disruption of the BSCB in peripheral blood vessels and, ultimately, in the absence of regeneration and in impaired motor function, in zebrafish, the revascularization of the injury site, with blood flow being observed at 7 dpi, occurs along with the regeneration of the spinal cord and the regain of motor function. By studying the regenerative response that occurs in zebrafish and understanding the events and mechanisms behind it, new ways to attenuate or even solve the consequences of SCI in mammals could be developed.

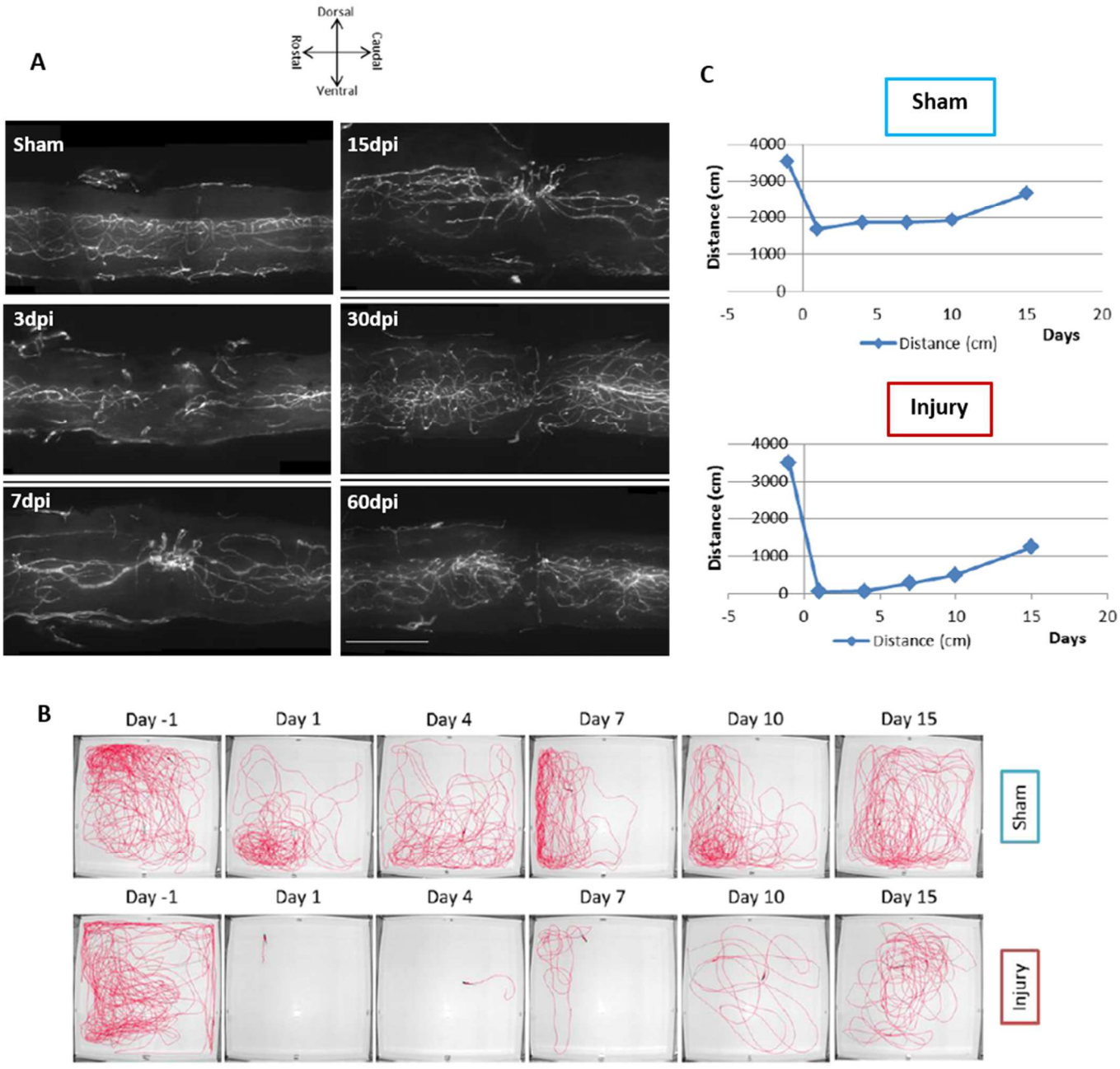

Figure 1.10 – **Vascular and functional recovery after spinal cord injury. (A)** Spinal cord vasculature was observed at different time points, (3, 7, 15, 30 and 60 dpi). Until 15dpi, an increase of blood vessels at the injury site is observes. At 30 and 60 dpi, a reorganization of the vessels at the injury site is seen. (**B** and **C**) Funtional swimming assays in injured fish were performed. At 15 dpi, injured fish were able to recover some their swimming ability. (Adapted from Maçarico, 2014)

1.4 Aims of the study

In this study, we took advantage of light sheet fluorescence microscopy to revisit the dynamics of the vasculature recovery after SCI to allow the observation of the full vasculature at the injury area, as previous work was only able to obtain portions of the target vasculature.

As previously mentioned, the vascular response of mammals, like humans, rat and mouse, and that of zebrafish to a SCI is quite distinct, with zebrafish being able to form new blood vessels at the injury site, in contrast to what happens in mammals. In addition, in mammals, blood vessels from areas adjacent to the injury become malfunctional, leaking blood to the spinal cord tissue. In zebrafish, although previous work from our lab showed that, at least at 7 dpi, the BSCB is reestablished, it was not known at what time after injury did the newly formed blood vessels regain their function. Therefore, in this work, the blood vessels of the previously mentioned spinal cords were observed in order to pinpoint the period of reestablishment of the BSCB. This was possible through the cardiac injection of a fluorescent compound, before spinal cord extraction, at defined timepoints.

Furthermore, since the recovery of the vasculature may be important to the regenerative process, in this work we also proposed to study the effects of the inhibition of the angiogenic process after SCI, regarding the vasculature at the injured area and motor function recovery. Previous work from our lab tried to inhibit angiogenesis using pharmacological inhibitors, with different routes of administration, without success. In this work, a transgenic zebrafish line with temperature inducible expression of *sflt1* was used in order to achieve this objective. Cardiac injection of a fluorescent compound was also done to observe the integrity of the BSCB.

Chapter 2. Methods & Materials

2.1 Animal Model

2.1.1 Zebrafish Husbandry

Adult zebrafish (*Danio rerio*) were kept in standard Tecniplast rack systems and were maintained at 28ºC, in standard pH and conductivity conditions (Westerfield, 2000). During the week, adult zebrafish were fed two meals of only dry food (SPAROS, Portugal) or dry food and a live feed, decapsulated *Artemia* (ZM Systems), when available. On the weekends and holidays, only a single dry food meal was given.

The surgical procedures involving adult zebrafish were done or supervised by users licenced by the Direcção Geral de Alimentação e Veterinária (DGAV). All the experiments involving animals were approved by the Animal User and Ethical Committees at Instituto de Medicina Molecular – João Lobo Antunes, in accordance with directives from DGAV (PORT 1005/92).

Fish with SCI were kept in individual 1L breeding tanks (external tank and internal tank with perforated bottom) (Tecniplast), in baths at 28ºC or at heat-shock temperature, in 1x Embryo Medium (reverse osmosis water with 5 mM NaCl; 0,17 mM KCl; 0,33 mM $CaCl_2 \cdot 2H_2O$; 0,33 mM $MgSO_4 \cdot 7H_2O$), and were only fed once a day, with decapsulated *Artemia,* after the second day of injury. The temperature of the bath was continuously monitored to avoid increase or decrease of set temperature. To avoid ammonia peaks and development of fungi or wound infections, the Embryo Medium and external tanks were changed daily.

For breeding, male and female zebrafish were placed in 1L breeding tanks before the end of the day, with divider. In the next morning, the divider was removed to initiate mating. Sometime later, embryos were collected and rinsed, first with reverse osmosis water and afterwards with 1x Embryo Medium with Methylene Blue (0.97 µM) (Sigma Aldrich) and were placed in petri dishes with 1x Embryo Medium with Methylene Blue. Embryos were then placed in the incubator at 28ºC until the start of procedures. Embryonic stages were confirmed according to Kimmel *et al*., 1995.

2.1.2 Zebrafish lines

In this study, the following zebrafish lines were used: Wildtype AB strain established in the fish facility at iMM-JLA, Tg(kdrl:EGFP)^{s843} (Jin *et al*., 2005) and Tg(kdrl:EGFP)^{s843}(hsp70l:sflt1; cryaa:cerulean)^{bns80} (Matsuoka *et al*., 2016). Wildtype AB zebrafish were only used as breeders with the other two lines, to obtain embryos or to start and establish new generations of adult zebrafish in the facility. Both transgenic zebrafish lines had expression of enhanced green fluorescence protein (EGFP) driven by the *kdrl* promotor, labelling blood vessels. The Tg(kdrl:EGFP) (hsp70l:sflt1; cryaa:cerulean) line hadan additional genetic construct where the expression of *sflt1* was activated upon a significant

increase of temperature, also known as heat-shock treatment. This construct also contained genetic information for a cyan fluorescent protein (CFP), cerulean, whose expression was driven by the *cryaa* promotor, labelling the eye lens.

2.2 Spinal cord injury

Adult zebrafish (5 - 9 months-old) were anesthetised by immersion in 0,016% (w/v) Tricaine-S solution. The fish were placed, left side up, on a moulding clay support covered with chromatography paper (GE Healthcare), on top of a cooling pad, as shown in **Figure 2.1**.

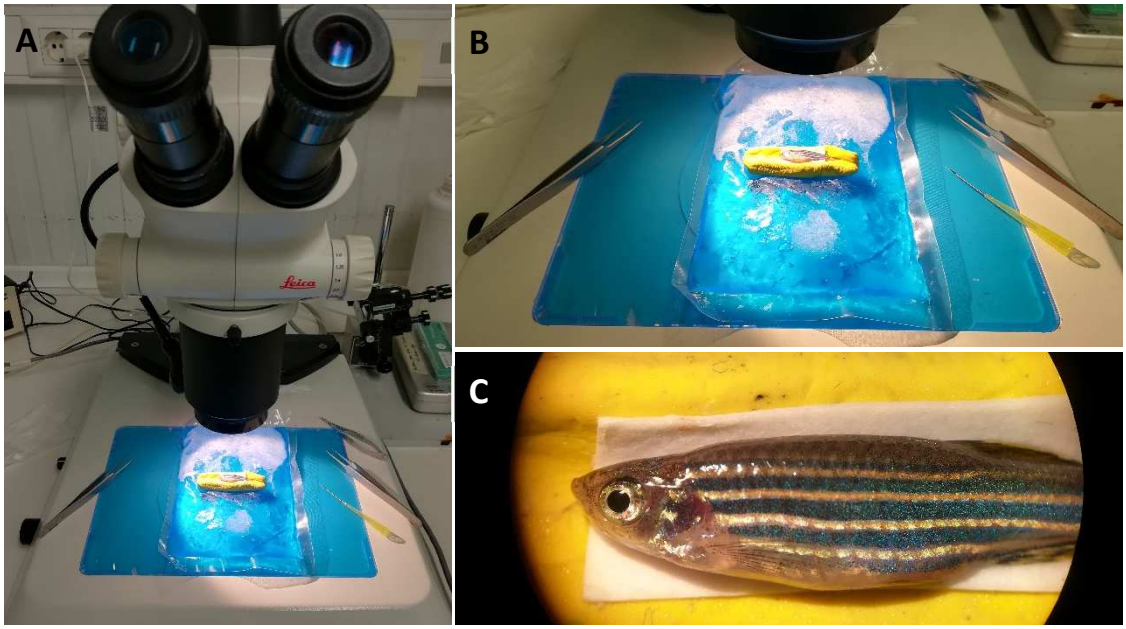

Figure 2.1 – SCI material and set-up. **(A)** Full working set up, **(B)** zoomed view and **(C)** surgery working view.

After removal of the scales, a longitudinal incision, parallel to the first light dorsal stripe, was made halfway between the base of the skull and the dorsal fin using surgical scissors (Vannas-Tübingen Spring Scissors - Straight, FST). The vertebral column and the spinal cord were exposed, and the spinal cord was compressed dorsoventrally using forceps (Dumont #55, FST) **(Figure 2.2**). After gently removing the forceps and bringing together the limits of the incision, the wound was sealed with Vetbond (3M) and the fish were allowed to recover in individual tanks. Sham injury fish were obtained following the same procedure without the compression of the spinal cord. (Fang *et al*., 2012) All surgical material was sterilized with 75% ethanol between procedures.

If at any point before the end of the experiment the injured fish showed abnormal behaviour or signs of decay after the injury procedure, the fish were euthanized using a lethal dose (>1500 mg/L) of Tricaine-S solution (MS222, Western Chemical Inc.).

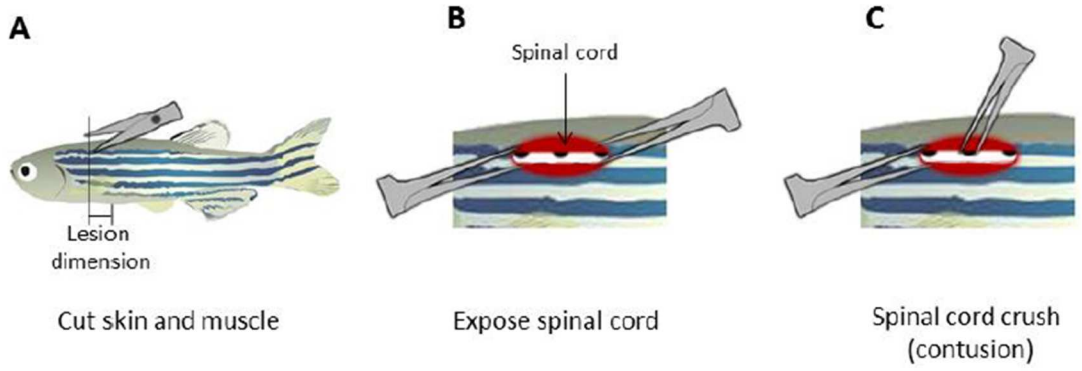

Figure 2.2 – Spinal cord injury procedure. (**A**) After scale removal, a clean longitudinal incision was done, (**B**) the spinal cord was gently exposed using forceps and (**C**) compressed dorsoventrally. (Adapted from Fang *et al*.,2012).

2.3 Inhibition of angiogenesis - Heat-shock Protocols

2.3.1 Heat-shock protocols in larvae for imaging

To confirm promoter activation of the hsp70l:sflt1 transgenic line after heat-shock and to assess the inhibitory effect of *sflt1* overexpression on angiogenesis, the development of the intersomitic vessels (ISVs) was followed.

Embryos at 17-somite stage, before the development of these vessels (Isogai *et al*., 2003), were subjected to 1 hour (h) heat-shock, in pre-warmed embryo medium, at 37ºC (Matsuoka *et al.*, 2016) and were observed at, approximately, 36 hours post fertilization (hpf).

Heat-shock at 34ºC was also done, with several periods of heat-shock: 30 minutes, 1h, 1h30, 2h, 4h, 6h, 8h, 10h,16h, 18h and 1 day. Heat-shock was induced at 17-somite stage and, once again, the embryos were observed at approximately 36hpf.

In addition, the development of the vasculature at standard temperature (28ºC) was likewise monitored at 36 hpf.

2.3.2 Heat-shock protocols in adults for imaging

Several heat-shock protocols for adult zebrafish were tested. Heat-shock protocols at 37ºC had a duration of 2h, twice a day, until 7 dpi with the difference between them being the day of the beginning of the protocol.

The following protocols were tested: heat-shock right after injury – **HS 37ºC (0 - 7) dpi**; heat-shock beginning at 3 dpi – **HS 37ºC (3 - 7) dpi**; heat-shock beginning at 4 dpi – **HS 37ºC (4 - 7) dpi**; and heat-shock beginning at 5 dpi, with an extra day of heat-shock before injury – **HS 37ºC (-1, 5 - 7) dpi**. In addition to these, an extended heat-shock protocol was tested, beginning at 4 dpi and ending at 14 dpi – **HS 37ºC (4 - 14) dpi**.

At 34ºC, the following protocols were tested: 6h heat-shock, twice a day, starting at 2 dpi – **HS 34ºC 6h (2 - 7) dpi**; and continuously at 34ºC, beginning at 2 dpi – **HS 34ºC cont. (2 - 7) dpi**. An extended version of the continuous protocol was also tested, starting at 2 dpi and ending at 14 dpi – **HS 34ºC cont. (2 - 14) dpi**.

2.4 Rhodamine Injection

Injured adult zebrafish were anesthetised by immersion in 0,016% (w/v) Tricaine-S solution. The fish were placed, ventral side up, in a foam support and the heart was exposed using forceps and surgical scissors (**Figure 2.3 A**). Tetramethylrhodamine dextran 10 kDa (3µg/µl), (ThermoFisher Scientific, D1824), here referred to as rhodamine, was injected directly in the heart using needles made from borosilicate capillaries (World Precision Instruments, Inc.) and inserted into an aspirator tube (Sigma, A5177). The procedure was done in an Olympus MVX10 microscope and the injection was followed using fluorescence. The injection was then confirmed by inspecting the presence of rhodamine inside the caudal fin blood vessels (**Figure 2.3 B**).

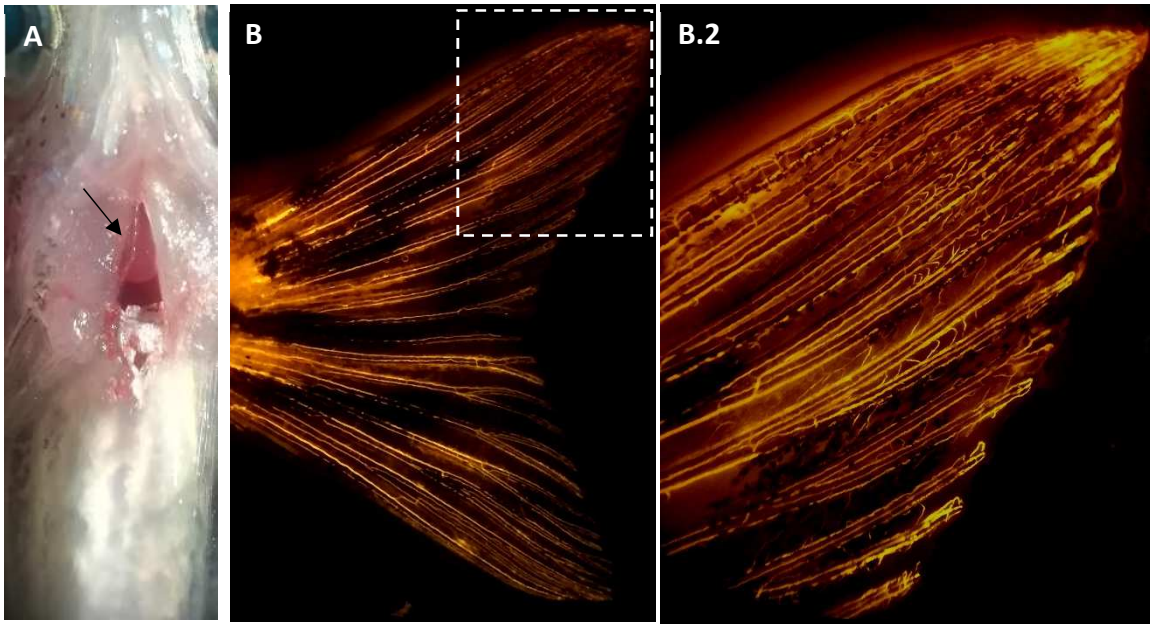

Figure 2.3 – **Rhodamine Injection Procedure**. (**A**) After anaesthesia, the fish's heart was exposed (arrow) and rhodamine was injected directly into the blood stream. (**B**) The injection's success was confirmed by the presence of rhodamine inside the caudal tail blood vessels. **B.1** is a close up of the selected area of image **B.**

2.5 Spinal cord extraction

The anesthetised fish were euthanized through decapitation using a scalpel blade and the vertebral column was dissected in cold 1x Phosphate Buffer Saline (1x PBS) (1.37mM NaCl, 0.27mM KCl, 1mM $Na_2HPO_4 \cdot 7H_2O$, 0,2mM KH_2PO_4). The samples were fixed using 4% paraformaldehyde (PFA) at 4ºC overnight. After fixation, the spinal cord was isolated from the vertebrae.

2.6 Immunohistochemistry

Two immunohistochemistry protocols for whole spinal cord were tested, with the main difference between them being the composition of the blocking solution. In both protocols, the primary and secondary antibodies used were the same: anti-GFP rabbit primary antibody (ThermoFisher Scientific, A6455) and anti-rabbit Alexa 488 goat secondary antibody (ThermoFisher Scientific, A-11034).

In the first protocol, spinal cords were incubated in Blocking Goat Serum (BGS) solution (1x PBS; 10% Goat Serum; 0,1% Triton X-100) for 2 days at 4ºC and then incubated with anti-GFP primary antibody solution (BGS with 2µl/ml of primary antibody) for another 2 days. The samples were twice washed in PBST (1x PBS; 0,1%(v/v) Triton X-100) and left in the roller during the day, and then incubated with secondary antibody solution (BGS with 1µl/ml of secondary antibody) for 2 days. Finally, the samples were twice washed in PBST.

For the second protocol, spinal cords were incubated in a different blocking solution (1x PBS; 1%(w/v) Bovine Serum Albumin (BSA); 1%(v/v) Dimethyl sulfoxide (DMSO); 0,05%(v/v) Triton X-100) for 2 days at 4ºC and then incubated with anti-GFP primary antibody solution (1x PBS; 1%(w/v) BSA; 0,1%(v/v) Triton X-100; 2µl/ml primary antibody) for another 2 days. The samples were twice washed in PBST (1x PBS; 0,1%(v/v) Triton X-100) and left in the roller during the day, and then incubated with secondary antibody solution (1x PBS; 1%(v/v) BSA; 0,1%(v/v) Triton X-100; 1µl/ml secondary antibody) for 2 days. Finally, the samples were twice washed in PBST.

2.7 Whole spinal cord clearing

The clearing protocol was adapted from the Sca*l*e protocol from Hama *et al*.,2015. Whole spinal cords were subjected to a clearing protocol before light sheet fluorescence microscopy acquisition. Samples were placed in Scale A2 (4M urea; 10%(w/v) glycerol; 0,1%(v/v) Triton X-100) for 3 days, at 4ºC. The samples were then incubated in Scale B4 (8M urea; 0,1%(v/v) Triton X-100) at 37ºC for 1 day and, afterwards, switched back to Scale A2 for a minimum of 3 days. At least a day before acquisition, the samples were incubated in Scale S4 (4M urea; 40%(w/v) Sorbitol; 10%(w/v) glycerol; 0,2%(v/v) Triton X-100; 15%(v/v) DMSO).

2.8 Motor Function Recovery Assay

A blind study of swimming ability and motor function recovery of heat-shocked, injured and sham-injury, fish was performed using a tracking protocol. Zebrafish from Tg(kdrl:EGFP) and Tg(kdrl:EGFP)(hsp70l:sflt1; cryaa:cerulean) transgenic lines were assigned a number and analysed one day before injury (-1 day), to take into account the swimming variability of each fish, and 1 day after

injury (1 dpi). From 2 dpi, the fish were subjected to a continuous heat-shock at 34ºC and their swimming ability was again analysed at 7 dpi, 14 dpi and 21 dpi. For each measurement, zebrafish were individually placed in a 35cm x 35cm tank filled with system water, illuminated from below. The trials were recorded using a camera placed above the tank and the tracking was done using Ethovision software (Noldus, Wageningen, The Netherlands). Each fish was allowed to freely explore the tank for 15 minutes – Open Field Test (Stewart *et al.*, 2012)- of which 5 minutes were done so the animal could acclimatise to the tank and the final 10 minutes to record the fish's movement. After each trial, the water of the tank was changed to avoid exposure of the next fish to stress hormones from previous ones. Different people were responsible for the injury and tracking procedure to ensure that the person recording the fish did not know their genotype. After the end of the experiment, the results of injured zebrafish were divided into the corresponding groups and their swimming distance for each fish per timepoint was analysed using Prism software (GraphPad Software). Swimming distances from both lines, for each tracking timepoint, were statistically compared using a two-way ANOVA multiple comparisons test (alpha of 0.05, with 36 degree of freedom (df)), with a Sidak test for multiple comparison corrections.

2.9 Image Acquisition & Analysis

Transmitted light and fluorescence images from adult zebrafish and from control and heat-shocked embryos were acquired either using a Zeiss AxioZoom V16 microscope (Carl Zeiss MicroImaging) with a PlanNeoFluar Z 1x objective, with GFP (excitation: 450 – 490 nm, emission: 500 – 550 nm) and RFP (Red Fluorescent Protein; excitation: 559 – 585 nm, emission: 600 – 690 nm) filter sets, or an Olympus MVX10 microscope (Olympus) with an Olympus MVPlapo 1x objective, and with GFP (excitation: 460 – 480 nm, emission: 495 – 540 nm), RFP (excitation: 535 – 555 nm, emission: 570 – 625 nm) and CFP (excitation: 425 – 445 nm, emission: 460 – 510 nm) filter sets. Both microscopes were equipped with monochromatic AxioCam MRm cameras (Carl Zeiss MicroImaging). The software used was ZEN 2012 Blue Edition (Carl Zeiss MicroImaging).

Before acquisition, spinal cord samples were observed to ensure sample integrity and level of transparency. Fluorescence images were, afterward, acquired with light sheet fluorescence microscopy (Weber *et al.*, 2014), using a Zeiss Lightsheet Z1 (Carl Zeiss MicroImaging) (**Figure 2.4**). Cleared spinal cords were put, caudal side first, inside size 1 capillaries (Carl Zeiss MicroImaging) and the capillaries placed in the appropriate metal support. When inside the scale S4 (refraction index = 1,44) filled chamber, the areas to acquire, injury site and caudal area, were exposed outside the capillary. The software used for sample positioning, definition of acquisition parameters and image acquisition was ZEN 2012 Black Edition (Carl Zeiss MicroImaging). A secondary camera was used to position the samples in front of the 20x Clr Plan-Neofluar clearing objective. The GFP expressed in blood vessels

and the injected rhodamine were excited with 488nm and 561nm wavelength laser units, respectively. Emitted light was directed to GFP (emission: 505 – 545 nm) or Cy3 (emission: 575 – 615nm) filter sets to reduce unspecific signal, before reaching the primary camera. With this method, thin optical slices were made using double-sided illumination, with left and right adjustable light sheets, and a z-stack of the complete target area of the cleared sample was obtained (Weber *et al*., 2014).

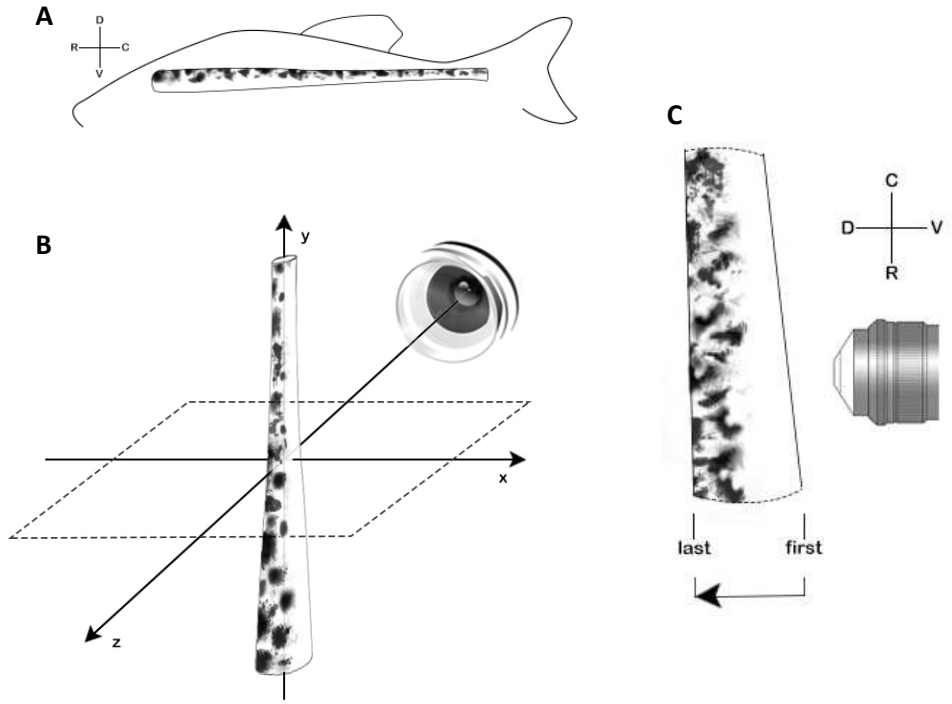

Figure 2.4 – **Light sheet microscopy acquisition**. Representation of (**A**) natural position of the spinal cord and body axis; (**B**) spinal cord placement for light sheet acquisition and coordinates (**x,y,z**), and (**C**) direction of z-stack acquisition and corresponding body axis according to the spinal cord placement; **D –** dorsal, **V –** ventral, **R –** rostral, **C –** caudal.

Preliminary images from spinal cord sample obtained in the motor functional recovery assay were preliminarily acquired using confocal laser point-scanning microscopy with a Zeiss LSM 880 (Carl Zeiss MicroImaging) equipped with a 25x LCI Plan-Neofluar objective, Argon (488 nm), DPSS 561-20 (561nm) laser units and Green (excitation : 450 nm – 490 nm; emission: 500 nm – 550 nm) and Red (excitation: 533 nm – 558 nm; emission: 570 nm – 640 nm) filter sets.

Maximum intensity orthogonal projections of the acquired z-stack images were done using ZEN 2012 Blue Edition and stitching of the tiles was done manually using Photoshop (Adobe).

Image analysis for heat-shock samples was done using a custom macro for FIJI software (Schindelin *et al*., 2012), written by Anna Pezzarossa from Edgar Gomes Lab, at iMM-JLA Lisbon. It required a .czi file of the acquired spinal cord z-stack as input and, when running, selection of regions of interest (ROI) to analyse. The following parameters were analysed: branch length and tortuosity (branch length/ euclidian distance).

Maximum intensity orthogonal projections of samples from the study of the reestablishment of the BSCB were analysed using FIJI and then Prism software (GraphPad Software). For each channel of a sample, a threshold was manually set to obtain the area percentage of the respective signal. Both channels areas were then compared, and a ratio was obtained. These values were then compared within timepoint, to calculate the mean and standard deviation, and statistically compared, between timepoints, using an unpaired T-test with a correction for multiple comparisons using the Holm-Sydak method to measure statistical significance, with a p value of < 0.05 and with 6 degrees of freedom (df) for comparisons between 1dpi and 3 dpi samples and 8df for the other compared samples.

Chapter 3.Results

3.1 Reestablishment of the Brain - Spinal Cord Barrier

Work done previously in our lab showed that new blood vessels are formed at the injury site during spinal cord regeneration in zebrafish. However, it was important to obtain information regarding their functionality as this could be one of the main differences between zebrafish and mammals, whose remaining blood vessels are not functional, further damaging the spinal cord tissue.

In order to observe the reestablishment of the BSCB, Tg (kdrl:EGFP) zebrafish at 1, 3, 5, 7, 14 and 30 dpi were subjected to cardiac injection of rhodamine. If these new blood vessels were functional, rhodamine would be retained due to the reestablishment of the BSCB. If not, rhodamine would be leaked to the surrounding tissue. Sham injuries were also done to ensure that the surgical procedure of exposing the spinal cord did not influence the overall vasculature. Spinal cord samples were isolated, fixed and subjected to a whole mount immunohistochemistry protocol, followed by a clearing protocol, in order to observe the vasculature and its overall recovery and gain of function through time, using light sheet microscopy.

3.1.1 Spinal cord vasculature after injury

For the 3, 5, 7 and 14 dpi timepoints, 5 samples were acquired (n = 5) (**Supplementary Figure 1-5**). Sham injury, 1 dpi (n = 3) and 30 dpi (n = 2) samples were also obtained. Representative images of all timepoints are shown in **Figure 3.1**. Sham injury showed the normal vasculature of the spinal cord in the absence of injury. At 1dpi, BSCB disruption was seen, with blood vessels being destroyed, and rhodamine leaking out to the spinal cord tissue. At 3 dpi, new blood vessels were already observed at the injury site. However, these did not contain rhodamine inside them, which was leaked to the spinal cord tissue. By contrast, blood vessels from areas adjacent to the injury were able to retain rhodamine. This indicated that the blood vessels at the injury site, contrary to what happened to those in adjacent areas, were not fully functional as they were not able to retain the injected compound. Two days later, at 5 dpi, an increase in the number of blood vessels at the injury site was observed, with some of them being now able to retain the injected compound. This indicated the gain of function of a portion of the blood vessels at the injury site. At 7 dpi, although a great number of blood vessels was still seen at the injury site, contrary to what happened after 3 dpi and 5 dpi, the majority of them were already able to retain rhodamine. This was again observed at 14 dpi. No obvious differences in terms vasculature and BCSB reestablishment were seen between 7 dpi and 14 dpi samples. At 30 dpi (**Figure 3.2**), only 2 samples were obtained. The samples were quite distinct, with sample **A** having thinner vessels at the injury site when compared with sample B. In both, however, the injury site was still visible, now with a decrease in the quantity of blood vessels at the injury site, when compared with previous timepoints. These blood vessels were able to maintain the injected compound inside them, being functional.

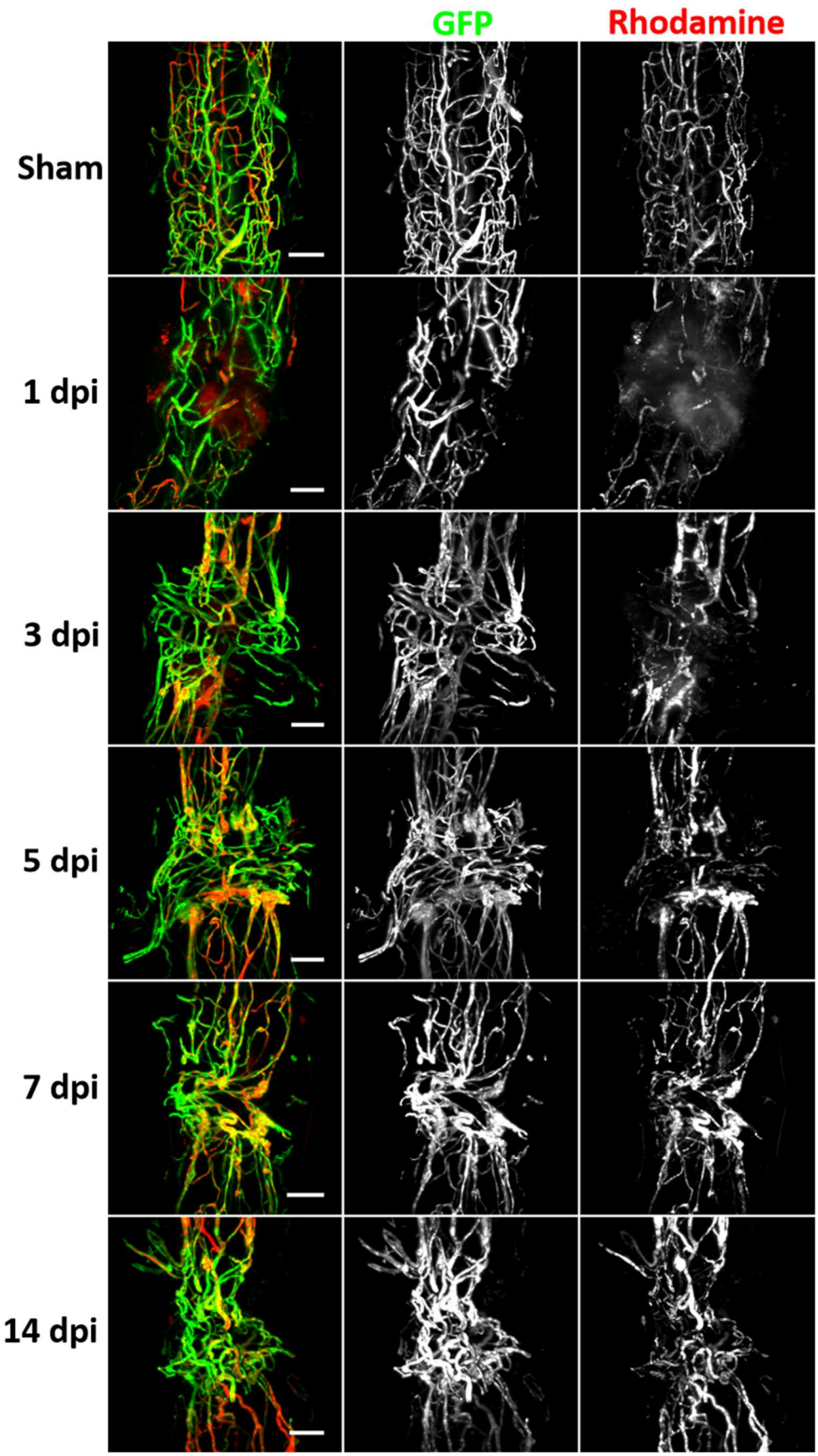

Figure 3.1 – Representative images of Sham and 1, 3, 5, 7 and 14 dpi of Tg (kdrl:EGFP) spinal cords. The images show an increase blood vessels (GFP) at the injury site, starting at 3dpi, and an increase in their functionality, at 5dpi, being able to retain rhodamine over time. **Scale bar : 100 µm**

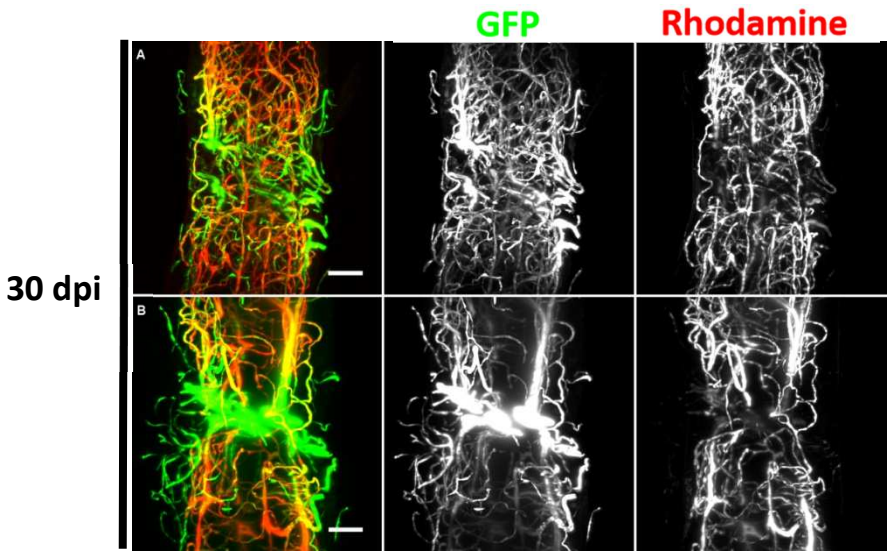

Figure 3.2 – Tg (kdrl:EGFP) 30 dpi samples. The injury site was still visible, now with less blood vessels (GFP). The vasculature was able to retain rhodamine. **Scale bar: 100 µm**

Throughout the analysed timepoints, a perceptible increase of rhodamine at the injury site occurs between 3 dpi and 7 dpi. This indicated that the major gain of function of the new blood vessels and, consequently, the reestablishment of the BSCB happened between these timepoints.

3.1.2 Quantification of the Reestablishment of the BSCB

Although a perceptible difference in the presence of rhodamine inside the newly formed blood vessels is seen, throughout the timepoints, it was important to quantify these results and confirm their significance. For this, a simple analysis of the orthogonal projection for Sham injury and 1, 3, 5, 7 and 14 dpi samples was done, firstly using Fiji and then Prism software. A threshold was defined for both channels of each sample and the area of the positive pixels measured, obtaining the percentage (%) of the positive area for each channel. It is important to note that blood vessels in injured areas are much brighter than those in adjacent areas, independently of the immunohistochemistry protocol used (although spinal cords subjected to the second protocol presented a more uniform GFP signal than those subjected to the fist protocol (images not shown)). Therefore, the threshold was manually set as to include fainter blood vessels, without losing definition of brighter ones. Samples were then analysed for the amount of rhodamine and GFP in the samples (ratio %red / %green), and the results (mean ± standard deviation) were plotted (**Figure 3.3**). Sham injuries, as the vasculature was not affected, had an almost perfectly matched % of rhodamine and GFP, having a ratio of 0.998 ± 0.0014. One day after injury, a ratio of 0.214 ± 0.038 was observed (although setting the threshold in these samples was more difficult due to the existence of leaked rhodamine in the tissues). At 3 dpi, a ratio of 0.342 ± 0.094, was obtained; over time, this ratio increased, being 0.496 ± 0.066 at 5 dpi and 0,706 ± 0.039 at 7 dpi. At 14 dpi, the ratio changed only slightly, being 0.738 ± 0.125.

The results for each timepoint were then compared, using an unpaired T-test statistical test with a correction for multiple comparisons using the Holm-Sydak method, with a p value of < 0.05, to measure statistically significance. Differences between 3 dpi and 5 dpi samples (P value = 0.016) and between 5 dpi and 7 dpi (P value = 0.0003) were found to be statistically significant but not those between 1 dpi and 3 dpi (P value = 0.076) and between 7 dpi and 14 dpi (P value = 0.614). This goes in accordance to what was previously mentioned and supports the idea that the BSCB reestablishment, with the timepoints tested, occurred mainly between 3 dpi and 7 dpi.

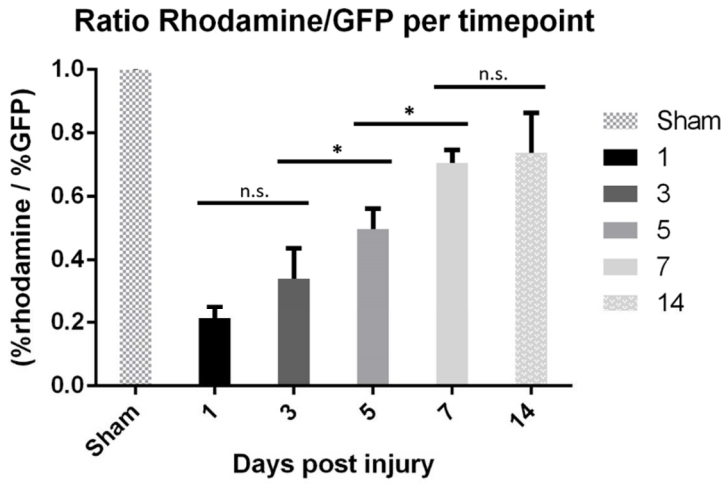

Figure 3.3 – Ratio rhodamine/GFP per timepoint. Mean ± standard deviation values regarding the ratio %rhodamine/%GFP, for Sham injury and days post injury timepoints, were calculated and plotted. ***** - Statistically significant; **n.s** – no significance

3.2 Inhibition of angiogenesis - Heat-shock treatment

In order to assess the importance of the angiogenic response observed during spinal cord regeneration, a genetic method was chosen to inhibit angiogenesis, as previous attempts with pharmacological methods were not successful. The transgenic Tg (kdrl:EGFP)(hsp70l:sflt1, cryaa:cerulean) zebrafish line was used, hereby abbreviated Tg (hsp70l:sflt1) (Matsuoka *et al*, 2016). This transgenic line has GFP labelled blood vessels due to the GFP driven expression by the *kdrl* promotor, which is a known receptor of the VEFG pathway and is present in ECs. This line also has a genetic construct that allows temperature inducible activation of the *hsp70l* promotor that drives the expression of *sflt1*. sFLT1 is the soluble form of a receptor also involved in VEGF signalling, and therefore in angiogenesis. However, and in contrast to KDRL, sFLT1 acts as a decoy receptor, controlling the availability of VEFG and restricting blood vessels formation. Due to this, this transgenic line can be used as a tool to inhibit the angiogenic process during regeneration.

3.2.1 Transgenic line tests – without Heat-shock

First, the ISVs development of Tg (hsp70l:sflt1) embryos was followed to ensure that, at normal temperature (28ºC), the *hps70l* promoter would not drive the expression of *sflt1* in the absence of heat-shock. Embryos were observed at approximately 36 hours post fertilization.

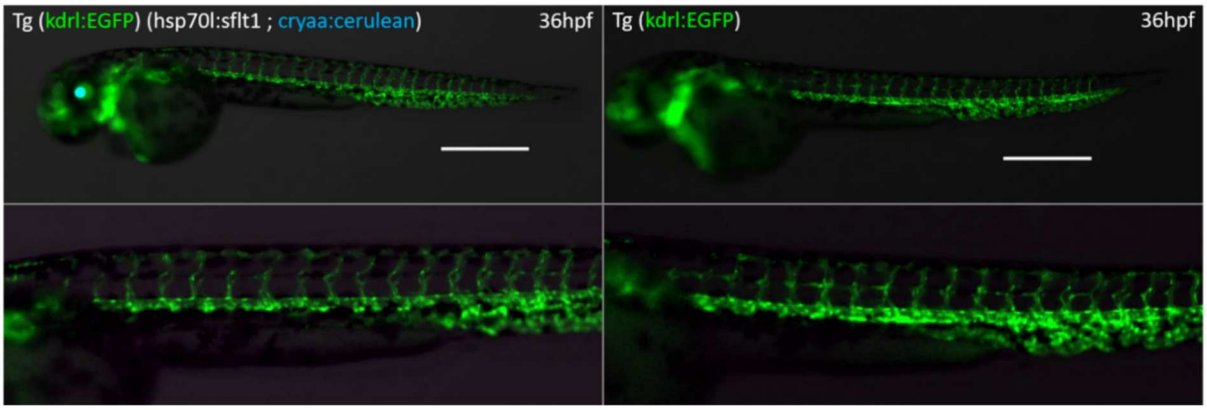

Figure 3.4 – Transgenic line tests without heat-shock. Embryos grown at 28ºC were observed at 36hpf. In the absence of heat-shock, Tg (hsp70l:sflt1) embryos developed normal ISVs, having the same vascular pattern as Tg (kdrl:GFP) siblings. **Scale bar: 500 µm**

Tg (hsp70l:sflt1) embryos showed the same vascular pattern as control Tg(kdrl:EGFP) siblings (**Figure 3.4**), demonstrating the normal development of the ISVs. This indicated that, at 28ºC, the *hsp70l* promoter was not activated, that is, *sflt1* overexpression was not induced.

Afterwards, and to guarantee that the repair and recovery of function of the vasculature of the spinal cord after injury followed what was observed with the Tg(kdrl:EGFP) line, the vasculature of injured Tg (hsp70l:sflt1) fish was analysed at 7 dpi and 14 dpi.

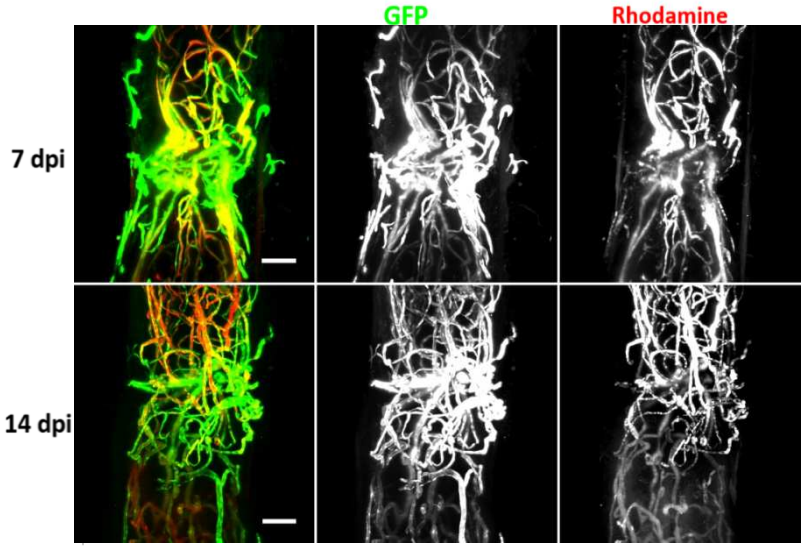

Figure 3.5 – Spinal cord injuries at 7 dpi and 14 dpi of Tg (hsp70l:sflt1). At both timepoints, many blood vessels are observed at the injury site. These blood vessels are able to retain rhodamine, being functional. **Scale bar: 100µm**

Representative images from 7 dpi (n = 4) and 14 dpi (n = 4) are shown in **Figure 3.5 (**all samples are shown in **Supplementary Figures 6 and 7)**. At 7dpi blood vessels were already seen at the injury site in Tg (hsp70l:sflt1) and most vessels retained the injected rhodamine, indicating that the vessels were functional. A week later, at 14 dpi many blood vessels were still observed at the injury site and, again, most retained the injected rhodamine.

This showed that, at 28ºC, no perceptible differences in the recovery of the vasculature at the injury site were seen, when compared to Tg (kdrl:EGFP) samples (**Figure 3.1**), as there were functional blood vessels at the injury site, at both timepoints and in both transgenic lines.

3.2.2 Heat-shock at 37ºC

Before beginning heat-shock experiments in injured adults, tests in embryos were performed using the protocol described in Matsuoka *at al.*, 2016. This was done to assess the ability of the Tg (hsp70l:sflt1) transgene to inhibit angiogenesis. Heat-shock was induced at 17-somite stage, before ISVs are formed, to observe their development in the presence of excess sFLT1. The 37ºC heat-shock protocol was then tested in Tg (hsp70l:sflt1) adult zebrafish with SCI. Tg (kdrl:EGFP) siblings were used as controls of the experiment.

3.2.2.1 37ºC Heat-shock tests in embryos

At this temperature, heat-shock was induced for 1 hour, at 17-somite stage. The experiment was done in three different trials, with multiple groups of embryos per trial. At approximately 36 hours post fertilization, Tg (hsp70l:sflt1) embryos did not develop ISVs, in contrast to control siblings (Figure **3.6**).

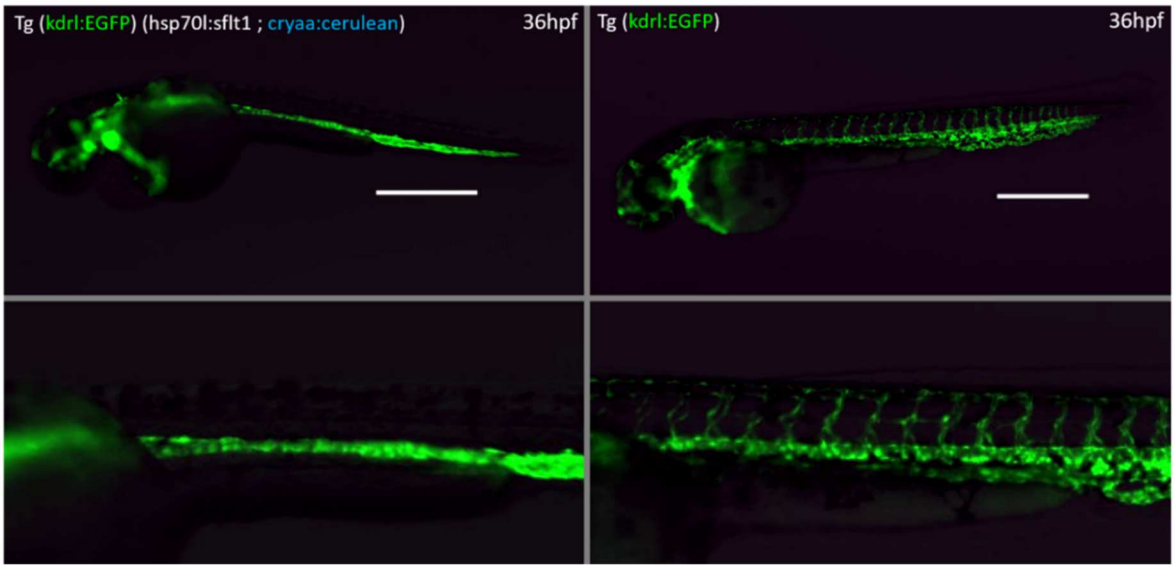

Figure 3.6 – Heat-shock at 37ºC in embryos. Heat-shock at 37ºC, for 1 hour, was induced in Tg (hsp70l:sflt1) and Tg (kdrl:EGFP) embryos. At 36 hpf, Tg (hsp70l:sflt1) embryos showed no ISV, in contrast to their Tg (kdrl:EGFP) siblings (number of trials = 3). **Scale bar: 500 µm**

This result confirmed that heat-shock at 37ºC was able to induce *sflt1* overexpression and inhibit ISVs development in embryos as previously described in the literature (Matsuoka et al., 2016).

3.2.2.2 37ºC Heat-shock in spinal cord injured adults

After observing the effect of the heat-shock induced overexpression of *sflt1* in embryos, heat-shock experiments in SCI zebrafish adults were performed. These experiments were done to determine if, after *sflt1* overexpression, there would be a decrease in the number blood vessels at the injury site. Additionally, the functionality of the blood vessels present at the injury site was tested through cardiac injection of rhodamine, as mentioned in **section 3.1**. The SCI heat-shock protocol at 37ºC was based on the protocol described in Azevedo *et al.*, 2011. At this temperature, several protocols were carried out. All were done at 37ºC, for 2 hours and twice a day, until 7 dpi, with the difference between them being the day of the beginning of the heat-shock protocol.

As it was important to initiate the heat-shock protocol before the increase in the number of the blood vessels at the injury site, the first protocol tested began right after injury - **HS 37ºC (0 - 7) dpi**. No survivors were obtained, with the fish dying after the first day of heat-shock, suggesting that immediately after injury fish are very sensitive to pronounced changes in water temperature.

A protocol beginning at 3 dpi was then tested - **HS 37ºC (3 - 7) dpi**. The 3 dpi timepoint was chosen as, in normal SCI procedures, fish that survive until this timepoint usually survive afterwards. However, in this heat-shock protocol too, no survivors were obtained, dying in the first or second day of heat-shock.

The next protocol used started later, at 5dpi, with an additional day of heat-shock before the injury procedure - **HS 37ºC (-1, 5 - 7) dpi**. Out of 41 Tg (hsp70l:sflt1) injured zebrafish, 6 reached 7dpi (15%) and only spinal cord samples from 4 survivors were obtained. With this protocol, most injured fish died even before the start of the heat-shock or right after the first heat-shock period. The four samples obtained all had blood vessels at the injury site although they were quite variable, in terms of quantity of blood vessels. The images shown in **Figure 3.7** represent opposing examples of the acquired samples. In both, knots of vessels were seen at the injury site (**Figure 3.7 arrow heads**). However, while in sample A there was no rhodamine inside the blood vessels present at the injury site (**Figure 3.7 A.2**), in sample B, these blood vessels were able to retain rhodamine (**Figure 3.7 B.2**).

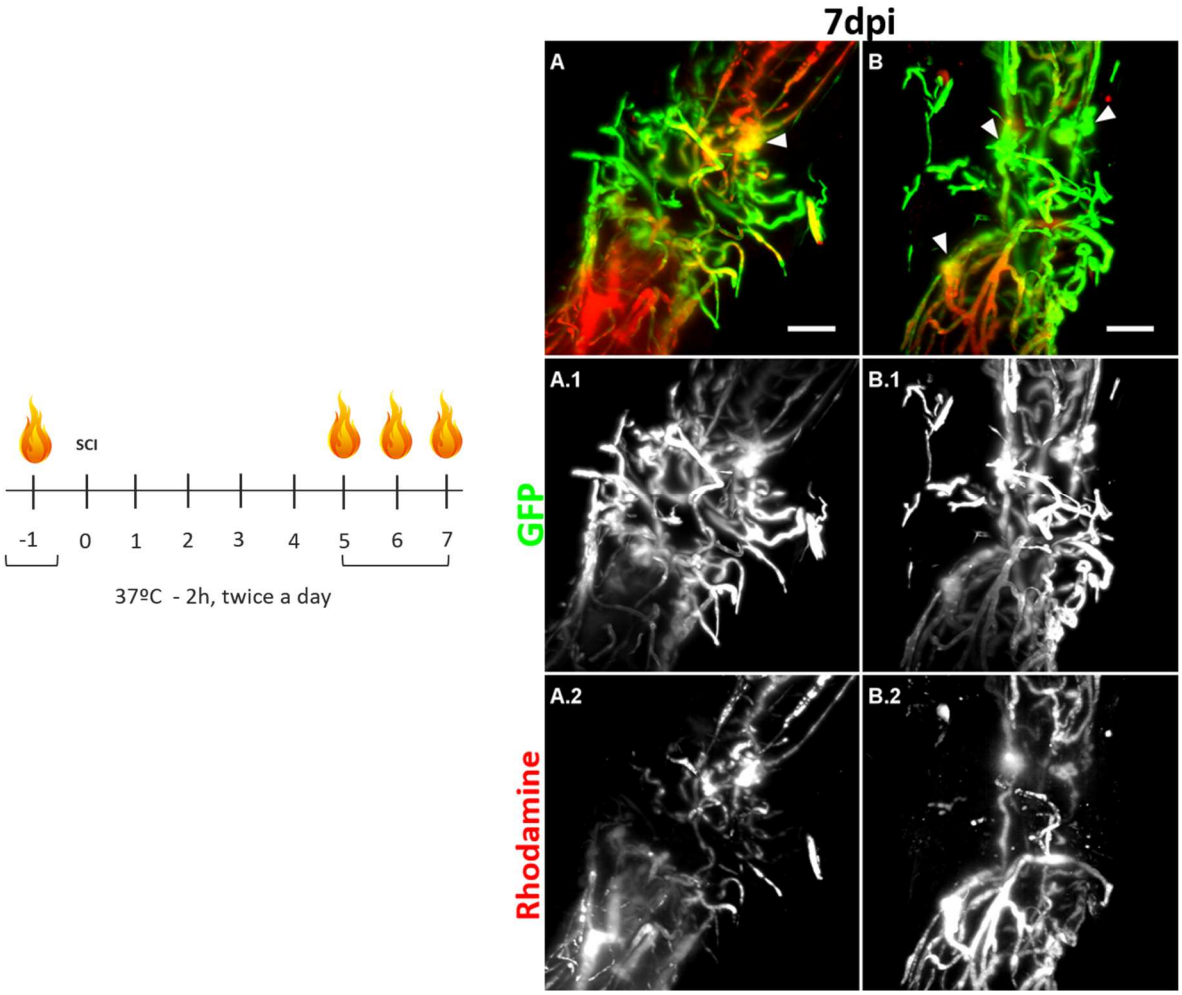

Figure 3.7 – Representation of the HS 37ºC (-1, 5 - 7) dpi protocol and representative Tg (hsp70l:sflt1) samples obtained. With this protocol, blood vessels were visible at the injury area (**A.1** and **A.2**). In some samples (**A.2**) rhodamine was not present in all blood vessels at the injury site, while in some (**B.2**) rhodamine is seen inside blood vessels at the injury site. Arrow heads indicate knots of blood vessels, observed in all samples. **Scale bar:** 100µm

As the heat-shock at the day before injury could be influencing the survival of the fish, a protocol without it and starting earlier, at 4dpi, was done - **HS 37ºC (4 - 7) dpi**. This protocol resulted in the biggest number of survivors from all of the protocols tested at this temperature: 7 out of 19 fish (37%) from Tg (hsp70l:sflt1) line and 5 out of 14 (36%) Tg (kdrl:EGFP). Spinal cord samples, 3 from the Tg (kdrl:EGFP) line and 6 from the Tg (hsp70l:sflt1), were obtained, processed and images were acquired. Again, the images in **Figure 3.8** show opposing examples of the Tg (hsp70l:sflt1) samples obtained. Tg (kdrl:EGFP) representative sample is also shown in **Figure 3.8**.

Like with the previous protocol, the vascular patterns observed in Tg (hsp70l:sflt1) samples were quite variable, ranging from having none or very few blood vessels at the injury site (**Figure 3.8 A.2**) to samples (**Figure 3.8 B.1**) that were similar to Tg (kdrl:EGFP) controls (**Figure 3.8 C.1**).

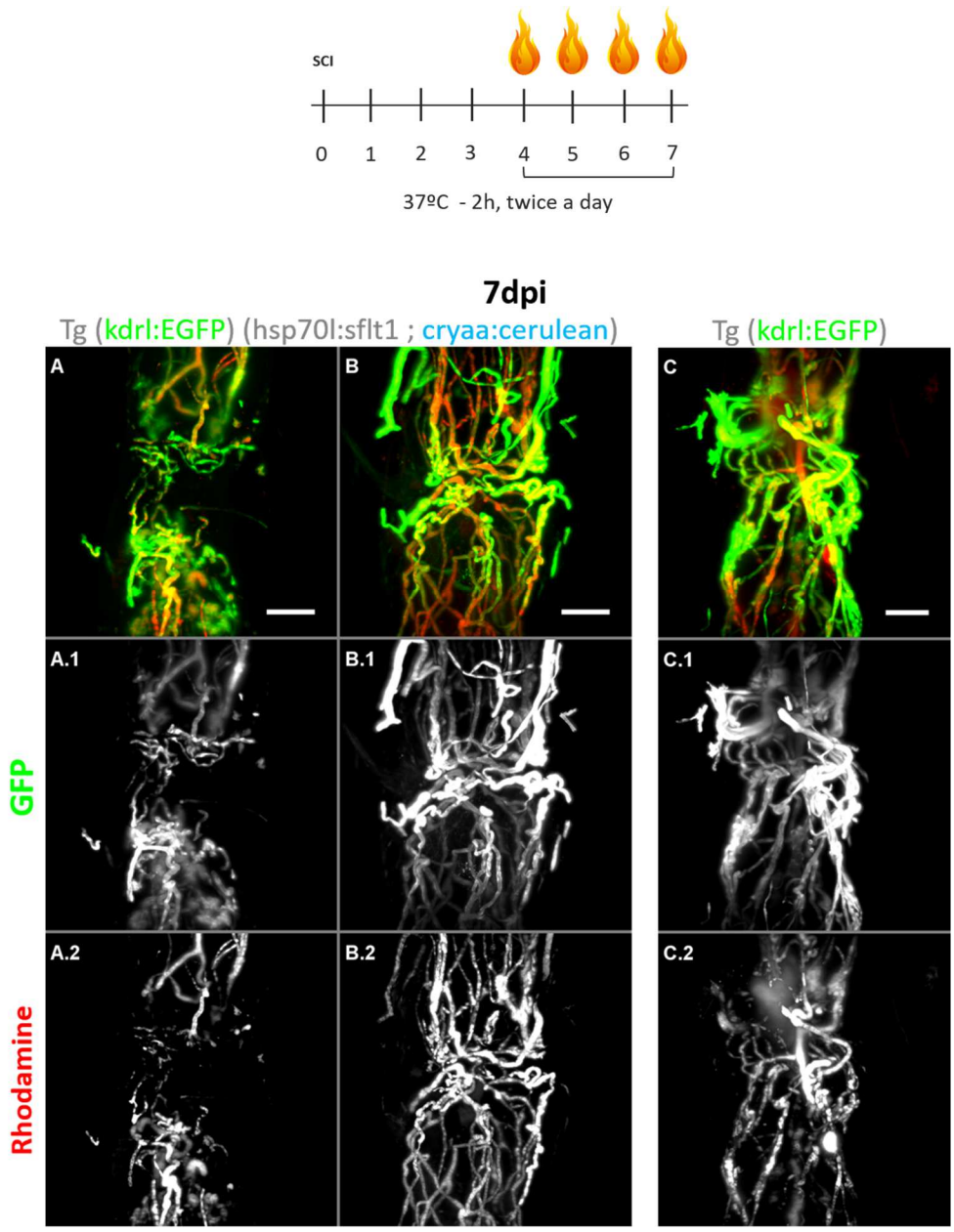

Figure 3.8 – Representation of the HS 37ºC (4 - 7) dpi and representative Tg (hsp70l:sflt1) and Tg (kdrl:EGFP) samples obtained. With this protocol, a sample with few blood vessels at the injury site was obtained (**A**). However, most samples had blood vessels at the injury site, as shown in **B**. All samples were able to retain rhodamine inside these vessels (A.2 and B.2) Most Tg (hsp70l:sflt1) samples showed no perceptible differences when compared with heat-shock controls (**C**). **Scale bar: 100 µm**

Since the previous protocol was the most successful in terms of injured fish survival, an extended version was done, starting again at 4 dpi and samples were collected at 14 dpi - **HS 37ºC (4 - 14) dpi**. This protocol was only performed in Tg (hsp70l:sflt1) fish and 3 survivors out of 7 (43%) injured fish were obtained, and the samples collected, processed and observed (**Figure 3.9**).

Although no heat-shock controls were done, the vasculature of the heat-shocked Tg (hsp70l:sflt1) fish was compared with non-heat-shocked samples from both Tg (kdrl:EGFP) controls and Tg (hsp70l:sflt1) fish (**Figure 3.1** and **3.5)**. When compared with these samples, perceptible differences are observed, with heat-shocked samples displaying fewer vessels at the injury site and, in the existing ones, rhodamine was not fully retained, with the vessels being leaky. Additionally, and when compared to samples from the previous protocol, the previously described differences were also observed. The sample shown in **Figure 3.9 A** was not subjected to the immunohistochemistry protocols although samples shown in **Figure 3.9 B** and **3.9 C** were. However, due to problems with the first immunohistochemistry protocol, GFP labelled interior vessels in the areas adjacent to the injury are not perceptible (**Figure 3.9 B.1** and **C.1**), only being visible through the injected rhodamine (**Figure 3.9 B.2** and **C.2**).

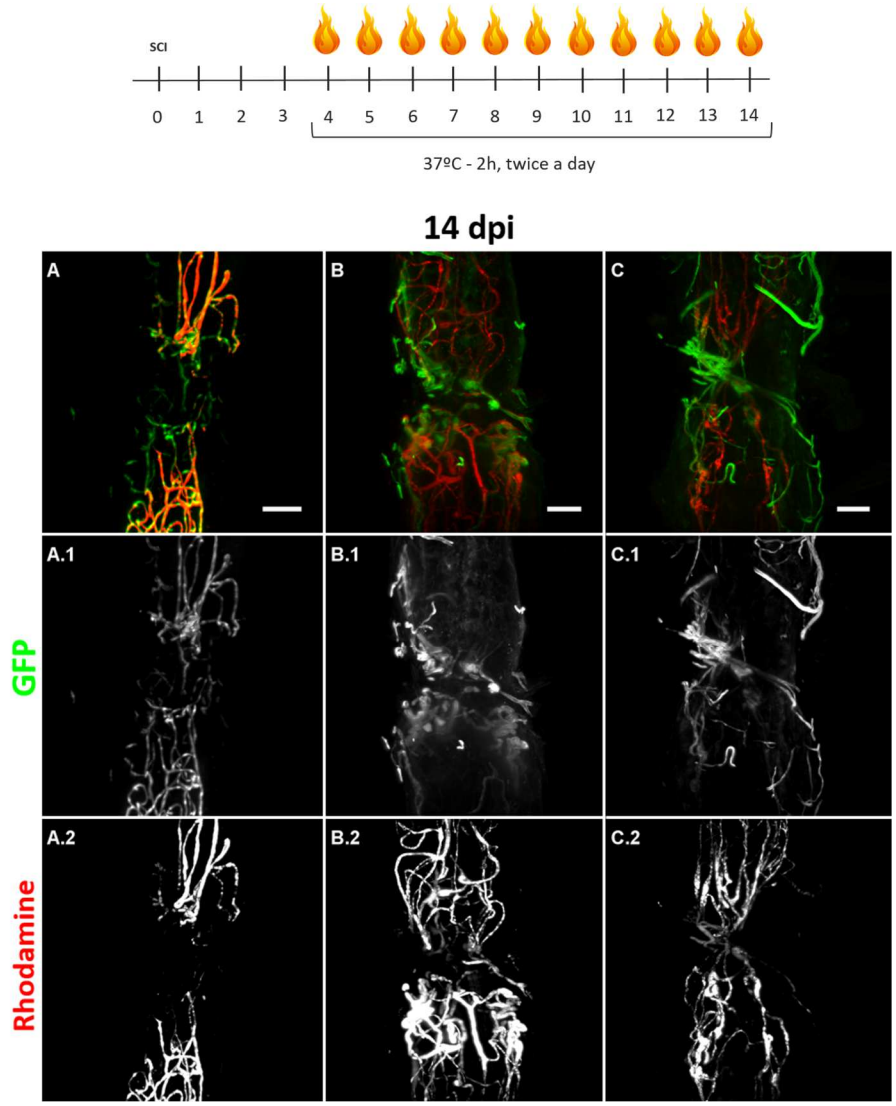

Figure 3.9 – Representation of the HS 37ºC (4 - 14) dpi protocol and Tg (hsp70l:sflt1) samples obtained. With this protocol, three samples were obtained. Despite the problems regarding the GFP labelling, due to the immunohistochemistry protocol used, all samples have less blood vessel at the injury site (A.1 to C.1), additionally confirmed by the absence of rhodamine in those vessels. **Scale bar: 100 µm**

Although more samples for this timepoint should be done in order to confirm these results, it seems that, at 14 dpi, the overexpression of *sflt1* has a perceptible effect in the recovery of the vasculature after an injury, in terms of quantity of blood vessels at the injury site and the function of their BSCB, when compared to non-heat-shocked 14 dpi Tg (hsp70l:sflt1) samples, shown in **Figure 3.5**. The same could not be observed in 7 dpi samples, independently of the protocol used. This may indicate that longer heat-shock periods are more effective than shorter ones. Additionally, heat-shock at 37ºC seemed to be quite aggressive for fish with SCI, as few survivors were obtained independently of the genotype. Only after 4 dpi fish showed better endurance to heat-shock treatment.

3.2.3 Heat-shock at 34ºC

As heat-shock at 37ºC was too strong for adult zebrafish too handle in the first days after SCI, as shown in the previous results, a protocol at 34ºC was also tested, first in embryos and then in SCI adult zebrafish.

3.2.3.1 34ºC Heat-shock tests in embryos

At 34ºC, different periods of heat-shock were tested to see if the inhibition of ISVs development could also be induced at a temperature lower than 37ºC. At this temperature, the experiment was repeated twice, with multiple groups of embryos per condition, per trial. Heat-shock was induced at 17-somite stage and embryos were again observed at 36hpf (**Figure 3.10**). After 30 minutes of heat-shock (**Figure 3.10 A**) some inhibition in the development of the ISVs was already observed in Tg (hsp70l:sflt1) embryos when compared to control siblings (**Figure 3.10 A''**). This inhibitory effect progressively increased with bigger periods of heat-shock (**Figure 3.10 B - F**), inhibiting the formation of ISVs from anterior to posterior regions, with no ISVs being visible after 4 hours of heat-shock (**Figure 3.10 E**). By contrast, control embryos developed normally (**Figure 3.10 B'' – F''**).

Longer periods of heat-shock at 34ºC were also tested in embryos to determine if long term exposure to 34ºC could still elicit a response from the *hsp70l* promoter, since an increase in temperature could lose the heat-shock effect (sudden change of temperature) if continued for a long period of time. After 8 hours (**Figure 3.10 G**) and 10 hours (**Figure 3.10 H**) of heat-shock, most embryos died and in the surviving ones the absence of ISVs was still observed, along with other development defects such as a delay in the development of the eyes, seen by the lack of cerulean (blue) signal. Controls showed normal ISVs development (**Figure 3.10 G'' and H''**). Longer heat-shock periods (16h, 18h and 1 day) were also tested, however no survivors were obtained.

When comparing both protocols, heat-shock at 37ºC was more effective than at 34ºC. One hour of heat-shock was enough to fully inhibit the formation of ISV with the protocol at 37ºC (**Figure 3.5**) but not with the one done at 34ºC (**Figure 3.10 B** and **B'**)

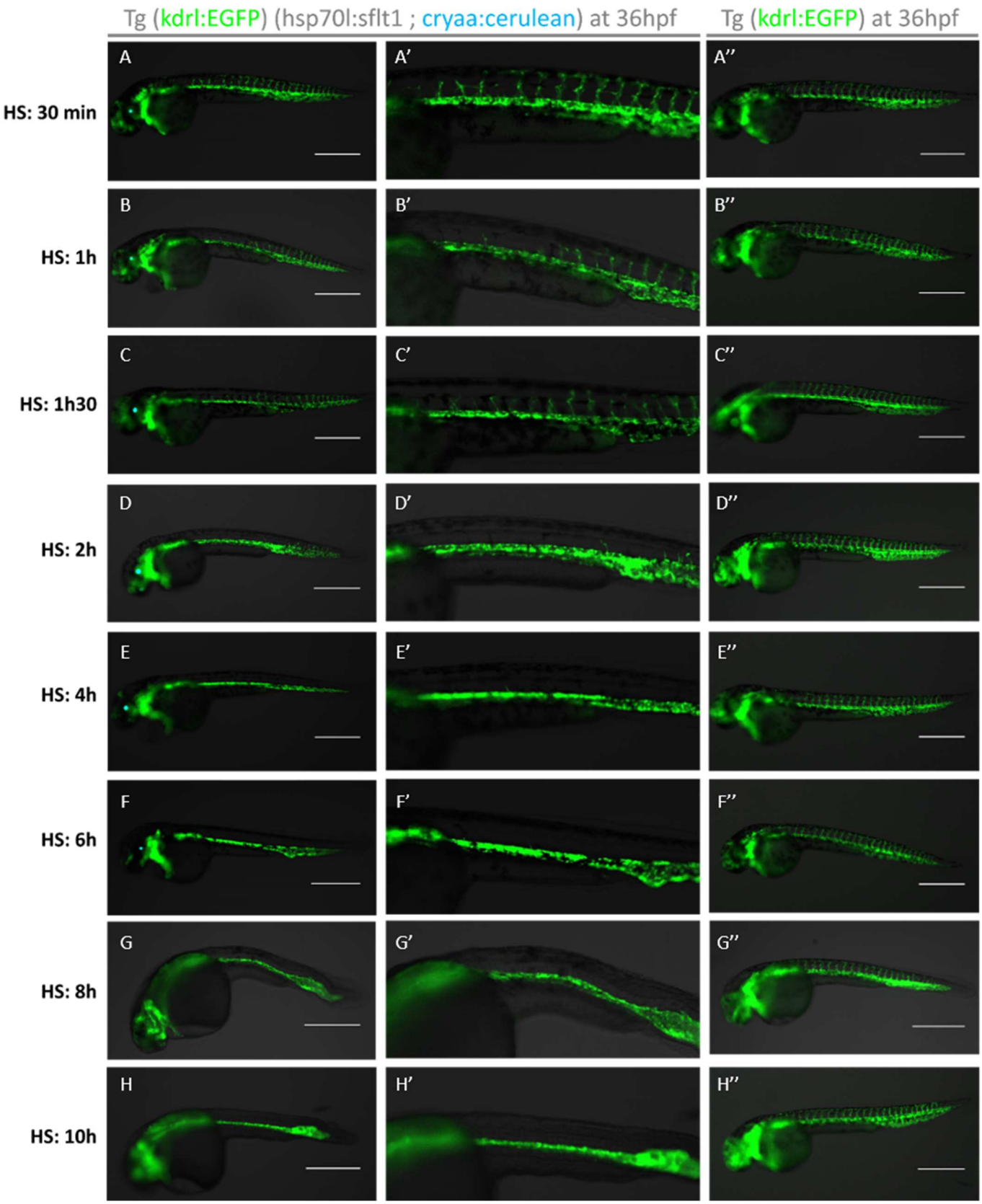

Figure 3.10 – Heat-shock at 34ºC in embryos. Heat-shock at 34ºC was performed, with different heat-shock periods. Embryos were observed at 36hpf (number of trials = 2). Throughout the heat-shock periods, Tg (hsp70l:sflt1) embryos (**A - H**) showed a decrease of ISVs formation, from anterior to posterior, with no ISVs being present after 4 hours of heat-shock (**E**). Tg (kdrl:EGFP) siblings exhibited normal ISV development (**A'' - H''**). **Scale bar: 500 µm**

Nevertheless, these results indicated that, even though longer heat-shock periods were needed to fully inhibit the development of the ISVs, a temperature of 34ºC was still able to activate the *hsp70l* promoter and drive the expression of *sflt1*.

3.2.3.2 34ºC Heat-shock in spinal cord injured adults

At this temperature, two distinct protocols were simultaneously tested: a 6h heat-shock, twice a day protocol and a continuous heat-shock protocol. Heat-shock was induced at 2 dpi, earlier than the protocols at 37ºC. With both protocols, survivors were obtained at 7 dpi.

With the first protocol - **HS 34ºC 6h (2 - 7) dpi**, out of 15 Tg (hsp70l:sflt1) fish only 5 survivors were obtained (33%), and 3 spinal cord samples acquired. The majority of the injured fish subjected to this protocol died after the first or second day of heat-shock, probably due to the changes of temperature at early stages of injury. While all samples showed, once again, the presence of knot-like GFP labelled structures, the existence of blood vessels at the injury site was still observed, with 2 out of the 3 samples being able to maintain rhodamine inside those vessels (showed in **Supplementary Figure 8**).

In the second protocol – **HS 34ºC cont. (2 - 7) dpi** (**Figure 3.11**) – the biggest number of survivors was obtained, out of all heat-shock protocols: 12 out of 24 (50%) Tg (hsp70l:sflt1) fish and 5 out of 15 (33%) Tg (kdrl:EGFP) fish. As Tg (hsp70l:sflt1) spinal cords were particularly frail, only 6 samples were obtained and acquired (**Figure 3.12**). From the Tg (kdrl:EGFP) survivors, 4 samples were acquired (**Figure 3.13**). Again, knot-like vessels were observed in all Tg (hsp70l:sflt1) samples and blood vessels were still present at the injury site of most samples, although a lot of variability was observed between samples (**Figure 3.12 A.1 to F.1).** Most samples, 4 out of 6, exhibited an unusual vasculature, with thick vessels at the injury site and adjacent areas (**Figure 3.12 A to D**), especially the sample shown in **Figure 3.12 B**, having an area of unconnected blood vessels at the injury site (**Figure 3.12 B.1**), further confirmed by the absence of rhodamine in the area (**Figure 3.11 B.2**). The remaining two samples (**Figure 3.12 E and F**) resembled Tg (kdrl:EGFP) controls, shown in **Figure 3.13**. Uninjured caudal areas (**Figure 3.12 A' – F'**), farther away from the injury site, were also acquired as an internal control of the vasculature of each sample.

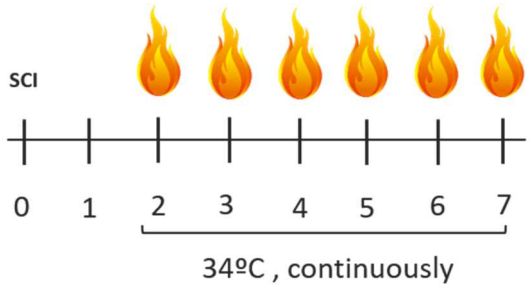

Figure 3.11 – Representation of the HS 34ºC (2 - 7) dpi, continuous protocol. With this protocol the biggest number of survivors was obtained

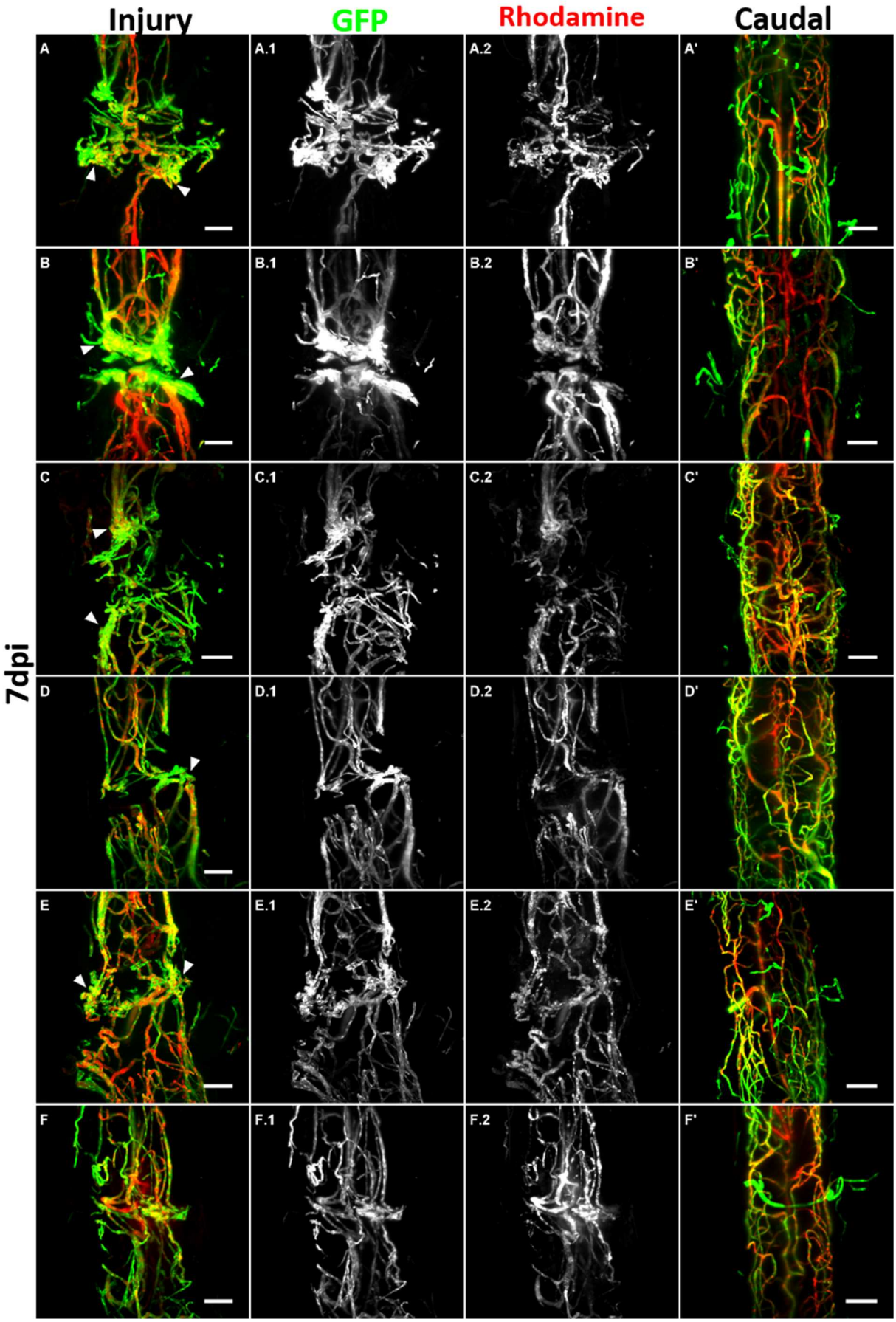

Figure 3.12 - Tg (hsp70l:sflt1) samples obtained with the HS 34ºC (2 - 7) dpi protocol. Injury (A – F) and Caudal (A' – F') areas from each sample. Although all samples had blood vessels (**A.1** to **F.1**), with rhodamine (**A.2** to **F.2**), at the injury site, most samples (**A** to **D**) showed abnormal looking vasculature, with knots of blood vessels (**arrowheads**) and thick vessels in areas adjacent to the injury. **Scale bar: 100 µm**

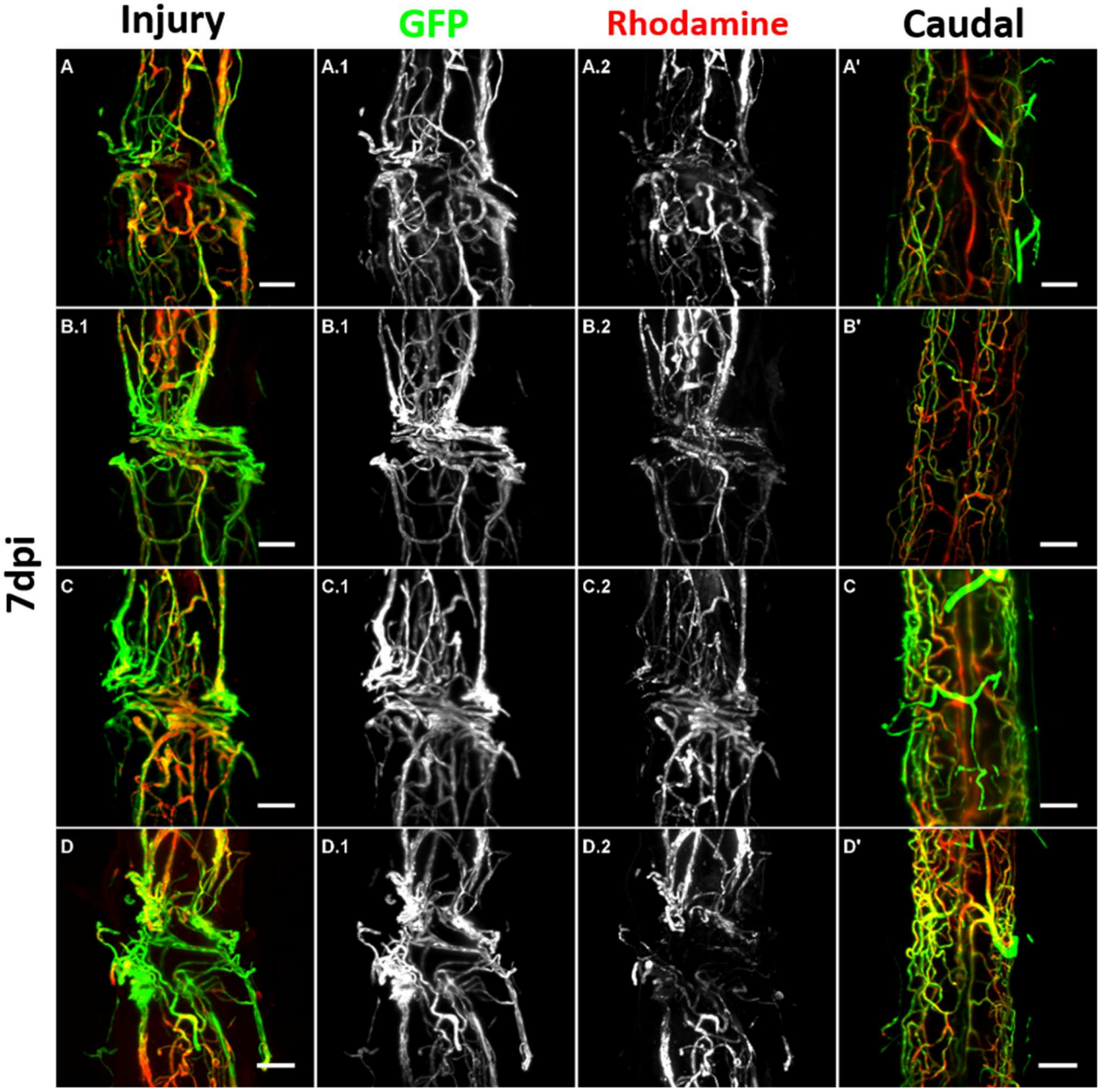

Figure 3.13 - Tg (kdrl:EGFP) samples obtained with the HS 34ºC (2 - 7) dpi protocol. Injury (A -D) and Caudal (A' – D') areas from each sample. Blood vessels (A.1 – D.1), containing rhodamine (A.2 – D.2), were observed at the injury site. **Scale bar: 100 µm**

In addition to the acquisition of single z-stacks from the injured area, larger portions of the Tg (hsp70l:sflt1) samples, which included injured areas and areas adjacent to the injury, were acquired. Once again, thick vessels are seen in areas adjacent to the injury, as previously mentioned (**Supplementary Figure 9**).

Despite the unusual vasculature seen in Tg (hsp70l:sflt1) samples when compared with controls, once again, full inhibition of the angiogenic process was not achieved with the 7 dpi protocol, as blood vessels were observed at the injury site.

An extended version of the continuous protocol was done, with samples being collected at 14 dpi – **HS 34ºC cont. (2 - 14) dpi.** Out of 6 injured fish from the Tg (hsp70l:sflt1) line, 2 survivors were obtained (33%) and samples from both fish were collected (**Figure 3.14**). The samples were quite distinct regarding the presence of blood vessels at the injury site, with the sample shown in **Figure 3.14 A.1** having more blood vessels than the one shown in **Figure 3.14 B.1**. However, both were unable to retain rhodamine inside the vessels at the injury site (**Figure 3.14 A.2** and **B.2**). This contrasts with what was observed in 14 dpi samples of the same transgenic line, previously shown in **Figure 3.5**.

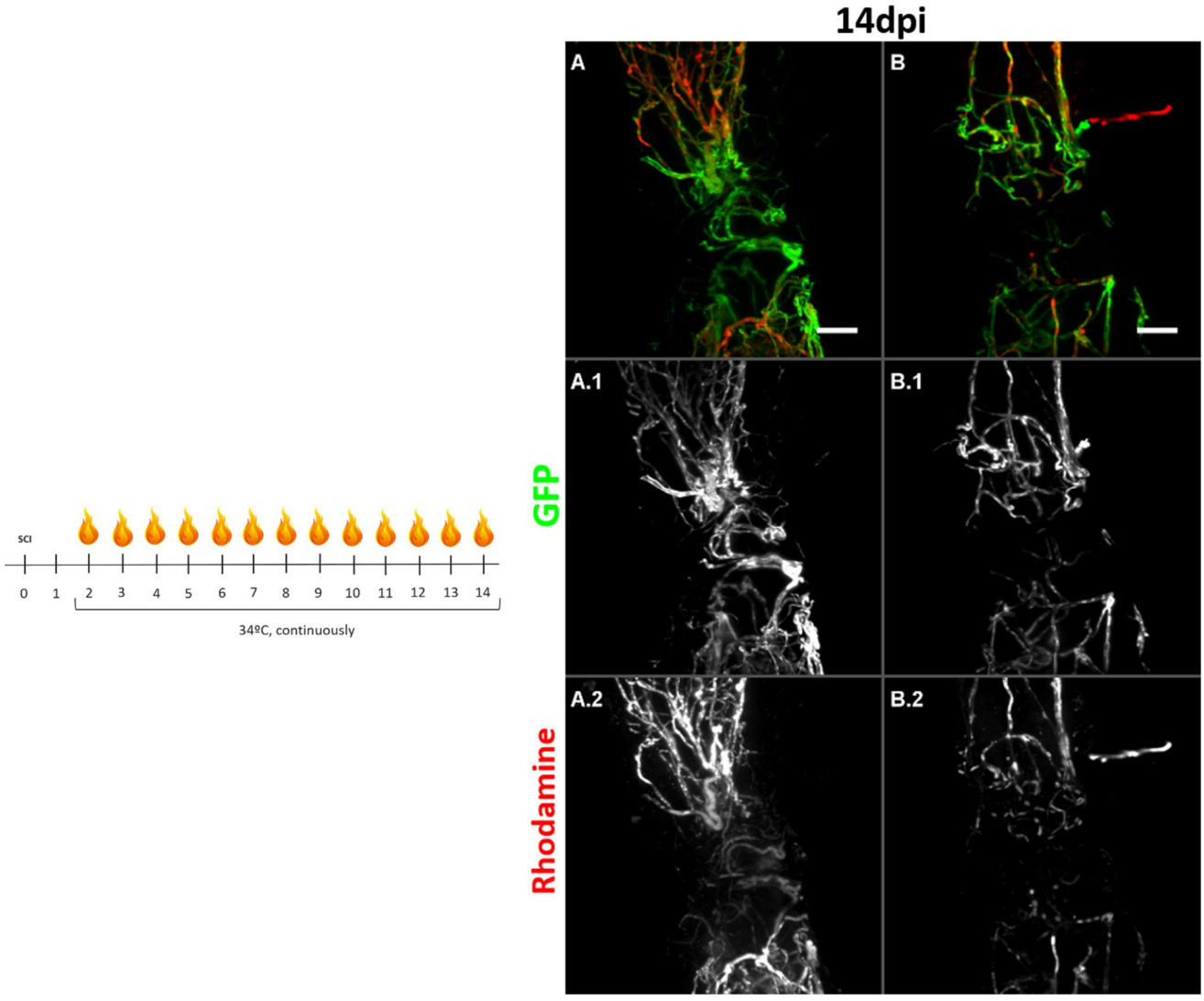

Figure 3.14 – Representation of the HS 34ºC (2 - 14) dpi protocol and Tg (hsp70l:sflt1) samples obtained. With this protocol, two samples were obtained. Both samples had less blood vessel at the injury site (**A.1** and **B.1**), with few being able to retain rhodamine (**A.2** and **B.2**). **Scale bar: 100 µm**

Once again, this seems to indicate that longer heat-shock periods, and therefore bigger periods of *sflt1* overexpression, may be more effective when it comes to decreasing the presence of blood vessels at the injury site, when compared with 7 dpi samples of the same protocol (**Figure 3.12**).

3.2.3.3 Image analysis and quantification

Image analysis with samples belonging to the **HS 34º cont. (2 – 7) dpi protocol** was done. Samples from Tg (kdrl:EGFP) and Tg (hsp70l:sflt1) were analysed, using a custom macro for FIJI software. This macro used original z-stack files, created a mask through identification of tubular structures present throughout the file and, after selection of a region of interest, created a skeleton of the identified structures, with information regarding branching and ending points (allowing the calculation of the euclidian distance) and branch length (**Figure 3.15**). With the information about euclidian distance and branch length, the tortuosity of the blood vessels was also calculated and compared. The results of this analysis are shown in **Figure 3.16**.

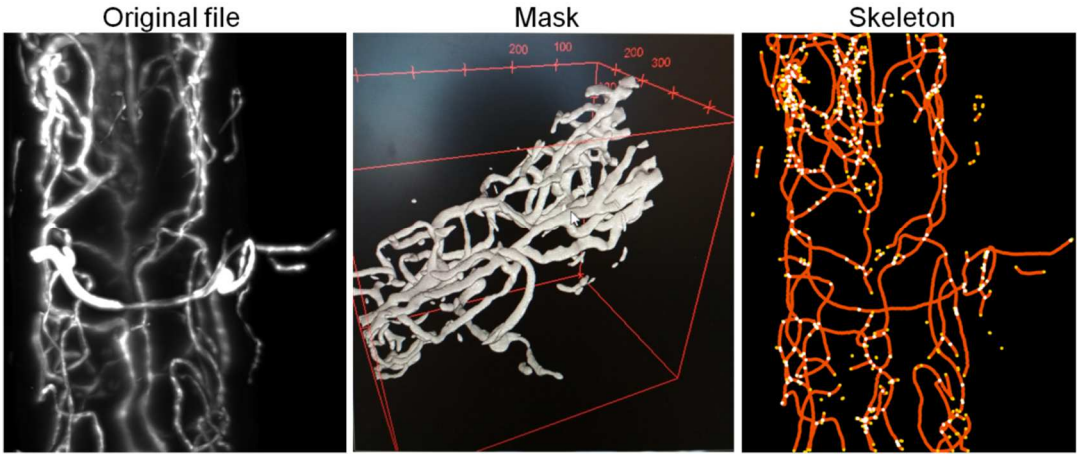

Figure 3.15 – Macro analysis steps. A custom macro was done to analyze the original z-stack files obtained using light sheet microscopy. Analyzing the file frame by frame, a mask was created by identification of tubular structures. From this mask, a skeleton of the vascular structure was done, containing information about branch length and branching and ending points. With the last two parameters, the euclidian distance of blood vessels could be calculated.

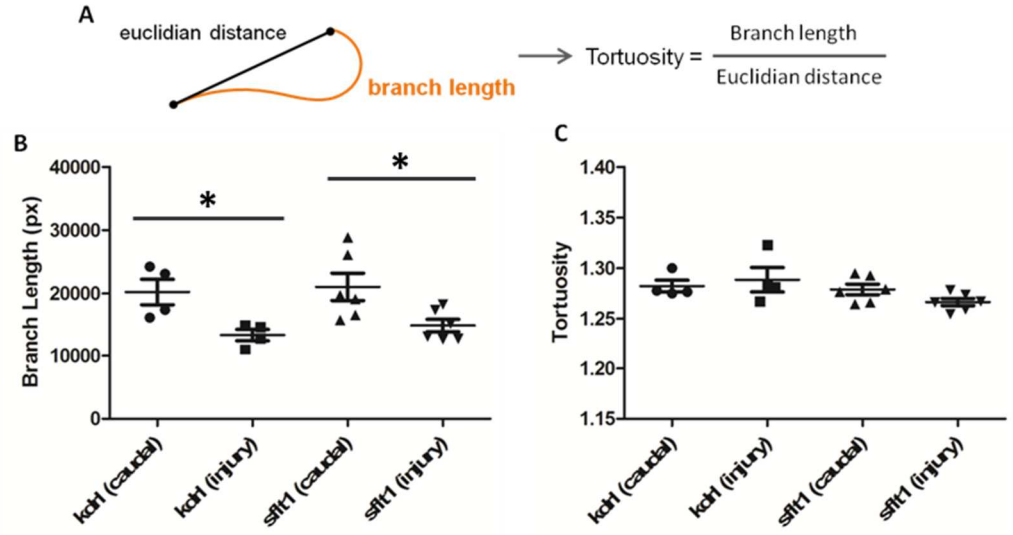

Figure 3.16 – Analysis of Tg(kdrl:EGFP) and Tg (hsp70l:sflt) injured and caudal acquisitions. (**A**) Representation of branch length, euclidian distance and tortuosity. (**B**) Branch length results for both lines and areas acquired. Caudal areas had significantly (*) smaller branches than injured areas. No significant differences in branch length were observed between lines, as happened with tortuosity (**C**).

Comparison between lines and between areas of acquisition, regarding branch length, only showed significant branch length changes between caudal and injured areas (for Tg (kdrl:EGFP), p value = 0.0213; for Tg (hsp70l:sflt1), p value = 0.0277). No differences were observed between Tg (kdrl:EGFP) and Tg (hsp70l:sflt1) samples, suggesting that the heat-shock protocol was not affecting the number of vessels in the injured region in Tg (hsp70l:sflt1) fish. However, the quantification method used needs to be optimized. The threshold used to identify blood vessels was defined by the user and was difficult to set due to differences in GFP levels between samples. As a result, information of blood vessels were either lost or exaggerated and substantially affected the measured branch length.

When comparing tortuosity, no significant differences were observed between lines and, additionally, between injured and caudal areas. This result was unexpected since a qualitative analysis of the images showed that vessels at the injury site were more tortuous than in adjacent regions. This discrepancy was likely due to the fact that the quantification method created mostly small branches and therefore underestimated tortuosity.

3.2.4 Motor function recovery assay

Using an Open Field Test, a motor function recovery assay, with Tg (hsp70l:sflt1) and Tg (kdrl:EGFP) zebrafish, was performed in order to assess the influence of *sflt1* overexpression over the recovery of motor function after SCI. This type of test is commonly used in neurobehavioral research to study the exploratory behavior of animal models in a novel environment and to screen and study existing or induced, in case of SCI, locomotor characteristics (Stewart *et al.*, 2012).

The protocol used is represented in **Figure 3.17**. In this assay, fish were allowed to freely explore the tank for 15 minutes, with their swimming paths being recorded after a 5-minute acclimatization. To avoid bias, the experimenter was blinded to the genotype of the fish being tracked, with each fish being assigned a number. Fish were tracked before (day -1) and after (1 dpi) injury, and then at 7, 14 and 21 dpi. Injured fish were placed at 34ºC, continuously, at 2 dpi.

Five fish from the Tg (kdrl:EGFP) line and six fish from the Tg (hsp70l:sflt1) line survived the heat-shock protocol and their tracking results (swimming path and total swimming distance) were organized in the respective groups and analysed. The results of the tracking protocol and examples of the swimming paths of fish from each line, per tracking timepoints, are shown in **Figure 3.18**.

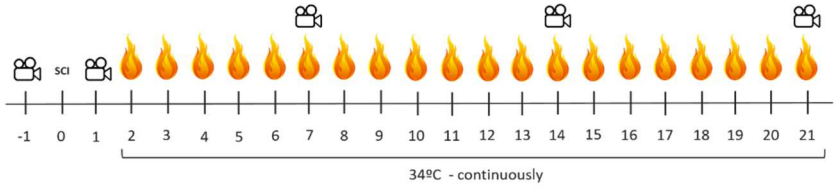

Figure 3.17 – Heat-shock tracking protocol. Protocol established for assessment of motor function recovery, using Tg (hsp70l:sflt1) and Tg (kdrl:EGFP) SCI zebrafish. Tracking of motor function was done at -1, 1, 7, 14 and 21 dpi. Heat-shock was induced, at 34ºC continuously, at 2 dpi.

Overall, after injury and throughout this assay, Tg (kdrl:EGFP) fish swam bigger distances than Tg (hsp70l:sflt1) fish (**Figure 3.18 A;** swimming distances shown in **Supplementary Table 1)**. One outlier for each group was obtained. Representative swimming paths are shown in **Figure 3.18 B.**

According to the literature (Stewart *et al.*, 2012), and as seen before SCI (-1 day), healthy fish explored the whole area of the tank, although with a preference for staying close to the walls. Immediately after injury (day 1), the distance swam by the fish was greatly reduced when compared to that before the injury. Over time, an increase of the swimming distance was observed in both groups, although more visibly for Tg (kdrl:EGFP) SCI fish. At 21dpi, the majority of Tg (kdrl:EGFP) fish (4 out of 5) exhibited a similar swimming pattern to that before the injury, although the swimming distance did not yet reach the initial levels. By contrast, Tg (hsp70l:sflt1) fish, (5 out of 6), exhibited lower swimming distances and, when compared to day -1, different swimming patterns. Additionally, 4 out of 6 Tg (hsp70l:sflt1) showed an abnormal curvature, usually at the injury site and only perceptible in the second week after injury, while Tg (kdrl:EGFP) fish appeared normal (**Figure 3.18 C**).

In order to eliminate individual variability, the swimming distance values of the timepoints after injury were normalized to the day before injury. The obtained results, mean ± standard deviation, were and plotted in **Figure 3.19** (values shown in **Supplementary Table 2).** Statistical testing, with a two-way ANOVA statistical test (alpha of 0.05) using Prism software, was then performed to check if the differences between the swimming distances of the transgenic lines were significant. The results are shown in **Figure 3.19** and only at 21dpi a statistically significant difference was found between the results for each transgenic line, with the differences seen at 7dpi and 14 dpi, although existent, not being statistically significant.

At 21 dpi, after the last tracking recording, rhodamine was injected, the fish were euthanized, and the spinal cords collected for observation of the vasculature (structure and function). A preliminary look at some of the spinal cord samples was done using confocal laser point-scanning microscopy (**Figure 3.20**). Swimming tracks, with increasing swimming distances are shown in **Figure 3.20 A** to **D**, with the corresponding images acquired, at the injury site (**B, D, F** and **H**) and at a caudal area (**B', D', F'** and **H'**). All samples analysed so far belonged to Tg (hsp70l:sflt1) fish. Tg (kdrl:EGFP) heat-shock controls were done but were not ready for acquisition by the end of this work. All Tg (hsp70l:sflt1) samples showed blood vessels at the injury site, with samples **B** and **H** showing a more complex vascular architecture than samples **D** and **F**. Despite having blood vessels, no rhodamine was observed at the injury site in samples **B, D** and **H**. In sample **F**, rhodamine was not observed at the injury site or at the caudal area acquired, probably indicating that the cardiac injection procedure was not successful.

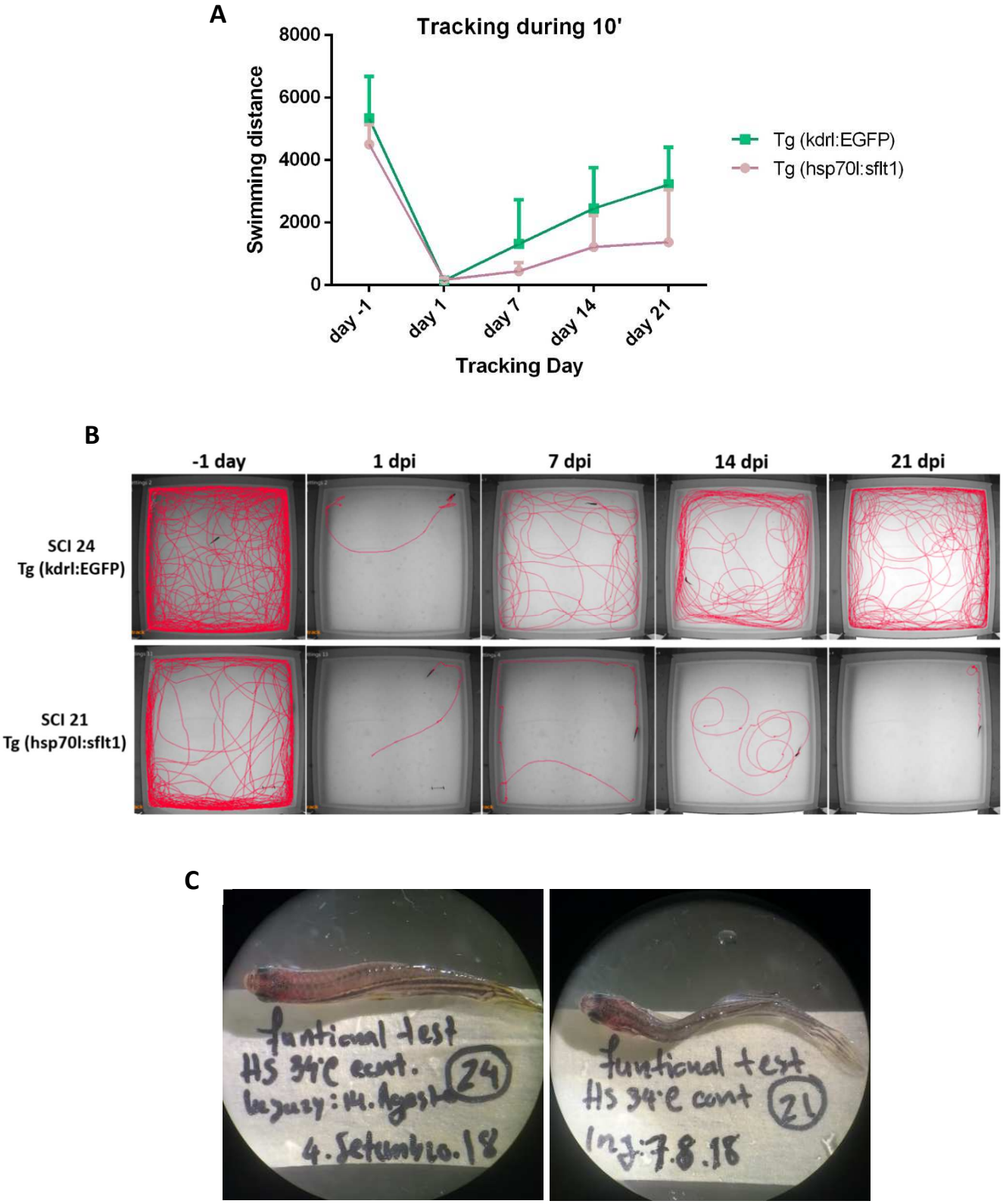

Figure 3.18 – Heat-shock tracking protocol results. (A) Graphic shows swimming distances, during ten-minute tracking, for Tg (kdrl:EGFP) and for Tg (hsp70l:sflt1) fish. Data obtained from every SCI fish was organized and grouped. Mean ± standard deviation was plotted for both groups, per tracking timepoint (**B**) Examples of swimming paths from SCI fish of each line, for every tracking timepoint. (**C**) Top view of the SCI fish shown in **B.** The majority of Tg (hsp70l:sflt1) fish were more frail looking and showed an abnormal curvature of the body- **number 21 -**, at the injury site, at 21 dpi, while most Tg (kdrl:EGFP) showed appeared normal - **number 20**.

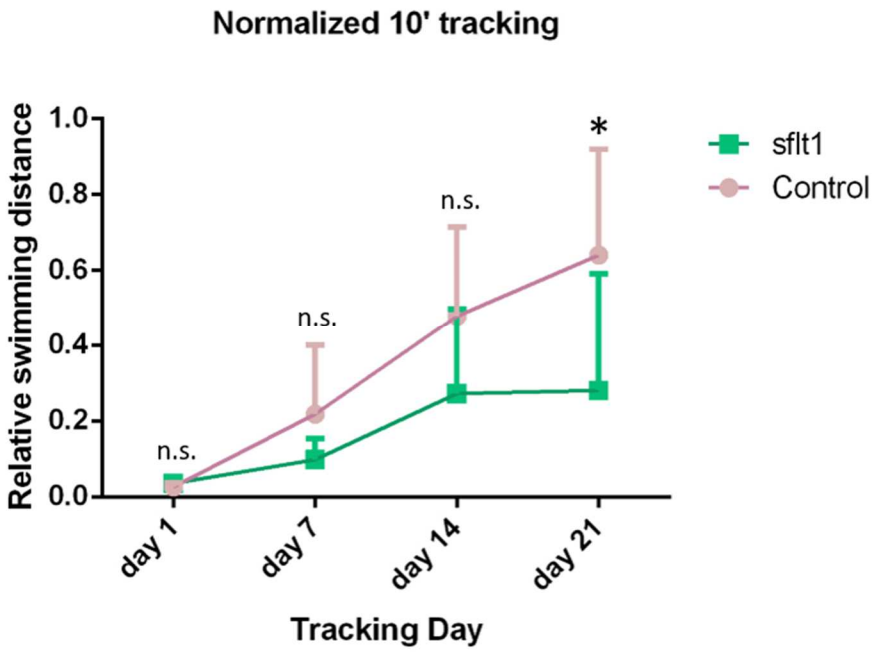

Figure 3.19 – Normalized heat-shock tracking protocol results. Values of swimming distances, per timepoint, for 10-minute tracking, after the injury were normalized using the ones from before the injury. These results were plotted, mean ± standard deviation, and statistically analysed. A significant difference (*) was found between the two transgenic lines, at 21dpi, but not regarding other timepoints (**n.s.** – not significance).

Although the presence of blood vessels at the injury site suggested that angiogenesis was not efficiently inhibited, the reestablishment of the BSCB seemed to be affected. All samples with a successful cardiac injection showed absence of rhodamine at the injury site.

To determine if the degree of revascularization of the injured region correlated with the swimming capacity of the fish, the swimming tracks of each fish were compared with the acquired images. Three of the samples showed some correlation between the distance swam and the density of blood vessels at the injury site (**Figure 3.20 C/D, E/F, G/H**). However, another fish with very limited motor function still presented a considerate amount of blood vessels at the injury site (**Figure 3.20 A/B**). Therefore, it is not possible to confirm if revascularization was impaired in Tg (hsp70l:sflt1) fish. Nevertheless, in all samples the vessels in the injured region were not functional as no rhodamine could be observed at the injury site, in contrast to its caudal area.

No further information regarding the analysis of the inhibition of angiogenesis can be concluded, as no non-heat-shock controls were made for this timepoint (21 dpi).

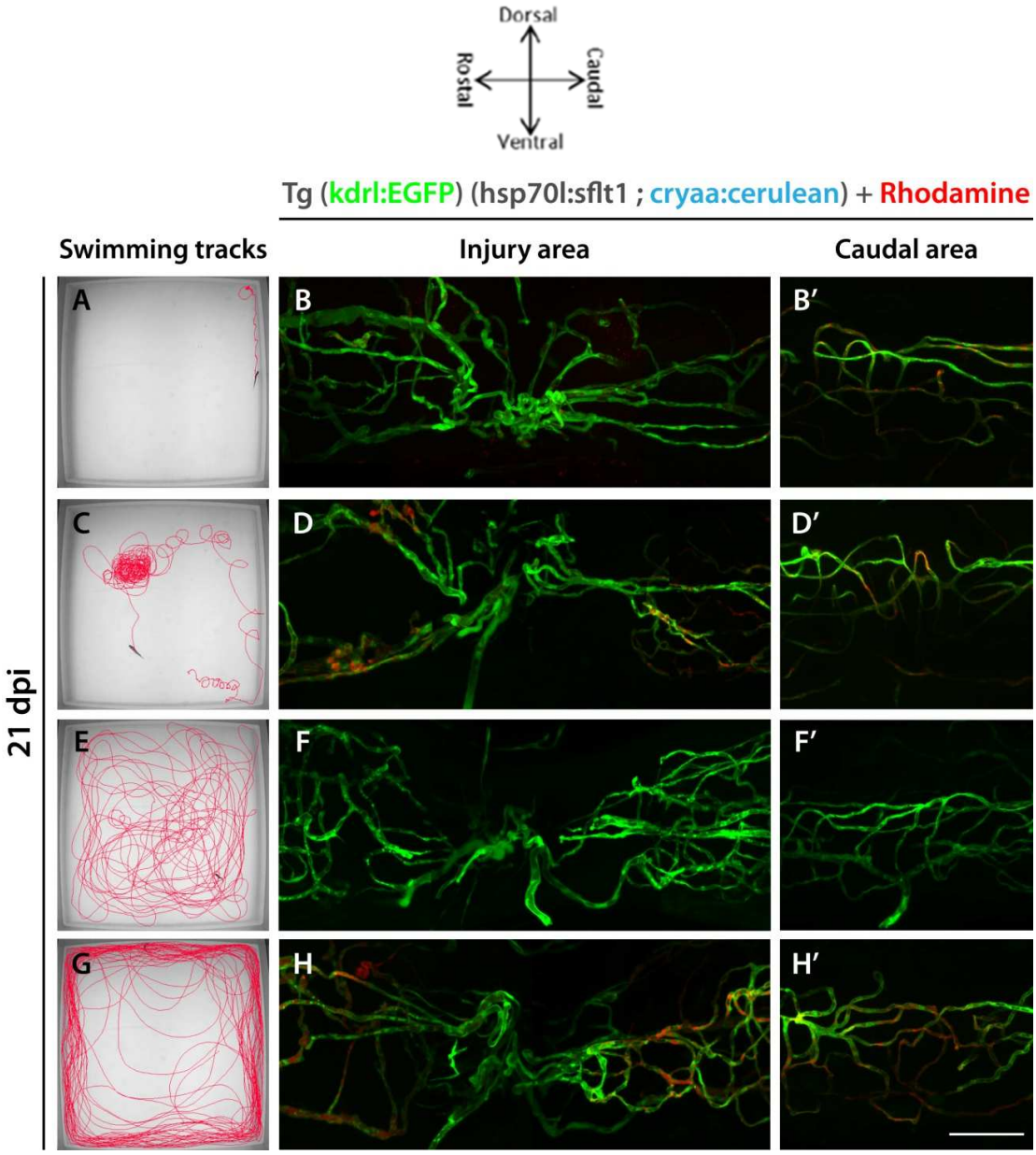

Figure 3.20 – Preliminary image acquisition of Tg (hsp70l:sflt1) spinal cords from the motor functional assay. Images **A, B, C** and **D** show the swimming track of the fish whose spinal cords were preliminarily observed, at the injured site (**B** to **H**) and at a caudal area (**B'** to **H'**), using confocal microscopy (**A**). At 21dpi, all samples showed a confluence of blood vessels at the injury site (**B, D, F** and **H**). Sample **F/F'** did not exhibited rhodamine throughout the sample. In the remaining samples (**B, D** and **H),** almost no rhodamine was observed at the injury site. **Scale bar**: 100 µm

To summarize, in this assay, our results showed that *sflt1* overexpression seems to affect the recovery of motor function after SCI. While the vascular pattern between samples seemed to be variable, the revascularization of the injured area appeared to be affected and, in most samples, no perfusion of these vessels was observed. Analysis of the full vasculature of these samples and of Tg (kdrl:EGFP) samples should be done and compared. Furthermore, an increase in the number of samples is also needed to confirm the obtained results and to determine the relation between vascular recovery after SCI and recovery of motor function.

Chapter 4. Discussion

4.1 Reestablishment of the Blood - Spinal Cord Barrier

One of the reasons for the persistent damage in injured spinal cord in mammals, after the primary injury, is the disruption of the BSCB and the consequent failure to reestablish a functional vascular network. Coupled with the formation of a glial scar and the presence of growth-inhibitory molecules, the endogenous attempts at self-repair are thwarted (Ahuja *et al.*, 2017; Oudega, 2012). By contrast, zebrafish are able to recover from a SCI. Additional work done in our lab showed that, throughout the regenerative process of the spinal cord and recovery of function, an increase of blood vessels at the injury site is observed and the consequent restructuring of these vessels, over time, occurs (Maçarico, 2014). However, before these studies, it was not known if these newly formed blood vessels were functional and, in case they were, at what point during the regenerative process did they become functional.

In this work it was confirmed that, throughout the regeneration of the spinal cord, new blood vessels were formed at the injury site, as shown in Maçarico, 2014. However, blood vessels were already observed at the injured area at 3 dpi, contrary to what is seen in the previously mentioned work. This could be related with the fact that the whole vasculature of the spinal cord was not acquired due to limitations of the maximum acquisition range of the microscopy method used, something that is overcome using light sheet fluorescence microscopy. Differences between researchers regarding the execution of SCI surgery should also not be excluded, as more severe injuries might cause more damage to the tissue than less severe ones, possibly delaying the vascular recovery (even if in both cases the paralysis of the posterior portion of the body, in the first week after injury, is confirmed). In the following timepoints, at one week and two weeks post injury, similar results were obtained, with the presence an unorganized confluence of blood vessels, originated from areas adjacent to the injury site, being seen. In Maçarico, 2014, rhodamine was injected in injured fish, at 7 dpi, to investigate the existence of blood flow in the confluence of vessels. The presence of the fluorescent compound was observed, not only indicating the existence of blood flow but also the correct functioning of these blood vessels, as the compound was retained inside them and not leaked to the surrounding tissue.

Taking it a step further, in this work, the functionality of the newly formed blood vessels was assessed, now at different timepoints, to observe the reestablishment of BSCB. Results showed a perceptible increase of the fluorescent compound injected into the blood stream at the injured area, from 3 dpi, where almost no rhodamine was present inside the blood vessels, to 7 dpi, where most blood vessels contained the injected compound. Before this period, at 1 dpi, no new blood vessels were observed at the injury site and the existing ones were not able to retain the compound, which visibly accumulated in the nervous tissue. At 14 dpi, no perceptible differences were observed when compared to 7 dpi samples. At 30 dpi, only two samples were obtained, and although distinct, a decrease of blood

vessels at the injury site and a reorganization of the existing ones were observed, when compared to earlier timepoints. In order to assess the percentage of vessels without rhodamine, the fluorescence density of the two channels (GFP and Rhodamine) was quantified. Thirty days post injury samples were not included in this analysis due to the sample size. Statistically significant differences were observed between 3 dpi and 5 dpi and between 5 dpi and 7 dpi, but not between 1 dpi and 3 dpi and between 7 dpi and 14 dpi. Once again, this data seemed to indicate that the main recovery of the BSCB, with the analysed timepoints, occurred between 3 dpi and 7 dpi. Despite these results, a more thorough analysis should be done to accurately demonstrate the existing differences between samples. The initial strategy was to analyze the original z-stack files, frame per frame for each channel and the channels then automatically compared, using a custom macro. However, since the macro was not working properly by the end this work, a simpler method was instead used, based on the same principles (comparing GFP and rhodamine channels) and using 2-dimensional projections of the original files.

Nevertheless, the previous results seem to indicate the existence of major differences regarding the vascular response after SCI between zebrafish and mammals, and may be one of the reasons allowing the regeneration of the spinal cord in zebrafish. Interestingly, previous works using the compression injury model showed that extensive loss of neurons is seen at 3 dpi and that neuronally determined proliferative cells are detected at 7 dpi (Hui *et al.*,2010). Additionally, motor function studies, previously performed in our lab, showed that after 7 dpi injured fish started to gradually regain their swimming ability (Maçarico, 2014). These timepoints correspond to ones used in this work and, when pieced together, seem to correlate neuronal death with the presence of a disrupted BSCB, at 3 dpi, and neurogenesis and beginning of functional recovery with a mostly recovered BSCB, at 7 dpi.

Different molecular and cellular players could be involved in the reestablishment of the BSCB in zebrafish. Angiopoietin-1 (Ang-1) plays an important role in vascular remodelling and stabilization and its administration reduces vascular permeability after ischemic injury. SCI studies done in rats showed that Ang-1 improves the integrity of the BSCB after injury and, together with VEGF, enhances the revascularization and tissue perfusion (Herrera *et al.*, 2010). Possible cellular players, like pericytes, can also be involved in the recovery of the BSCB as they are responsible for the stabilization of newly formed blood vessels (Oudega *et al.*, 2012). In fact, work done in our lab to study the distribution of pericytes after SCI showed that, between 3 dpi and 5 dpi, new blood vessels are already covered by pericytes. This timing is consistent with the recovery of the BSCB seen in our results.

Future studies should be done to assess the correlation between tissue revascularization and neuron distribution, not only by observing the presence and functionality of blood vessels and the presence of proliferative cell, neurons and of neuronally determined cells in the SCI samples, but also by interfering with the vascular recovery and observing the resulting consequences, either by inhibiting of vessels formation (with the main target being endothelial cell) or by interfering with vessel

stabilization (with the main target being pericytes). The inhibition of blood vessel formation was tested in this work and the results are discussed in the topic bellow. The identification and characterization of new cellular and molecular players involved in the reestablishment of the BSCB after SCI would also be important to understand the mechanisms that occur during spinal cord regeneration in zebrafish. The target players could be molecules that are known to be downregulated after SCI or molecules already tested and that showed a promising effect in vessel stabilization in mammals or cell types that are known to influence and stabilize blood vessels. This study could be done with the use/construction of transgenic lines, in situ hybridization assays in injured spinal cord sections or immunohistochemistry assays in injured spinal cord sections or whole spinal cords or even using molecular biology methods, like qPCR, to assess the expression level of these molecules at different timepoints after injury.

4.2 Inhibition of angiogenesis

Recovery of motor function, neurogenesis and vascular recovery, as mentioned in the previous topic, seem to have correlated time frames. In order to investigate if the formation of new blood vessels was essential to the spinal cord regenerative process, the consequences of the inhibition of the angiogenic process during spinal cord regeneration were studied. As previous work using pharmacological inhibitors was not successful, a genetic approach was tested, using a transgenic zebrafish line – the Tg (hsp70l:sflt1) line – with a temperature inducible promoter (*hsp70l*) controlling the expression of a *sflt1*, a soluble form of a VEGF receptor, known for being an angiogenic regulator through the control of VEGF availability (Chappell and Bautch, 2010). When at a higher temperature, *sflt1* overexpression should occur, inhibiting the angiogenic responses taking place. Several heat-shock protocols were tested and, when the most adequate one was established, in terms of injured fish survival and effect on the angiogenic response, a motor function recovery assay was performed.

4.2.1 Heat-shock protocols

Using the previously mentioned transgenic line, different protocols, at two distinct temperatures, 37ºC and 34ºC, were tested in this work, first in embryos and afterwards in adults.

During development and after heat-shock induction in embryos, at either temperature, the inhibition of the ISVs formation was observed in Tg (hsp70l:sflt1) embryos, but not in Tg (kdrl:EGFP) controls. These vessels were chosen as a target to test the transgenic line since their formation, through sprouting angiogenesis, is relatively well described (Gore *et al.,* 2012). Additionally, due to their positioning, disturbances in the development of these vessels would be easily observed. Heat-shock at 37ºC proved to be more efficient than at 34ºC, with only 1 hour of heat-shock being sufficient to completely inhibit ISV development. This goes in accordance to what is described in Lele *et al.*, 1997, as heat-shock induced at a higher temperature (37ºC) resulted in an increased heat-shock promoter activation and gene expression than when at a lower temperature (34ºC).

Interestingly, with heat-shock at 34ºC, increasing heat-shock periods showed increasing levels of ISV inhibition, initially affecting only anterior regions and gradually inhibiting more posterior regions. Somite development occurs from anterior to posterior regions and ISV formation likely follows the same pattern. ISVs are derived from the dorsal aorta in response to VEGF that is produce by the somites (Childs *et al.*, 2002; Gore *et al.*, 2012; Kimelman and Martin, 2012). As such, a decrease of VEGF availability by *sflt1* overexpression could affect ISV development in more anterior regions first and, with the increase of heat-shock duration, the effect would expand posteriorly, producing the observed phenotypes.

After confirming the ability of the Tg (hsp70l:sflt1) line to inhibit angiogenic mechanisms, heat-shock was carried out in injured adults. Most protocols tested had a low survival rate, especially those initiated right after or in the first few days after injury. This was especially true with protocols at 37ºC, which had lower survival than protocols at 34ºC. This indicated that fish with SCIs, regardless of having the hsp70l:sflt1 transgene or not, were especially sensitive to temperature changes at early stages of SCI. Additionally, heat-shock before the injury procedure greatly conditioned the survival of Tg (hsp70l:sflt1) fish. This could be due to the influence of *sflt1* overexpression over the angiogenic process associated with wound healing, as to perform a SCI a wound has to be opened in order to expose the spinal cord. The most successful protocol, with a 50% survival rate of Tg (hsp70l:sflt1) line, was the one where fish had a continuous exposure to 34ºC since 2 dpi. This protocol avoided changes of temperature that, as previously mentioned, proved to be fatal to injured fish. Additionally, this protocol was the only one that, at 7 dpi, resulted in the biggest number of spinal cords samples with an abnormal vasculature at the injury site, while in many samples from other protocols the effects were variable, and some samples were even similar to Tg (kdrl:EGFP) samples. Despite the observed differences, when doing a quantitative analysis of the Tg (hsp70l:sflt1) and Tg (kdrl:EGFP) samples obtained with the 34ºC continuous protocol, no differences regarding branch length and tortuosity were observed at 7 dpi. Optimization of the custom macro, used to perform this analysis, is still needed. The signal of the blood vessels of injured areas is higher than that of adjacent areas, due to the density of vessels and the high expression of angiogenic proteins like KDRL (whose promoter was used to drive GFP expression). As such, information of adjacent blood vessels with low GFP-signal is sometimes not taken in account and might ultimately influence our analysis. Therefore, a solution for the definition of an appropriate threshold is needed to improve the quality of our quantification.

Using this transgenic line, regardless of the protocol used, no full inhibition of the angiogenic process was observed at 7 dpi, with most samples having blood vessels at the injury site. In many samples, the presence of very thick blood vessels and/or knots of vessels was observed. By contrast, at 14 dpi, with both temperatures, samples with some vascular defects were obtained, regarding the presence of blood vessels at the injury site and the functionality of these vessels. These results seem to indicate that longer heat-shock periods, and therefore longer periods of *sflt1* overexpression, may be

more effective when compared to shorter protocols (7 dpi). Even though these results look promising, more samples and heat-shock controls should be acquired and analysed to confirm this hypothesis.

One of the simplest explanations regarding the differences observed between 7dpi and 14dpi, with both heat-shock temperatures, could be the low efficiency of the heat-shock induced activation of the *hsp70l* promoter in the spinal cord, a more interior tissue, when compared to more exterior tissues. In this case, even heat-shock at 37ºC, for 2 hours, would not be enough to drive the expression of *sflt1* to completely inhibit the angiogenic effect at 7dpi. After another week of interference with the endogenous revascularization attempts, the nervous tissue would begin to sustain damage, possibly slowing the angiogenic process and BSCB reestablishment, explaining the results observed at 14dpi. Due to the high mortality observed with the tested temperatures, an increase of temperature or of heat-shock duration at 37ºC was not possible. Nevertheless, this hypothesis could be tested by comparing *sflt1* heat-shock induced expression levels in the spinal cord and in a more external tissue, like the caudal fin.

The limited success of using pharmacological and genetic methods that target VEGF to inhibit sprouting angiogenesis raises interesting questions regarding the angiogenic process involved during spinal cord regeneration. ISV formation in embryos occurs through sprouting angiogenesis and full inhibition of their development was obtained using the Tg (hsp70l:sflt1) transgenic line. However, the same could not be completely accomplished in adult zebrafish after SCI, as mentioned above, where in most cases thick blood vessels or knots of vessels were observed. These structures are not characteristic of a sprouting angiogenesis mechanism and might indicate that the angiogenic response during spinal cord regeneration might not fully occur through this process, and instead occur through a combination with different angiogenic mechanisms, like with intussusceptive angiogenesis, also known as splitting angiogenesis. This angiogenic mechanism is observed during development (Caduff *et al*., 1986; Karthik *et al.*, 2018) and in pathological conditions (Ronca *et al.*, 2017) and is described by the formation of thinner blood vessels through the splitting of preexisting thicker ones, initiated by the establishment of intraluminal pillars (Gianni-Barrera *et al.*, 2014). The mechanisms involved in the regulation of this type of angiogenesis are not completely clear, although results described in the literature indicate that while VEGF signaling might promote splitting angiogenesis, it may not be essential to this process (Baum *et al.*, 2010). Other molecular players, like angiopoetin-1 and -2 and their tyrosine kinase receptors Tie1 and Tie2, seem to be involved in splitting angiogenic during embryonic development (Logothetidou *et al.,* 2017; Patan, 1998). However, this pathway is not exclusive to this type of angiogenesis, as it has likewise been associated with sprouting angiogenesis (Savant *et al.*, 2015). Splitting angiogenesis also seems to be influenced by heamodynamic factors, being stimulated in areas of increased blood flow but low shear stress. The combination of both of these angiogenic processes has been described in chicken embryos regarding lung (Makanya *et al.*, 2007) and kidney (Makanya *et al.*, 2005) development and, more recently, in zebrafish for the caudal vein plexus development (Karthik *et al.*, 2018). The existence

of a combinatory angiogenic process, during spinal cord regeneration, could potentially explain the existence of blood vessels at the injury site even in the presence of an anti-angiogenic factor like sFLT1, as the splitting angiogenic process would not be completely dependent of this pathway. To test this hypothesis, first the confirmation that sprouting angiogenesis is not being activated after heat-shock should be performed. This could be done through qPCR analysis of the expression levels, of the injured portion of the spinal cord of samples with and without heat-shock. This analysis would target genes whose expression is activated or repressed by the VEGF pathway. After this confirmation, an analysis and comparison of gene expression of Tg (hsp70l:sflt1) and Tg (kdrl:EGFP) heat-shock fish and Tg (hsp70l:sflt1) non- heat-shocked fish could be done, through RNAseq of sorted endothelial cells from the injured area. This would not only show changes triggered by *sflt1* expression but could also allow the identification of potential players involved in the revascularization process seen at these timepoints. Additionally, a more thorough analysis of the thick vessels and knots of vessels, using objectives that allow a bigger amplification of the target regions, could be done to assess the presence of transluminal pillars, a hallmark of intussusceptive analysis.

An alternative explanation for the limited effect of the Tg (hsp70l:sflt1) line in adults could be the presence of potential hypoxia-driven compensatory mechanisms, such as the increase of VEGF expression (Pugh and Ratcliff, 2003). In this hypothesis, the initial hypoxia induced response after injury, known to activate the expression of pro-angiogenic factors, would be blocked by the overexpression of *slft1*. With a longer exposure to hypoxia, and with the accumulation of hypoxia-inducible factors, an increase in pro-angiogenic factors would occur and, ultimately, the heat-shock induced expression of *sflt1* would not be sufficient to inhibit angiogenesis. Over time, persistent exposure to hypoxia would result in cell death, and consequently a decrease in hypoxia-driven expression, possibly explaining the results observed at 14dpi. This hypothesis could be tested by assessing the levels of VEGF of heat-shock samples, at different timepoints, through qPCR.

Regardless of the possible mechanism involved in the formation and maintenance of blood vessels at the injury site, ultimately the use of the Tg (hsp70l:sflt1) line, using the described protocols, proved to be inefficient in inhibiting the angiogenic response that occurs during spinal cords regeneration. Different approaches could be pursued in order to continue this study. Another genetic approach could be used, such as the Tg(hsp70l:dn-vegfaa) line, could be used. This line relies on temperature inducible expression of a dominant negative VEGF, with antagonistic effects, and its use has been proven successful in the inhibition of angiogenesis during heart regeneration (Marín-Juez *et al.*, 2016). A future pharmacological approach that could also be investigated is the use of a triple inhibitor of the VEGF, PDGF and FGF pathways, that are involved in the angiogenic response as previously mentioned, with the objective of inhibiting all angiogenic responses that could result after injury.

4.2.2 Motor Function Recovery Assay

After observing the results of the heat-shock protocols, a motor functional recovery assay was done. After choosing the heat-shock strategy with the most effective results and highest survival rate - the 34ºC continuous protocol - a tracking protocol was established. Initially, this tracking protocol was planned to span from 2 dpi to 30 dpi. However, due to the perceptible degradation in the physical condition of Tg (hsp70l:sflt1) fish, it was shortened to 21 dpi. Overall, Tg (hsp70l:sflt1) performed worse, regarding the recovery of normal swimming pattern and total swimming distance, and at 21 dpi appeared more affected than Tg (kdrl:EGFP) fish. Statistical significance regarding total swimming distance was only observed at 21dpi, although swimming distance differences start at 7 dpi.

A preliminary observation of the vasculature and of axonal regeneration of the spinal cords of the tracked fish was done. However, only some of the samples were observed due to time constraints, as this assay was initiated in the last months of this internship. As such, a comparison with the obtained controls was not possible as these were still in the samples processing phase.

Four samples of the Tg (hsp70l:sflt1) line were acquired using confocal point-scanning microscopy. In all samples, blood vessels were observed at the injury site, although the revascularization of the area seemed to be affected. Additionally, in three of the samples, no rhodamine was observed at the injury site, indicating that the BSCB was not functional. In the remaining sample, no rhodamine was observed throughout the spinal cord, indicating that the injection protocol was not successful.

Again, s*flt1* overexpression seemed to be not only affecting the recovery of motor function but also partially inhibiting the recovery of the vasculature at 21 dpi. In addition to the damages caused by the absence of a functional BSCB, the depletion of VEGF could also be affecting axonal regrowth as this growth factor not only is associated with the angiogenic process but also promotes neuro protection and axonal guidance (Almodovar *et al.*, 2011; Khaibullina *et* al., 2004; Rosentein and Krum, 2004). In this work, the axonal recovery was to be observed, however, the immunohistochemistry protocol applied was not successful and did not label axons specifically (data not shown).

A new assay, with a bigger sample size, should be done to confirm the functional results obtained in this work. Additionally, future studies should assess the axonal regrowth in these samples in order to investigate and clarify the relation between inhibition of angiogenesis and persistent disruption of the BSCB with motor function and axonal recovery in zebrafish.

4.3 Concluding remarks

In this work we confirmed the reestablishment of the BSCB and identified its recovery time-frame after SCI in zebrafish. These results, together with results described in the literature, represent important steps to fully understand the regenerative process that occurs after SCI in zebrafish. Regarding the inhibition of angiogenesis during spinal cord regeneration, our results appear to indicate that while the Tg (hps70l:sflt1) transgenic line was very efficient inhibiting angiogenesis when used in a developmental context, the same could not be observed in a regenerative context, with the effects being variable. Nevertheless, some differences in the vascular architecture of the spinal cord, after *sflt1* overexpression, were observed when comparing Tg (hsp70l:sflt1) samples with controls of experimental settings and with transgenic line controls. Additionally, our results suggest that the vasculature is important for functional recovery. This work is, therefore, the basis for future studies aiming to understand how the vascular system contributes to spinal cord regeneration.

Bibliography

Ahuja, C.S., Wilson, J.R., Nori, S., Kotter, M.R.N., Druschel, C., Curt, A., Fehlings, M.G., 2017. Traumatic spinal cord injury. Nature Reviews Disease Primers 3, 17018.

Almodovar, C.R. De, Fabre, P.J., Knevels, E., Coulon, C., Segura, I., Haddick, P.C.G., Aerts, L., Delattin, N., Strasser, G., Oh, W., Lange, C., Vinckier, S., Haigh, J., Fouquet, C., Henderson, C., Gu, C., Alitalo, K., 2011. VEGF mediates commissural axon chemoattraction through its receptor Flk1. Neuron 70, 966–978.

Assinck, P., Duncan, G.J., Hilton, B.J., Plemel, J.R., Tetzlaff, W., 2017. Cell transplantation therapy for spinal cord injury. Nature Neuroscience 20, 637–647.

Baptiste, D.C., Fehlings, M.G., 2007. Update on the treatment of spinal cord injury. Progress in Brain Research 161, 217–233.

Bartanusz, V., Jezova, D., Alajajian, B., Digicaylioglu, M., 2011. The blood-spinal cord barrier: Morphology and clinical implications. Annals of Neurology 70, 194–206.

Baum, O., Suter, F., Gerber, B., Tschanz, S.A., Buergy, R., Blank, F., Hlushchuk, R., Djonov, V., 2010. VEGF-A promotes intussusceptive angiogenesis in the developing chicken chorioallantoic membrane. Microcirculation 17, 447–457.

Becker, C.G., Becker, T., 2008. Adult zebrafish as a model for successful central nervous system regeneration. Restorative neurology and neuroscience 26, 71–80.

Becker, T., Becker, C.G., 2014. Axonal regeneration in zebrafish. Current Opinion in Neurobiology 27, 186–191.

Bussmann, J., Lawson, N., Zon, L., Schulte-Merker, S., Ekker, M., Mullins, M., Postlethwait, J., Westerfield, M., 2008. Zebrafish VEGF receptors: A guideline to nomenclature. PLoS Genetics 4, 4–5.

Caduff, J.H., Fischer, L.C., Burri, P.H., 1986. Scanning electron microscope study of the developing microvasculature in the postnatal rat lung. The Anatomical Record 216, 154–164.

Chamberlain, J.D., Meier, S., Mader, L., Von Groote, P.M., Brinkhof, M.W.G., 2015. Mortality and longevity after a spinal cord injury: Systematic review and meta-analysis. Neuroepidemiology 44, 182–198.

Chappell, J.C., Bautch, V.L., 2010. Vascular development genetic mechanisms and links to vascular disease, Current Topics in Developmental Biology. Elsevier Inc.

Chappell, J.C., Taylor, S.M., Ferrara, N., Bautch, V.L., 2009. Local Guidance of Emerging Vessel Sprouts Requires Soluble Flt-1 (VEGFR-1). Dev Cell 17, 377–386.

Chappell, J.C., Wiley, D.M., Bautch, V.L., 2011. How blood vessel networks are made and measured. Cells Tissues Organs 195, 94–107.

Cheshire, W.P., Santos, C.C., Massey, W.E., Howard, J.F., 1996. Spinal cord infarction: Etiology and outcome. Neurology 47, 321–330.

Childs, S., Chen, J.-N., Garrity, D.M., Fishman, M.C., 2002. Patterning of angiogenesis in the zebrafish embryo. Development 129, 973–982.

Cristante, A., Barros, T., Marcon, R., Letaif, O., Rocha, I., 2012. Therapeutic approaches for spinal cord injury. Clinics 67, 1219–1224.

Cross, M.J., Dixelius, J., Matsumoto, T., Claesson-Welsh, L., 2003. VEGF-receptor signal transduction. Trends in Biochemical Sciences 28, 488–494.

Curtis, E., Martin, J.R., Gabel, B., Sidhu, N., Rzesiewicz, T.K., Mandeville, R., Van Gorp, S., Leerink, M., Tadokoro, T., Marsala, S., Jamieson, C., Marsala, M., Ciacci, J.D., 2018. A First-in-Human, Phase I Study of Neural Stem Cell Transplantation for Chronic Spinal Cord Injury. Cell Stem Cell 22, 941–950.e6.

Diaz Quiroz, J.F., Echeverri, K., 2013. Spinal cord regeneration: where fish, frogs and salamanders lead the way, can we follow? Biochemical Journal 451, 353–364.

Dietz, V., Grillner, S., Trepp, A., Hubli, M., Bolliger, M., 2009. Changes in spinal reflex and locomotor activity after a complete spinal cord injury: A common mechanism? Brain 132, 2196–2205.

Fang, P., Lin, J.F., Pan, H.C., Shen, Y.Q., Schachner, M., 2012. A Surgery Protocol for Adult Zebrafish Spinal Cord Injury. Journal of Genetics and Genomics 39, 481–487.

Ghosh, S., Hui, S.P., 2018. Axonal regeneration in zebrafish spinal cord. Regeneration 5, 43–60.

Gianni-Barrera, R., Bartolomeo, M., Vollmar, B., Djonov, V., Banfi, A., 2014. Split for the cure: VEGF, PDGF-BB and intussusception in therapeutic angiogenesis. Biochemical Society Transactions 42, 1637–1642.

Gore, A. V, Monzo, K., Cha, Young R.Weinstein, B.M., 2012. Vascular Development in the Zebrafish. Cold Spring Harbor perspectives in medicine a00668.

Hagen, E.M., 2015. Acute complications of spinal cord injuries. World Journal of Orthopedics 6, 17.

Hama, H., Hioki, H., Namiki, K., Hoshida, T., Kurokawa, H., Ishidate, F., Kaneko, T., Akagi, T., Saito, T., Saido, T., Miyawaki, A., 2015. ScaleS: An optical clearing palette for biological imaging. Nature Neuroscience 18, 1518–1529.

Herrera, J.J., Sundberg, L.M., Zentilin, L., Giacca, M., Narayana, P.A., 2010. Sustained Expression of Vascular Endothelial Growth Factor and Angiopoietin-1 Improves Blood–Spinal Cord Barrier Integrity and Functional Recovery after Spinal Cord Injury. Journal of Neurotrauma 27, 2067–2076.

Hui, S.P., Dutta, A., Ghosh, S., 2010. Cellular response after crush injury in adult zebrafish spinal cord. Developmental Dynamics 239, 2962–2979.

Jin, S.-W., Beis, D., Mitchell, T., Chen, J.-N., Stainier, D.Y.R., 2005. Cellular and molecular analyses of vascular tube and lumen formation in zebrafish. Development 132, 5199–5209.

Kang, Y., Ding, H., Zhou, H., Wei, Z., Liu, L., Pan, D., Feng, S., 2017. Epidemiology of worldwide spinal cord injury: a literature review. Journal of Neurorestoratology Volume 6, 1–9.

Kari, G., Rodeck, U., Dicker, A.P., 2007. Zebrafish: An emerging model system for human disease and drug discovery. Clinical Pharmacology and Therapeutics 82, 70–80.

Khaibullina, A.A., Rosenstein, J.M., Krum, J.M., 2004. Vascular endothelial growth factor promotes neurite maturation in primary CNS neuronal cultures. Developmental Brain Research 148, 59–68.

Kimelman, D., Martin, B.L., 2012. Posterior Patterning in Early Development: Three Strategies. Wiley Interdisciplinary Reviews: Developmental Biology 1, 253–266.

Kimmel, C.B., Ballard, W.W., Kimmel, S.R., Ullmann, B., Schilling, T.F., 1995. Stages of embryonic development of the zebrafish. Developmental dynamics 203, 253–310.

Kirshblum, S.C., Waring, W., Biering-Sorensen, F., Burns, S.P., Johansen, M., Schmidt-Read, M., Donovan, W., Graves, D.E., Jha, A., Jones, L., Mulcahey, M.J., Krassioukov, A., 2011. International standards for neurological classification of spinal cord injury. The Journal of Spinal Cord Medicine 34, 547–554.

Kolte, D., McClung, J.A., Aronow, W.S., 2015. Vasculogenesis and Angiogenesis, Translational

Research in Coronary Artery Disease: Pathophysiology to Treatment. Elsevier Inc.

Lele, Z., Engel, S., Krone, P.H., 1997. hsp47 and hsp70 Gene Expression Is Differentially Regulated in a Stress- and Tissue-Specific Manner in Zebrafish Embryos. Developmental Genetics 21, 123–133.

Logothetidou, A., Vandecasteele, T., Van Mulken, E., Vandevelde, K., Cornillie, P., 2017. Intussusceptive angiogenesis and expression of Tie receptors during porcine metanephric kidney development. Histology and Histopathology 32, 817–824.

Maçarico, T.F.R.R., 2014. Uncovering the effect of low doses of ionizing radiation in angiogenesis during spinal cord regeneration. Tese de Mestrado. Faculdade de Ciências. Universidade de Lisboa.

Makanya, A.N., Hlushchuk, R., Baum, O., Velinov, N., Ochs, M., Djonov, V., 2007. Microvascular endowment in the developing chicken embryo lung. American Journal of Physiology-Lung Cellular and Molecular Physiology 292, L1136–L1146.

Makanya, A.N., Stauffer, D., Ribatti, D., Burri, P.H., Djonov, V., 2005. Microvascular growth, development, and remodeling in the embryonic avian kidney: The interplay between sprouting and intussusceptive angiogenic mechanisms. Microscopy Research and Technique 66, 275–288.

Marcus, E.M., Jacobson, S., Sabin, T.D., 2014. Integrated Neuroscience and Neurology: A Clinical Case History Problem Solving Approach, 2nd ed. Oxford University Press.

Marín-Juez, R., Marass, M., Gauvrit, S., Rossi, A., Lai, S.-L., Materna, S.C., Black, B.L., Stainier, D.Y.R., 2016. Fast revascularization of the injured area is essential to support zebrafish heart regeneration. Proceedings of the National Academy of Sciences 113, 11237–11242.

Martirosyan, N.L., Feuerstein, J.S., Theodore, N., Cavalcanti, D.D., Spetzler, R.F., Preul, M.C., 2011. Blood supply and vascular reactivity of the spinal cord under normal and pathological conditions. Journal of Neurosurgery: Spine 15, 238–251.

Matsuoka, R.L., Marass, M., Avdesh, A., Helker, C.S.M., Maischein, H.M., Grosse, A.S., Kaur, H., Lawson, N.D., Herzog, W., Stainier, D.Y.R., 2016. Radial glia regulate vascular patterning around the developing spinal cord. eLife 5, 1–24.

Mautes, A.E.M., Weinzierl, M.R., Donovan, F., Noble, L.J., 2000. Vascular Events After Spinal Cord Injury: Contribution to Secondary Pathogenesis. Physical Therapy 80, 673–687.

McDonough, A., Martínez-Cerdeño, V., 2012. Endogenous proliferation after spinal cord injury in animal models. Stem Cells International 2012.

Meletis, K., Barnabé-Heider, F., Carlén, M., Evergren, E., Tomilin, N., Shupliakov, O., Frisén, J., 2008. Spinal cord injury reveals multilineage differentiation of ependymal cells. PLoS Biology 6, 1494–1507.

Mescher, A.L., 2013. Chapter 9 Nerve Tissue & the Nervous System. Junqueiras's Basic Histology Text and Atlas, 13th ed. McGraw-Hill Education.

Nandoe Tewarie, R.D.S., Hurtado, A., Bartels, R.H.M. a, Grotenhuis, J.A., Oudega, M., 2010. A clinical perspective of spinal cord injury. NeuroRehabilitation 27, 129–39.

Oudega, M., 2012. Molecular and cellular mechanisms underlying the role of blood vessels in spinal cord injury and repair. Cell and Tissue Research 349, 269–288.

Patan, S., 1998. TIE1 and TIE2 receptor tyrosine kinases inversely regulate embryonic angiogenesis by the mechanism of intussusceptive microvascular growth. Microvascular Research 56, 1–21.

Pugh, C.W., Ratcliffe, P.J., 2003. Regulation of angiogenesis by hypoxia: Role of the HIF system. Nature Medicine 9, 677–684.

Reimer, M.M., Sorensen, I., Kuscha, V., Frank, R.E., Liu, C., Becker, C.G., Becker, T., 2008. Motor Neuron Regeneration in Adult Zebrafish. Journal of Neuroscience 28, 8510–8516.

Ribatti, D., Crivellato, E., 2012. "Sprouting angiogenesis", a reappraisal. Developmental Biology 372, 157–165.

Ronca, R., Benkheil, M., Mitola, S., Struyf, S., Liekens, S., 2017. Tumor angiogenesis revisited: Regulators and clinical implications. Medicinal Research Reviews 37, 1231–1274.

Rosenstein, J.M., Krum, J.M., 2004. New roles for VEGF in nervous tissue - Beyond blood vessels. Experimental Neurology 187, 246–253.

Savant, S., La Porta, S., Budnik, A., Busch, K., Hu, J., Tisch, N., Korn, C., Valls, A.F., Benest, A. V., Terhardt, D., Qu, X., Adams, R.H., Baldwin, H.S., Ruiz de Almodóvar, C., Rodewald, H.R., Augustin, H.G., 2015. The Orphan Receptor Tie1 Controls Angiogenesis and Vascular Remodeling by Differentially Regulating Tie2 in Tip and Stalk Cells. Cell Reports 12, 1761–1773.

Schindelin, J., Arganda-Carreras, I., Frise, E., Kaynig, V., Longair, M., Pietzsch, T., Preibisch, S., Rueden, C., Saalfeld, S., Schmid, B., Tinevez, J.-Y.J.-Y., White, D.J., Hartenstein, V., Eliceiri, K., Tomancak, P., Cardona, A., Liceiri, K., Tomancak, P., A., C., 2012. Fiji: An open source platform for biological image analysis. Nature Methods 9, 676–682.

Sharif-Alhoseini, M., Khormali, M., Rezaei, M., Safdarian, M., Hajighadery, A., Khalatbari, M.M., Safdarian, M., Meknatkhah, S., Rezvan, M., Chalangari, M., Derakhshan, P., Rahimi-Movaghar, V., 2017. Animal models of spinal cord injury: A systematic review. Spinal Cord 55, 714–721.

Steward, O., Willenberg, R., 2017. Rodent spinal cord injury models for studies of axon regeneration. Experimental Neurology 287, 374–383.

Stewart, A.M., Gaikwad, S., Kyzar, E., Kalueff, A. V., 2012. Understanding spatio-temporal strategies of adult zebrafish exploration in the open field test. Brain Research 1451, 44–52.

Ten Dijke, P., Arthur, H.M., 2007. Extracellular control of TGFβ signalling in vascular development and disease. Nature Reviews Molecular Cell Biology 8, 857–869.

Tetzlaff, W., Alexander, S.W., Miller, F.D., Bisby, M.A., 1991. Response of facial and rubrospinal neurons to axotomy: changes in mRNA expression for cytoskeletal proteins and GAP-43. The Journal of neuroscience : the official journal of the Society for Neuroscience 11, 2528–44.

Thuret, S., Moon, L.D.F., Gage, F.H., 2006. Therapeutic interventions after spinal cord injury. Nature Reviews Neuroscience 7, 628–643.

Tventen, L., 1976. SPINAL CORD VASCULARITY III - The spinal cord arteries in man. Acta Radiologica 17, May. 257–273.

Van De Graaff, K.M., 2001. Chapter 11 Nervous Tissue and the Central Nervous System. Human anatomy, 6th ed. McGraw-Hill Education.

Wang, H., Liu, X., Li, R., Zhang, P., Chu, Z., Wang, C., Liu, H., Qi, J., Lv, G., Wang, G., Liu, B., Li, Y., Wang, Y., 2017. Effect of glial cells on remyelination after spinal cord injury. Neural Regeneration Research 12, 1724.

Weber, M., Mickoleit, M., Huisken, J., 2014. Light sheet microscopy, 1st ed, Methods in Cell Biology. Elsevier Inc.

Attachments

1.Suplementary Figures

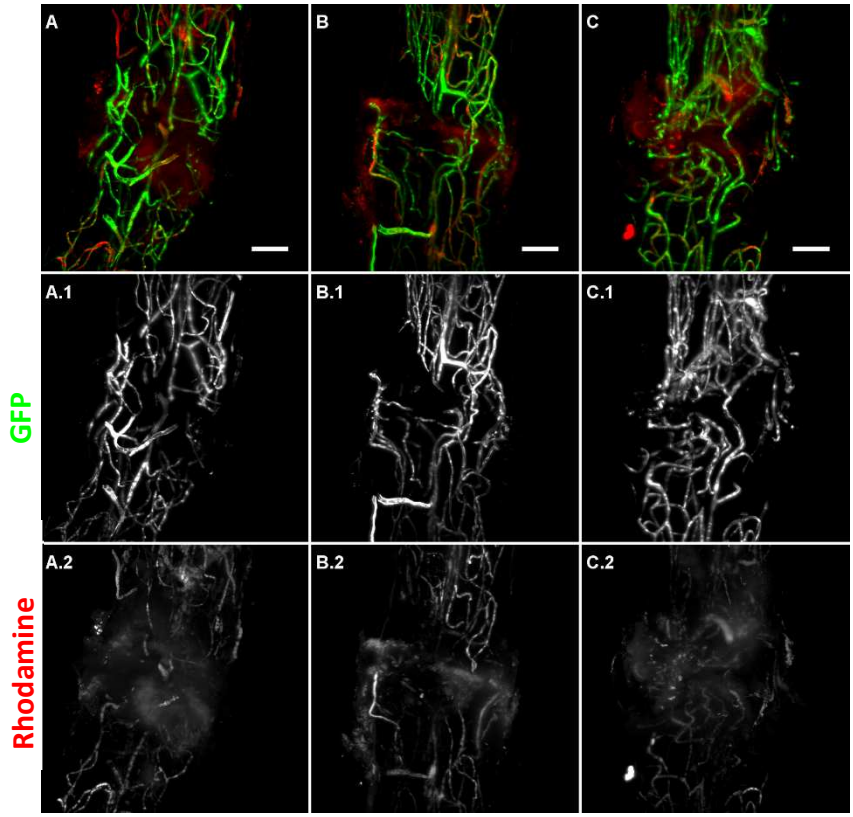

Supplementary Image 1 – Vasculature of Tg (kdrl:EGFP) samples after 1 dpi. At 1 dpi, the vasculature was disrupted (**A.1 – C.1**), with rhodamine leaking and accumulation in the nervous tissue (**A.2 – C.2**) **Scalebar:** 100µm

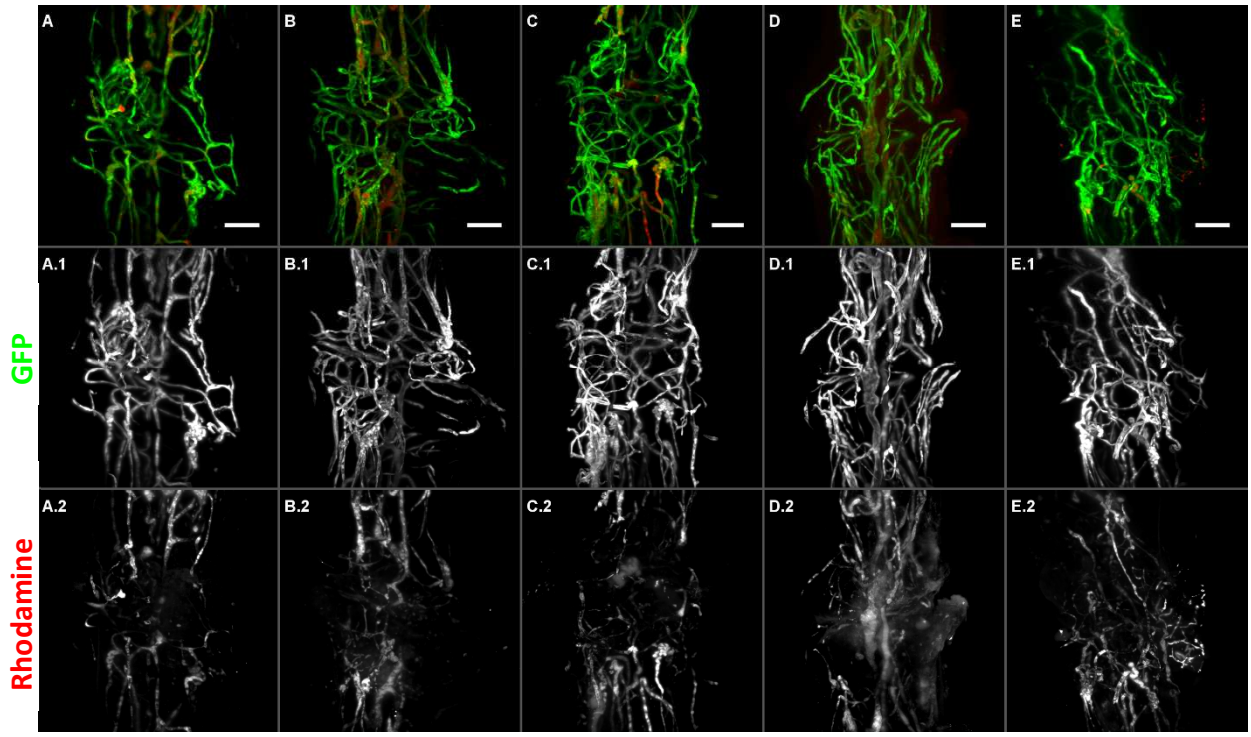

Supplementary Image 2 – Vasculature of Tg (kdrl:EGFP) samples at 3 dpi. At 3 dpi, new blood vessels were already seen at the injury site (**A.1 – E.1**). Most blood vessels did not contain rhodamine. Additionally, rhodamine was observed in the tissues (**A.2 – E.2**) **Scalebar:** 100µm

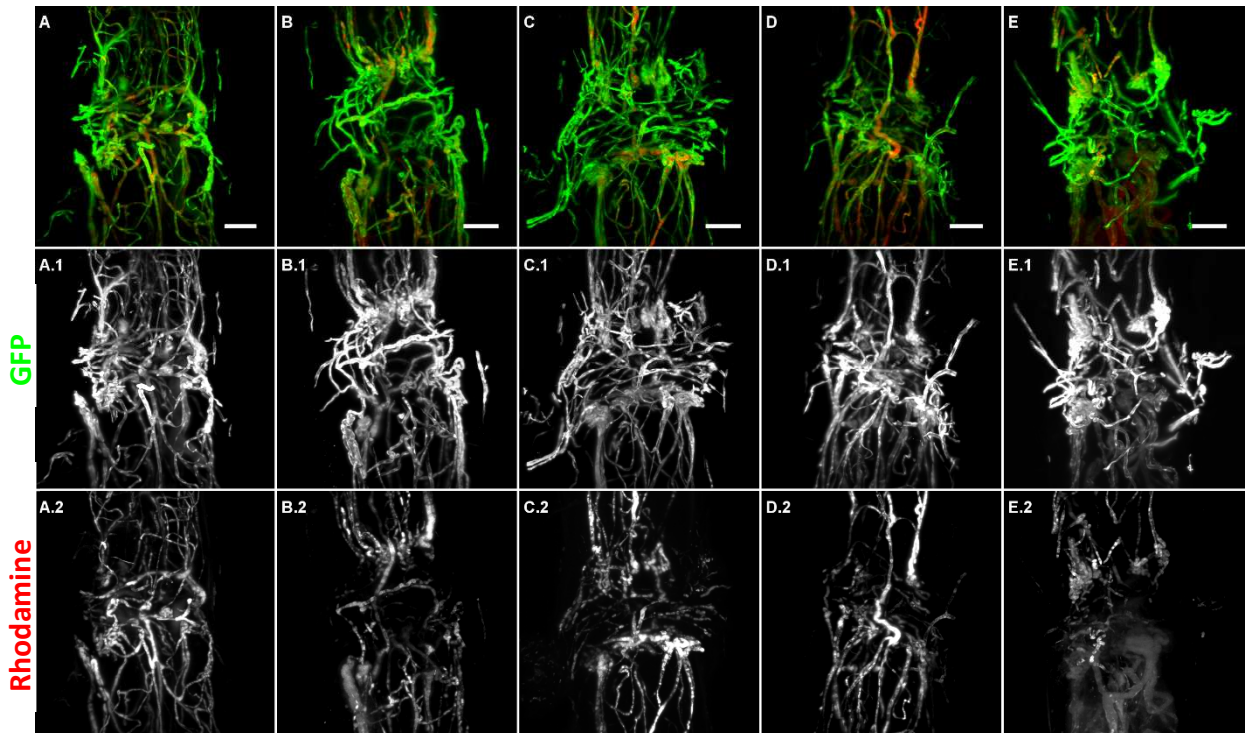

Supplementary Image 3 – Vasculature of Tg (kdrl:EGFP) samples at 5 dpi. At 5 dpi, more new blood vessels were seen at the injury site (**A.1 – E.1**). At this timepoint, many blood vessels were already able to retain rhodamine (**A.2 – E.2**) **Scalebar:** 100µm

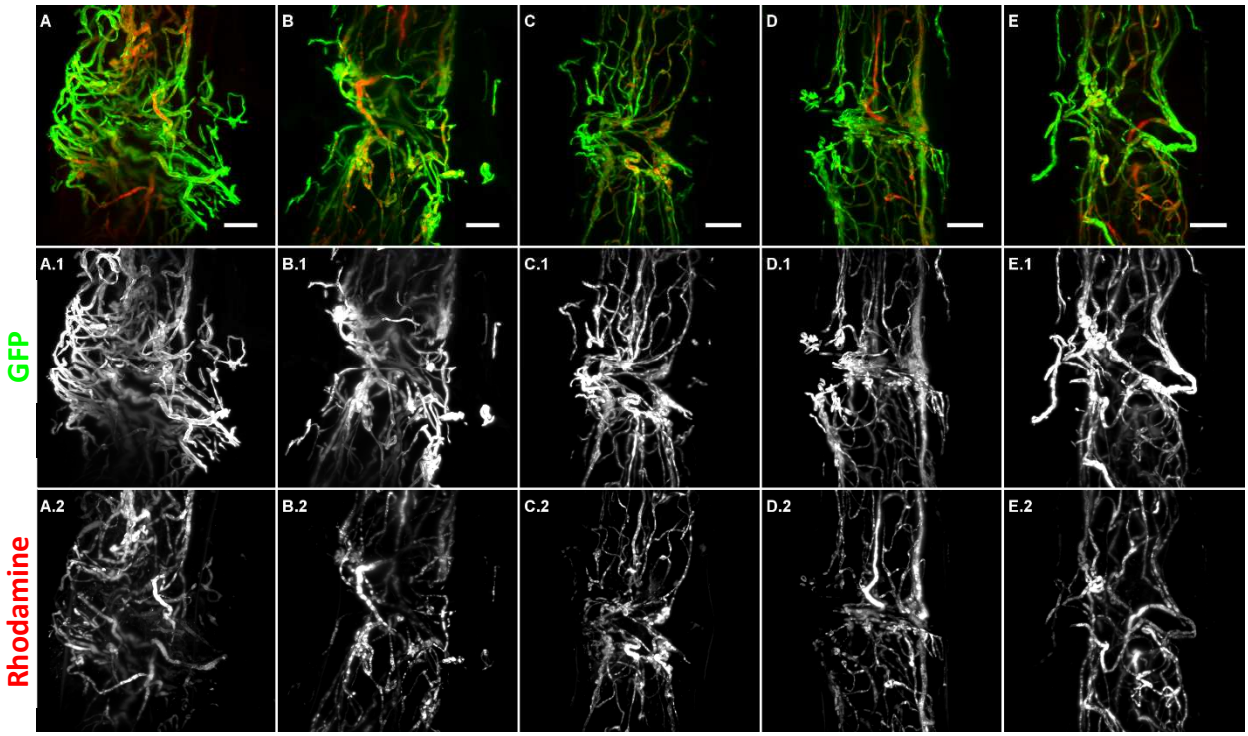

Supplementary Image 4 – Vasculature of Tg (kdrl:EGFP) samples at 7 dpi. At 7 dpi, many blood vessels were still seen at the injury site (**A.1 – E.1**). At this timepoint, most vessels contained rhodamine (**A.2 – E.2**) **Scalebar:** 100µm

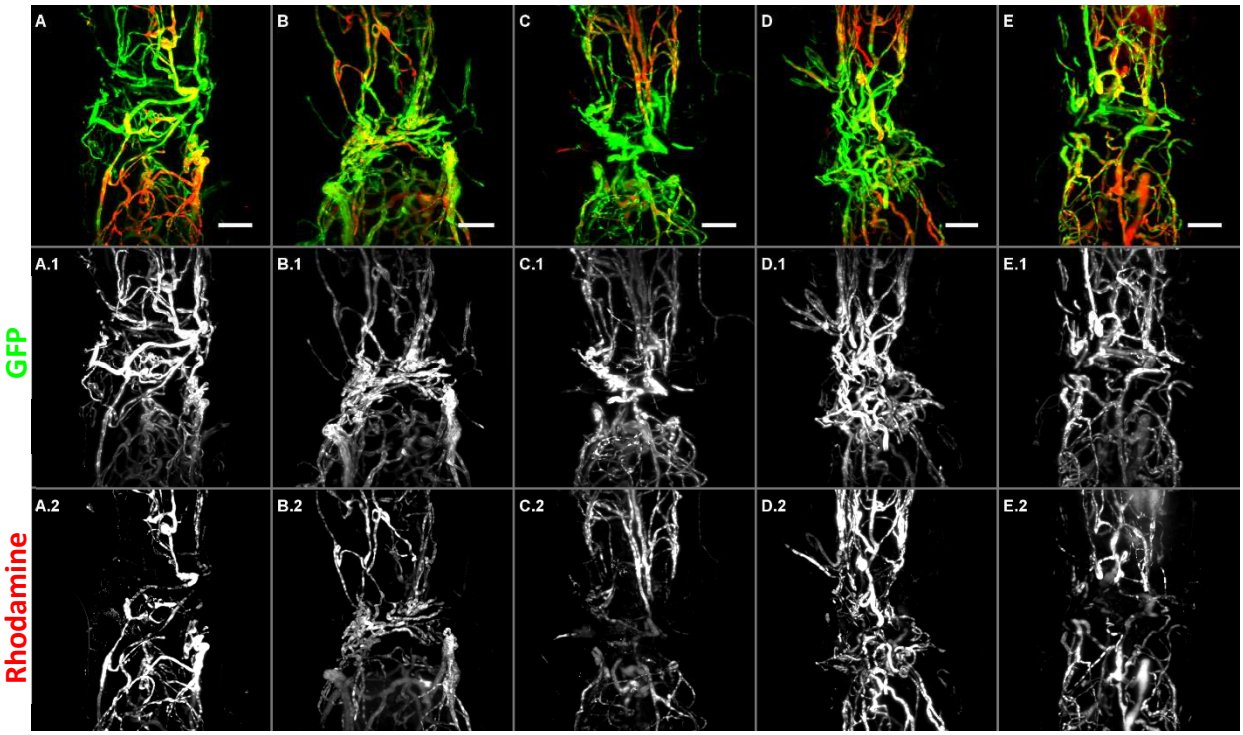

Supplementary Image 5 – Vasculature of Tg (kdrl:EGFP) samples at 14 dpi. At 14 dpi, no significant differences were observed, when compared with samples with 7dpi, regarding the quantity of blood vessels (**A.1 – E.1**) and their ability to retain rhodamine (**A.2 – E.2**). **Scalebar:** 100µm

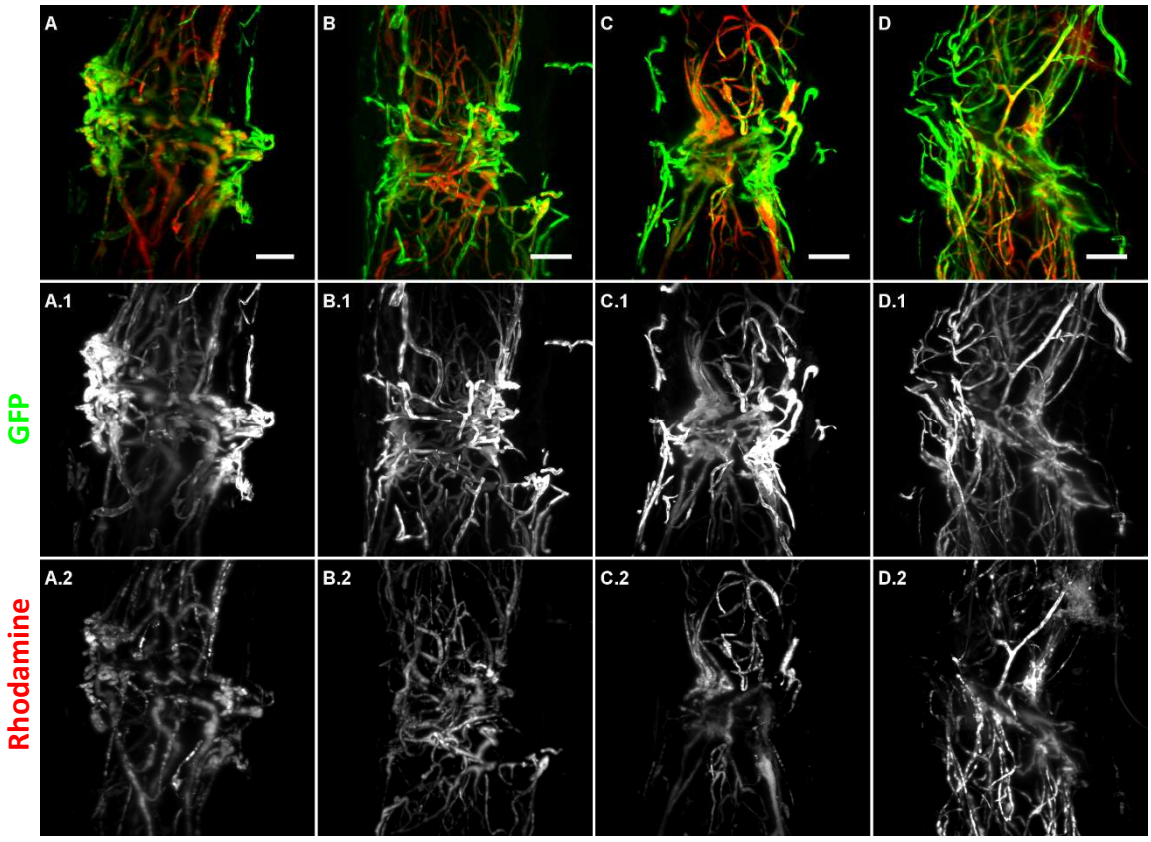

Supplementary Image 6– Vasculature of Tg (hsp70l:sflt1) samples at 7 dpi. Tg (hsp70l:sflt1) fish were maintained at 28ºC. At 7 dpi, many blood vessels were seen at the injury site (**A.1 – D.1**). At this timepoint, most vessels contained rhodamine (**A.2 – D.2**) **Scale bar:** 100µm

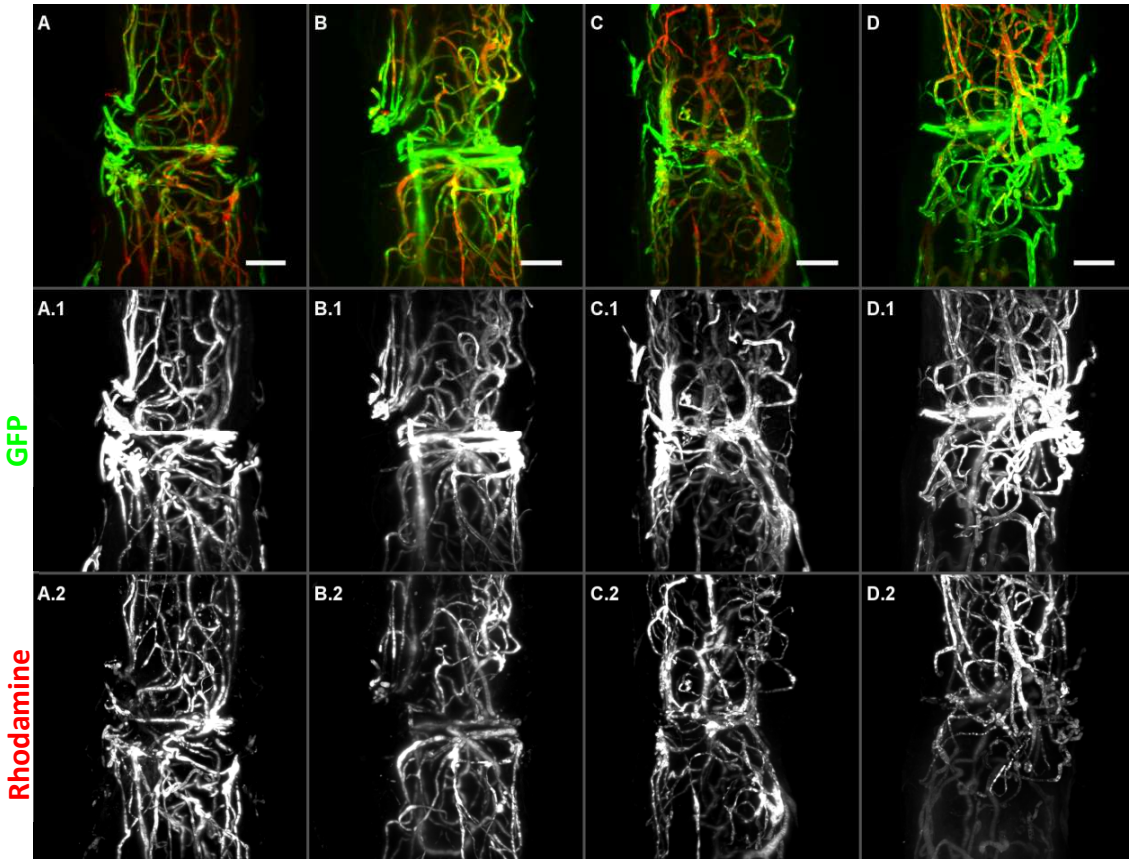

Supplementary Image 7 – Vasculature of Tg (hsp70l:sflt1) samples at 14 dpi. Tg (hsp70l:sflt1) fish were maintained at 28ºC. At 14 dpi, no significant differences were observed, when compared with samples with 7dpi, regarding the quantity of blood vessels (**A.1 – E.1**) and their ability to retain rhodamine (**A.2 – E.2**). **Scalebar:** 100µm

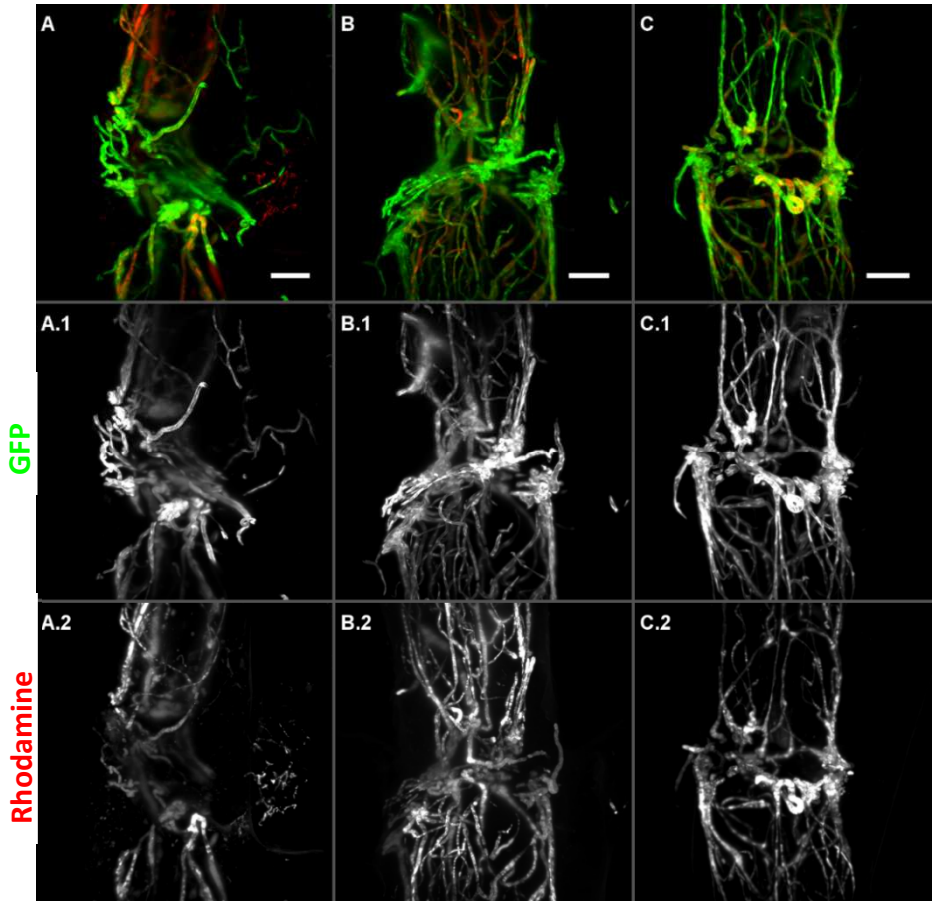

Supplementary Image 8 –Tg (hsp70l:sflt1) samples with 7 dpi obtained with the 34ºC, for 6 hours, twice a day, heat-shock protocol. All the samples showed blood vessels at the injury site (**A.1 – C.1**) with rhodamine inside (**A.2 – C.2**) **Scalebar:** 100µm

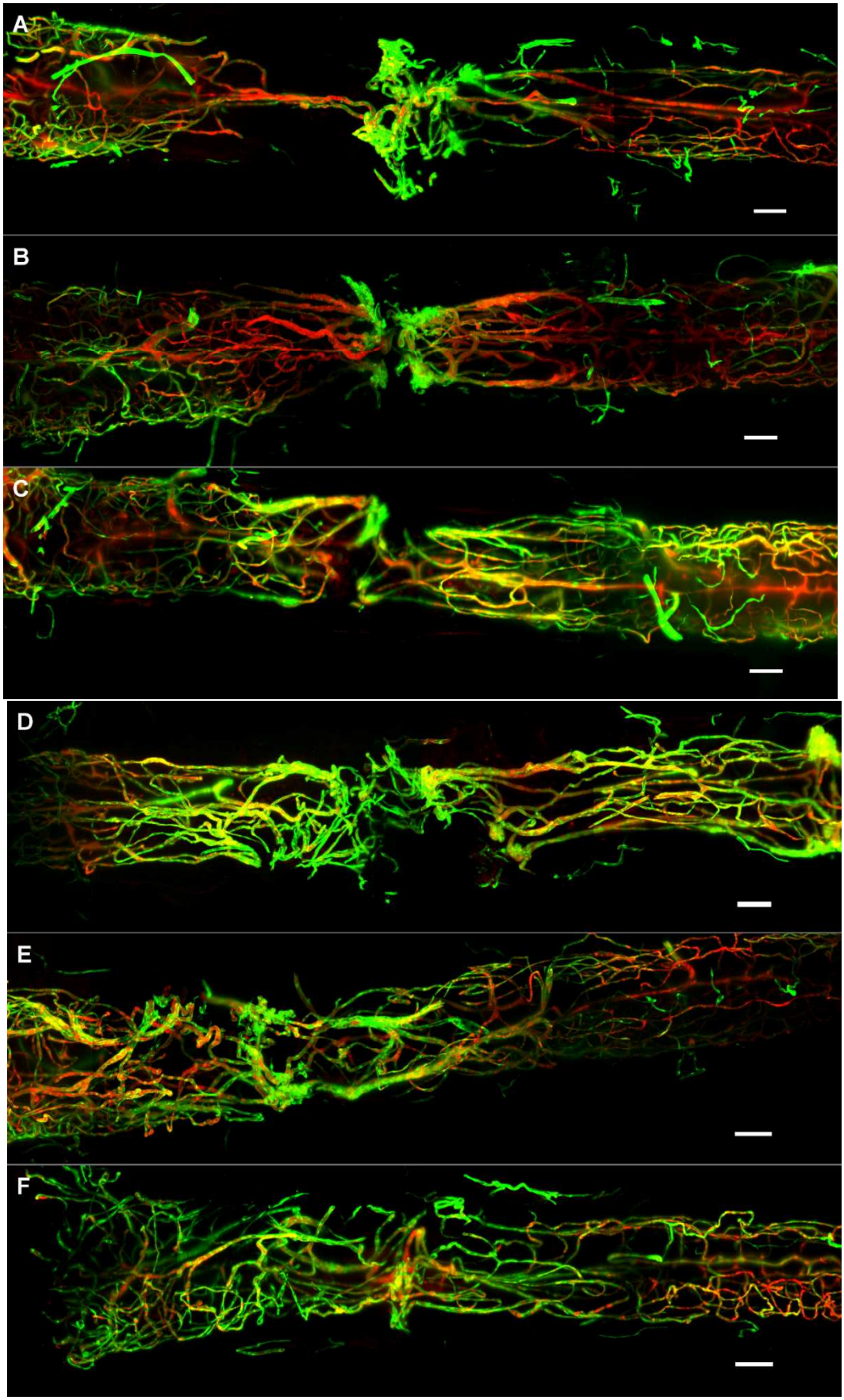

Supplementary Image 9 –Tiles from Tg (hsp70l:sflt1) samples with 7 dpi obtained with the 34ºC continuous heat-shock protocol. In most samples, knots of vessels are observed at the injury site (**A –** E). Additionally, thick vessels are observed at the injury site and in adjacent areas. **Scalebar:** 100µm

2.Suplementary Tables

Supplementary Table 1 –Mean values ± standard deviation of the swimming distances, during 10 minutes, of Tg (hsp70l:sflt1) and Tg (kdrl:EGFP). With the heat-shock tracking protocol until 21 dpi, Tg (hsp70l:sflt1) fish swam less distance that controls.

	Mean swiming distances (cm) ± SD (cm)	
Tracking day	Tg (kdrl:EGFP)	Tg (hsp70l:sflt1)
-1	5321.474 ± 1347.689	4503.976 ± 620.239
1	138.094 ± 48.265	165.665 ± 52.877
7	1306.878 ± 1417.102	443.473 ± 276.041
14	2452.579 ± 1302.663	1218.945 ± 1005.242
21	3216.920 ± 1185.538	1373.116 ± 1673.606

Supplementary Table 2 –Mean values ± standard deviation of the swimming distances normalized to -1day, during 10 minutes, of Tg (hsp70l:sflt1) and Tg (kdrl:EGFP). Normalization of the swimming values was done to take into account individual variability. Again, controls performed better than Tg (hsp70l:sflt1) after the heat-shock tracking protocol.

	Normalization to day -1 ± SD	
Tracking day	Tg (kdrl:EGFP)	Tg (hsp70l:sflt1)
1	0.021 ± 0.011	0.036 ± 0.009
7	0.219 ± 0.181	0.099 ± 0.055
14	0.479 ± 0.236	0.273 ± 0.224
21	0.641 ± 0.278	0.282 ± 0.309